

Mari Nyhaug

Dye-sensitized solar cells with zinc oxide electrodes

Improving the electrodeposition of ZnO and investigating the electrode lifetime

Master's thesis in Nanotechnology

Supervisor: Professor Svein Sunde

June 2019

Mari Nyhaug

Dye-sensitized solar cells with zinc oxide electrodes

Improving the electrodeposition of ZnO and investigating the electrode lifetime

Master's thesis in Nanotechnology
Supervisor: Professor Svein Sunde
June 2019

Norwegian University of Science and Technology
Faculty of Natural Sciences
Department of Materials Science and Engineering



Norwegian University of
Science and Technology

Preface

This master's thesis marks the end of 5 years attending the masters program in Nanotechnology (MTNANO) at the Norwegian University of Science and Technology (NTNU). The thesis is a continuation of the work performed in TMT4510 - Nanotechnology, specialization project, and builds on the report "Fabrication of zinc oxide photoanodes for use in dye-sensitized solar cells by combining the methods electrochemical deposition and doctor blading". The work is a part of the electrochemistry group at the Department of Materials Science and Engineering.

Acknowledgements

First of all, I would like to thank my supervisor Professor Svein Sunde for excellent guidance. Thanks goes to Henrik Erring Hansen for great discussions and for sharing the programs from his project work with me. The ALD-deposition of TiO_2 was kindly performed by Abdulla Bin Afif from the Department of Mechanical and Industrial Engineering. The Research Council of Norway is acknowledged for the support to the Norwegian Micro- and Nano-Fabrication Facility, NorFab, project number 245963/F50. Finally, thanks go to Nils R. Mulder and Håvard Katle Fjon for proofreading, and as always to my friends and family for always putting a smile on my face.

Sammendrag

Fargestoff-solceller er et spennende område innen fornybar energi. Disse solcellene åpner nye anvendelsesområder sammenlignet med silisium-cellene som dominerer dagens marked. Fargestoff-solceller kan lages gjennomsiktige eller med mange forskjellige farger, noe som åpner for bruk i bygninger og dekorative vinduer. I denne masteroppgaven har jeg forsket på hvordan man enkelt kan lage fargestoff-solceller av materialet sinkkoksidd.

Sinkkoksidd er et materiale som er enkelt å lage i mange forskjellige nanostrukturer, også ved lav temperatur. En syntese ved lav temperatur er fordelaktig med hensyn til energiforbruk under produksjon. I tillegg åpner det for muligheten til å lage bøyelige solceller av plast. For at fargestoff-solcellene skal fungere optimalt må sinkkoksiddet lages krystallinsk og porøst. En metode for å oppnå dette er elektrokjemisk utfelling. Metoden baserer seg på reduksjon av nitraterne i en vandig sinknitrat-løsning. Reaksjonen produserer hydroksidd-grupper som øker pH-en i løsningen og får sinkkoksidd til å felle ut og deponere på arbeidselektroden. Arbeidselektroden er en glassbit som er dekket med en elektrisk ledende tynnfilm (FTO-glass) på den ene siden.

I en fargestoff-solcelle fester man et fargestoff til overflaten av sinkkoksiddet. Dette er grunnen til at sinkkoksiddet må være porøst. Porene gjør at materialet har en stor overflate hvor fargestoffet kan feste seg. Det er fargestoffet som absorberer energien fra sola og gjør den om til elektrisk energi. Det er derfor viktig å ha mange fargestoff-molekyler på overflaten av sinkkoksiddet.

Elektrokjemisk utfelling av sinkkoksidd kan utføres på flere forskjellige måter. I denne masteroppgaven er forskjellige metoder og aspekter ved syntesen undersøkt for å finne den beste måten å lage sinkkoksidd-elektroder ved en lav temperatur.

Tre forskjellige elektrokjemiske metoder er prøvd for å oppnå ønsket potensial på arbeidselektroden: konstant strøm (galvanostatisk), konstant potensial (potentiostatisk) eller syklisk potensial. Arbeidet fant at et syklisk potensial gir bedre filmer enn både konstant potensial og konstant strøm.

En utfordring med den elektrokjemiske utfellingen er at filmene ikke er porøse nok. For å løse dette kan man tilsette eosin Y i sinknitrat-løsningen. Eosin Y er et fargestoff som også kan brukes i fargestoff-solceller, men som ikke gir så høy virkningsgrad. Det

kan derimot brukes som en «form» under syntesen av sinkoksidet. Når man har eosin Y i nitrat-løsningen under syntesen, fester molekylene seg på overflaten av sinkoksidet og tvinger sinkoksid til å gro rundt det. På den måten lager eosin Y en pore. Man kan si at eosin Y «holder av» en plass for fargestoffet man skal bruke i den ferdige cellen. Etter syntesen kan eosin Y enkelt fjernes i en basisk løsning av kaliumhydroksid for å gjøre plass til et annet, bedre fargestoff.

Det mest interessante funnet i denne masteroppgaven er at det er sannsynlig at lys hjelper veksten av sinkoksid ved å eksitere elektroner i eosin Y-molekylene. Dette hjelper elektrontransporten under syntesen og gjør at mer sinkoksid felles ut og fester seg på arbeids Elektroden. Det resulterer i tykkere filmer, som er bra fordi det da blir et større areal hvor fargestoffet kan feste seg. Med fargestoff i nitratløsningen og belysning under syntesen, ble fargestoff solceller med elektroder av elektrokjemisk utfelt sinkoksid, belagt med fargestoffet N719, forbedret fra å ikke kunne generere en fotostrøm, til en virkningsgrad på 3.42% når belyst med lys med bølglengde 512 nm.

Et problem med sinkoksid i fargestoff-solceller er at det veldig lett brytes ned. Fargestoffene bør festes til overflaten av sinkoksidet, med såkalte ankergrupper. Karboksylsyregrupper er ofte brukt til dette, men de bryter ned sinkoksid. Dette vil korte ned levetiden til den ferdige solcellen, og skal solcellene bli konkurransedyktige må dette løses. Hvordan to forskjellige fargestoffer, N719 og eosin Y, bryter ned cellen har derfor blitt undersøkt. N719 har to slike syregrupper, mens eosin Y ikke har noen. Solcellen med fargestoffet N719 har en 37.7% dårlige kvantevirkningsgrad etter 15 dager, mens cellen med eosin Y var ubrukelig etter bare noen timer. Dette viser at det er nødvendig å ha ankergrupper, men samtidig understrekes viktigheten av å lage mer stabile fargestoff-solceller.

Det ble forsøkt å dekke sinkoksidet med et tynt lag av titandioksid. Titandioksid er et mer stabilt materiale, og tanken var at det skulle beskytte sinkoksidet. 100 nm med titandioksid ble lagt oppå sinkoksidet med atomlag-deponering (ALD), men det viste seg å være for tykt. Porene i sinkoksidfilmen ble tettet og prøven ødelagt. Tynnere lag ble ikke prøvd, grunnet at ALD-maskinen var i ustand i en lang periode.

Arbeidet med denne masteroppgaven har vist at det er mulig å lage brukbare fargestoff-solceller av sinkoksid. Elektrokjemisk utfelling er en enkel lavtemperatur-metode for å legge en porøs og krystallinsk film av sinkoksid på et ledende substrat. Ved å tilføre eosin Y i sinknitrat-løsningen vil sinkoksidfilmene bli mer porøse. Ved å eksponere syntesen for lys, tilføres flere elektroner til reaksjonen og mer sinkoksid blir utfelt. Det største problemet med sinkoksid-fargestoff-solceller er at de brytes raskt ned av syregrupper på fargestoffene. Å dekke prøven med titandioksid kan være en løsning, men 100 nm er for tykt.

Abstract

Dye-sensitized solar cells (DSSCs) are an exciting area within the field of renewable energy. These solar cells open up for new areas of application compared to the silicon solar cells that dominate the market today. DSSCs can be made transparent and in different colors, and can, therefore, be used in buildings and windows. In this master's thesis, the manufacture and degradation of DSSC with electrodes of zinc oxide (ZnO) have been investigated.

ZnO is a material easily manufactured into many different nanostructures, also at low temperatures. A low-temperature synthesis is beneficial, both with regards to energy consumption during the manufacture and the utilization of temperatures sensitive substrates. Plastic substrates make flexible solar cells a reality. The ZnO in DSSCs must be crystalline and porous. A method to achieve this is electrochemical deposition. The method is based on the reduction of nitrate ions in an aqueous solution of zinc nitrate. The reaction produces hydroxyl groups, which increases the pH near the working electrode, making ZnO precipitate and deposit onto the working electrode. The working electrode is a piece of glass coated with fluorine-doped tin-oxide (FTO-glass) on one side.

The electrodeposition was performed using three different techniques: galvanostatic (constant current), potentiostatic (constant potential) and potentiodynamic (cycling the potential between two vertex potentials). Potentiodynamic resulted in films that were white and homogeneous, in contrast to potentiostatic and galvanostatic, which were either black or inhomogeneous.

A challenge with the standard electrodeposition is that the deposited films are not porous enough. A solution to this is to add the dye-molecule eosin Y to the zinc nitrate solution to make hybrid dye/ZnO-films. During this hybrid electrodeposition, eosin Y will adsorb to the surface of ZnO, inhibiting growth in that area. The ZnO will be forced to grow around the eosin Y, and a pore is thus created. The eosin Y deposited during the electrodeposition can easily be removed by a potassium hydroxide solution at a pH of 10.5, leaving bare ZnO. The electrode can then be re-loaded with another dye before assembling the solar cell.

The most interesting result in this master's thesis is that exposing the hybrid elec-

trodeposition to light from a solar simulator appear to increase the growth of ZnO. This is due to photoelectrons being excited in the eosin Y-molecules. If this photoassisted hybrid electrodeposition deposits more ZnO, it means a larger surface area where the dye-molecules can adsorb will be created. This will increase the current generation in the solar cell. Through this work, the performance of DSSCs with ZnO-electrodes made by electrodeposition was improved from not producing any photocurrent at all, to a conversion efficiency of 3.42% at 512 nm.

A problem with ZnO in DSSCs is fast degradation. The lifetime of the solar cell is too short for the cell to have any commercial value. In this work, it was investigated how two different dyes, N719, and eosin Y, degrade ZnO-cells. Dye molecules should be attached to the surface of ZnO by an anchoring group. A common anchoring group is the carboxyl acid group, which N719 has two of. Eosin Y does not have any anchoring groups. The total quantum efficiency of N719/ZnO-cells had decreased by 37.7% in 15 days, while the eosin Y/ZnO-cell was useless after a few hours. This shows that the acidic anchoring groups of N719 corrode the ZnO, but that anchoring groups are needed to make the dye-molecules stay at the surface of ZnO. Better suited dye-molecules are needed for ZnO-DSSCs to improve.

It was investigated if a thin layer of titanium dioxide (TiO₂) on top of the ZnO would increase the lifetime of the ZnO-cells. TiO₂ is a more stable material, and is also the material that is most commonly used in DSSCs. A 100 nm layer of TiO₂ was deposited on the ZnO by atomic layer deposition (ALD), this was unfortunately too thick. The pores in the ZnO were clogged by the TiO₂. Thinner layers of TiO₂ were not attempted as the ALD-machine broke down.

Contents

Preface	i
Sammendrag	iii
Abstract	v
1 Introduction	1
2 Theory	3
2.1 Solar energy	3
2.2 Semiconductors	4
2.3 Sensitizing dyes	7
2.4 Dye-sensitized solar cells	8
2.4.1 Basic principles	8
2.4.2 Efficiency loss	11
2.4.3 Efficiency calculations	12
2.5 Characterization	13
2.5.1 Characterization cell	13
2.5.2 Current-voltage curves and quantum efficiency	14
2.5.3 Electrochemical impedance spectroscopy	16
2.5.4 Time constants	18
2.5.5 Recombination modeling in Python	19
2.5.6 Profilometer	20
2.5.7 Scanning electron microscopy	20
2.5.8 X-ray diffraction	20
2.6 Electrodeposition	21
2.7 Doctor blading	24
2.8 Atomic Layer Deposition	25

3	Experimental	27
3.1	Electrode manufacture	27
3.2	Photoelectrochemical characterization	31
3.3	Material characterization	32
4	Results	33
4.1	Electrodeposition of zinc oxide	33
4.1.1	Electrochemical technique	33
4.1.2	SE, HE and PHE	35
4.1.3	Crystal structure of electrodeposited films	42
4.1.4	Changes in deposition environments	43
4.2	Degradation	47
4.3	Atomic layer deposition of titanium dioxide	53
5	Discussion	55
5.1	Electrodeposition of zinc oxide	55
5.1.1	Comparison of electrochemical technique	55
5.1.2	Comparison of SE, HE, and PHE	56
5.1.3	Changes in deposition environments	58
5.1.4	Future outlook of electrodeposition	60
5.2	Degradation	61
5.2.1	Anchoring groups	61
5.2.2	Degradation of the ZnO/N719-electrode	62
5.3	Atomic layer deposition of titanium dioxide	65
6	Conclusions	67
7	Further work	69
	References	71
	Appendix	76
A	Chemicals and materials	77
A.1	List of chemicals and materials	77
B	Supplementary results	79
B.1	Electrodeposition of ZnO	79
B.2	Degradation	82

<i>CONTENTS</i>	ix
C Python script	83
D Risk Assessment	93

Chapter 1

Introduction

In 2018, the Intergovernmental Panel on Climate Change (IPCC) published a report saying that by 2030, the world needs to reduce carbon emissions by almost 50% [1]. To achieve this, there is a huge need for efficient and affordable renewable energy sources. Solar cells are a part of the solution. In the strategic report "*Energi21*", from the Norwegian Ministry of Petroleum and Energy, it is highlighted that solar power production should be a strategic focus area within research and industry [2]. Norway should gain a strong international position within the field and building integrated solar cells are listed as one of the focus areas.

Dye-sensitized solar cells (DSSCs) are an exciting area of research, and promise low-cost solar cells with new areas of application. Ever since O'Regan and Grätzel presented a DSSC with a ground breaking conversion efficiency of 7.9% in 1991 [3], the interest for the new solar cell technology has grown in the research community. Today the best DSSCs in literature have a conversion efficiency of about 13% [4]. The cells have a theoretical efficiency of about 20% [5], and if achieved, they will be able to compete with silicon cells (Si-cells). This is, however, not necessarily the goal, as DSSCs can be used in areas where Si-cells cannot. Furthermore, DSSCs perform better than Si-cells at high temperatures [5] and in low flux light [6]. DSSCs also open up for new applications such as flexible solar cells and windows. At the Swiss Tech convention center in Switzerland, the facade is made of colorful DSSCs. These solar cell windows do not only produce electricity, they also shield the inside room from the sun, reducing the need for air conditioning [7]. Furthermore, the cells look good and can be customized with regards to color by changing the sensitizing dye. The aesthetics of a technology should not be underestimated, especially since they may take up large areas in buildings and cities.

The best DSSCs today are made of titanium dioxide (TiO_2). A prominent, alternative material to TiO_2 is zinc oxide (ZnO). Some advantages of ZnO are faster electron transport [8] and the ability to produce crystalline materials at low temperatures [9]. A

low-temperature synthesis of dye-sensitized solar cell photoanodes is beneficial as it requires less energy, and temperature sensitive substrates can be used. The main problem with ZnO is the chemical instability, making DSSCs with ZnO degrade fast [8, 10, 11].

An simple way of making ZnO is electrodeposition. It is a low temperature synthesis based on the reduction of nitrate ions in an aqueous solution of zinc nitrate. However, the preceding project work found that electrodes made by electrodeposition were unable to produce a photocurrent [12]. The reason was suggested to be too dense films. However, there are many aspects to the synthesis that could be changed to optimize the deposition of ZnO. One such aspect is the addition of dye molecules into the zinc nitrate solution [13].

Aim of this work

The main goal of this master's thesis was to make dye-sensitized solar cells with zinc oxide as the semiconducting material. Preferably, the ZnO should be made at a low temperature. The main goal can be divided into the three following objectives.

The first objective was to improve the electrodeposition of zinc oxide onto a conductive substrate from a zinc nitrate solution. Different aspects of the synthesis were investigated. Three different electrochemical techniques were compared: potentiodynamic, galvanostatic and potentiostatic. The results of electrodeposition with and without eosin Y in the zinc nitrate solution were investigated, along with the effect of light exposure during the electrodeposition. In addition, the effect of temperature and zinc nitrate concentration were examined.

The second objective was to investigate the degradation of ZnO-electrodes, and the effect of acidic anchoring groups. This was done by comparing the performance of two electrodes sensitized with different dyes, namely eosin Y and N719.

The third objective was to see if a thin protective layer of titanium dioxide on top of the zinc oxide would improve the lifetime of ZnO-electrodes sensitized with N719.

Chapter 2

Theory

2.1 Solar energy

Solar cells are devices that can convert solar energy into electrical energy. This is possible by the photovoltaic effect. Photons from the sun excites electrons in the solar cell material and the electrons are forced, by the asymmetric nature of the cell, through a circuit to do work [14]. The leading technology within the field of solar cells uses the semiconductor silicon as the solar cell material [15].

The sun emits photons of a wide range of wavelengths. A photon is a *packet* of energy that travels as a wave [14]. Its wavelength (λ) and energy (E) are related according to the relation

$$E = \frac{hc}{\lambda}, \quad (2.1)$$

where h is Planck's constant and c is the speed of light. From this relation it is obvious that photons with shorter wavelengths have more energy than photons with long wavelengths. The spectrum of wavelengths emitted from the sun is close to the spectrum from a black body of temperature 5760 K [14]. This is, however, outside the atmosphere surrounding the Earth. When the photons travel through the atmosphere, some wavelengths are absorbed by gas molecules such as water and carbon dioxide. To account for this, the a factor called "*air mass*" is used. Air mass accounts for the amount of air the photons have had to travel through in order to reach the Earth's surface. In literature a reference spectrum called air mass 1.5 or AM1.5 is used. It is defined to have an total irradiance of 1000 W m^{-2} at the surface of the Earth. The AM 1.5 spectrum is plotted in Figure 2.1. The total irradiance is the integral over all wavelengths.

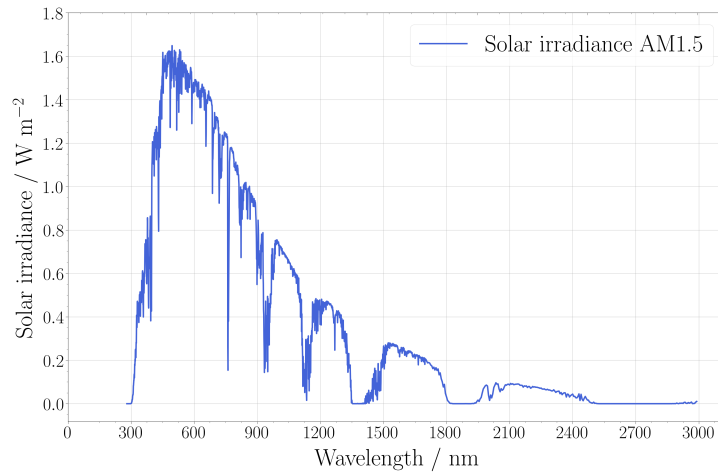


Figure 2.1: The standard AM 1.5 solar spectrum [16].

2.2 Semiconductors

All solar cells are based on semiconductor technology. A semiconductor is a material that has an excited state which is separated from its ground state by a band gap [14]. These states are normally referred to as the conduction band and the valence band, respectively. The band gap is an energy range where there are no states for charge carriers, and usually spans about 1-3 eV [17]. This is much larger than the thermal energy ($k_B T$), while comparable to the energy of photons irradiated by the sun. Incident photons can excite electrons across the band gap [14]. The differences in energy band gaps of metals, semiconductors and insulators are illustrated in Figure 2.2.

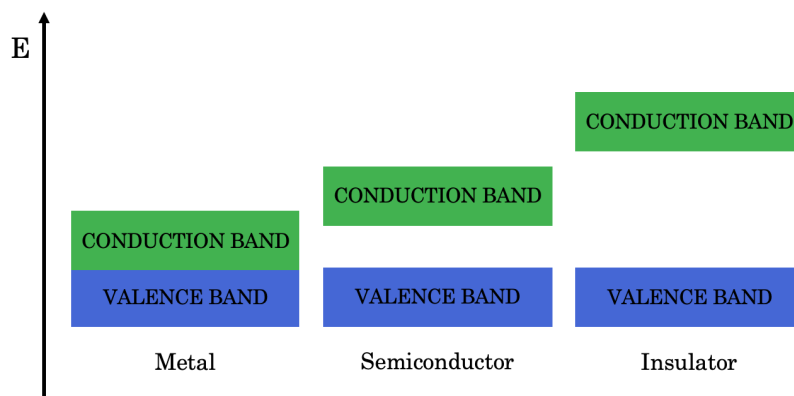


Figure 2.2: Illustration of the band gap in metals, semiconductors and insulators [17].

The charge carriers in a semiconductor are electrons and holes. A hole is the absence of an electron in the valence band. If the conduction band has the same amount electrons as the valence band has holes, the semiconductor is said to be intrinsic [18]. In reality, semiconductors are extrinsic, meaning that either electrons or holes dominate as the majority charge carrier. For ZnO, the majority charge carriers are electrons, and it is therefore referred to as an n-type semiconductor [18].

The density of states for electrons is a function describing the density of available states for electrons to occupy at a given energy level [17]. In the band gap the density of states is zero. The probability of an electron filling a state at a given energy is described by the Fermi-Dirac distribution. The Fermi level is defined as the energy where the Fermi-Dirac distribution yields $\frac{1}{2}$. For semiconductors the Fermi level is, by definition, situated in the band gap.

When a semiconductor is used as an electrode in an electrochemical cell, the interface between the electrolyte and the semiconductor becomes of special interest [8]. At equilibrium, the Fermi level of the semiconductor will align with the redox-potential in the electrolyte [18]. This causes bending of the energy bands in the semiconductor, creating a space charge region near the surface in the semiconductor [8, 18, 19]. This is illustrated in the top situation in Figure 2.3. The space charge region in the conduction band is depleted of electrons. This is due to the fact that electrons seek lower energies. When a bias is applied, the bands will bend even further, but the energy at the surface cannot move. The situation is illustrated in the middle illustration of Figure 2.3. The edge of the band gap is pinned, but can be changed through surface adsorption. The bottom illustration in Figure 2.3 is when a bias is applied so that the bands are flat, with no space charge region, this is referred to as the flatband potential of the semiconductor [19].

Electron transfer at an semiconductor/electrolyte interface is described by the Gerischer model, which is derived in detail by Memming [18]. For an electron transfer to happen, the conduction band of the semiconductor must align with the density of states in the electrolyte [18]. The electron transfer happens by tunneling, and the electron travels "horizontally" on the energy scale. In an electron transfer from the conduction band to the electrolyte, the edge of the conduction band has to align with the empty states of the electrolyte. When the electron transfer is the other way, the edge of the conduction band has to be aligned to the filled states in the electrolyte.

Many of the properties of a semiconductor is derived from the periodicity of the semiconductor crystal lattice, however, at the surface, the periodicity is broken [18]. This introduces surface defects, creating intermediate energy states at the interface. These states can be filled with electrons and reduce the electron transport in the cell [8]. Intermediate states can also be created at the grain-boundaries in the cell, and are often

referred to as trap states. These states can be positioned in the band gap. Depending on where in the band gap they are situated, they either contribute to electron transport through a process called hopping, or to recombination.

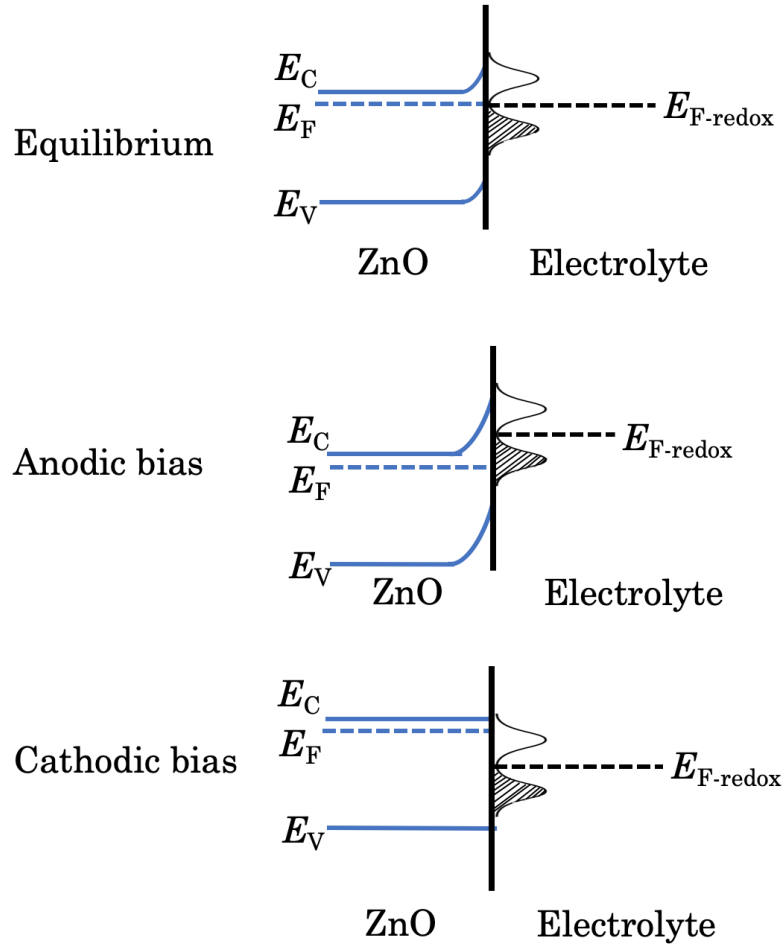


Figure 2.3: Illustration of the position and bending of the energy bands in ZnO at equilibrium (top), anodic bias (middle), and cathodic bias (bottom). The bell-curves on the electrolyte side represent the density of states in the electrolyte. The shaded area represent the filled states and the corresponding white area is the empty states. The vertical axis in the figure is energy, and the horizontal axis is position. The figure is based on a figure by Memming [18].

2.3 Sensitizing dyes

In DSSCs, sensitizing dye-molecules are utilized to absorb photon energy. The dyes are organic molecules or metal-organic complexes able to absorb energy from the sun. The adsorption is similar to the process in a semiconductor, but instead of conduction band and valence band, the energy levels in the dye is often referred to as the lowest unoccupied molecular orbital (LUMO) and the highest occupied molecular orbital (HOMO).

A good sensitizing dye should be panchromatic [20]. This means that it should be able to absorb light of different wavelengths. These wavelengths should correspond well with the solar spectrum that reaches Earth [4]. Ideally, natural organic dyes should be used, as they are non-hazardous and cheap [5]. The dyes could either be harvested from plants abundantly grown in nature or synthesized in a lab. Nature has chosen chlorophyll as the sensitizer for all plants. It is therefore reasonable to think that chlorophyll should be a good sensitizer for DSSC as well. This has, however, been shown not to be the case [21]. In fact, all natural dyes show rather poor efficiencies, with less than 1% conversion efficiency usually being reported [8, 22, 23]. Even with extremely low production cost, the power produced by the natural-dye-cells is not enough to compete with other solar cell technologies.

Two well studied, yet and different, dyes are N719 and eosin Y. Their chemical structures can be seen in Figure 2.4. N719 has carboxyl acid anchoring groups, while eosin Y does not have any anchoring groups. The price of them are also quite different. From a supplier such as Sigma-Aldrich, N719 costs 3720 NOK g⁻¹, while eosin Y costs 124 NOK g⁻¹.

N719 has an energy gap of 1.91 eV and the absorption peaks are located at 535 nm, 395 nm and 312 nm [24]. Though the light absorption of N719 fits well with the irradiation from the sun, there are, however, two problems with N719. First of all, it contains ruthenium which is an expensive metal. This drives the price of the solar units up [4]. Secondly, due to the two carboxyl acid anchoring groups, it will corrode electrodes of ZnO [8].

Eosin yellowish (eosin Y), is a xanthene dye and has its absorption peak at 517 nm, in the green range of visible light [25]. In ethanol, eosin Y absorbs light ranging from 450 nm to 575 nm [26], which is narrower than N719. The energy gap of eosin Y is about 2.2 eV [27].

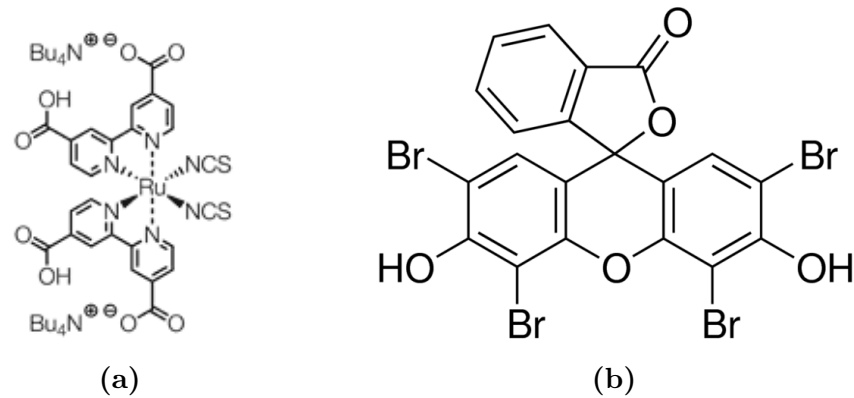


Figure 2.4: Chemical structures of (a) N719 [24] and (b) eosin Y [28].

2.4 Dye-sensitized solar cells

2.4.1 Basic principles

There are three main parts to a DSSC: a wide-band gap semiconductor, a light absorbing dye and an electrolyte [8]. These are assembled between two transparent and conductive substrates. Usually, glass slides coated with fluorine-doped tin oxide (FTO) are used. It is only the coating which is conductive, meaning that the conductivity of the substrates is a property of the surface and not the bulk. There is also a counter electrode, often platinum, and electrical contacts to connect the cell to an outer circuit. A schematic of a cell is presented in Figure 2.5

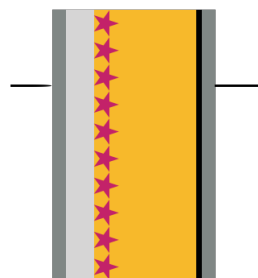
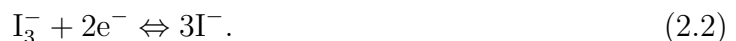


Figure 2.5: Schematic of a dye-sensitized solar cell. The stars represent dye-molecules, the yellow is the electrolyte, the light gray area is ZnO, the dark grey is FTO and the black is the platinum counter electrode.

The overall principle of a DSSC is the same as for Si-cells. A photon excites an

electron, which creates a current that can be utilized to perform work. This, however, is where the comparison ends. While the semiconductor absorbs the photons in a Si-cell, the dye performs this part in a DSSC [14, 5]. The band-gap of the semiconductor in the DSSC is about 3 eV, which is too wide to absorb most of the photons emitted from the sun, the energy gap of the dye is better suited for the task [29]. Together, the dye and the semiconductor do the same job as the asymmetric silicon-semiconductor in a Si-cell. The dye generates photoelectrons and the semiconductor keeps the charges separated and transports them to the FTO where they can enter the outer circuit. The driving force for the charge transport is a concentration gradient of electrons in the semiconductor resulting in diffusion of electrons. [8, 30]. When the electrons reach the counter electrode, they reduce a redox-pair in the electrolyte. This reduced species then travels to the dye/electrolyte interface and regenerates the dye, completing the circuit. A common redox-pair is I_3^-/I^- , which is reduced and oxidized by the reaction



The semiconductor in a DSSC is a porous metal oxide thin film [8]. Titanium dioxide (TiO_2) is the most common material, but ZnO is also widely researched. Only dye molecules in contact with the semiconductor will be able to transfer excited electrons and contribute to the photocurrent, meaning that more adsorbed dye will generate more current [9]. The semiconductor should therefore have a large surface area, where the dye can adsorb.

A large surface area can be obtained by manufacturing nanomaterials. Nanomaterials are materials with at least one dimension in the range between 1 nm and about 100 nm, and their small size give them a large surface-to-volume ratio [31]. As illustrated in Figure 2.6, making the electrodes out of nanomaterials result in a large surface area relative to the material used.

Less material also gives a more directional path for the electrons to travel in [9]. This is desirable, as it will reduce the transport time, and thus lower the probability of recombination in the cell. From the aspect of fast electron transport alone, nanorods are the best structures to use, as they allow the electrons to move in only one dimension. However, the rods have a small surface area for the dye to adsorb onto. According to Vittal *et al.* [9], the ideal structure to use in DSSCs is two-dimensional nanosheets which have large surface areas and only allow the electrons to travel in the plane, limiting the electron movement to two dimensions.

The dye molecules should be attached to the semiconductor surface with an anchoring group creating a covalent bond [5, 32, 33, 34]. This will make the dye-molecules stay at the surface and not diffuse into the electrolyte solution. In addition, the anchoring groups

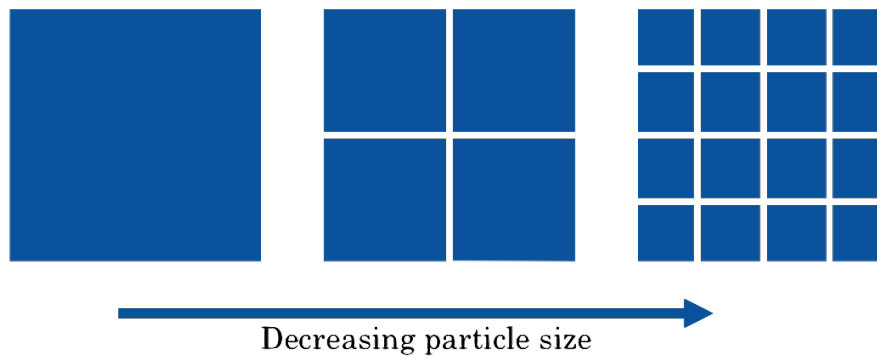


Figure 2.6: Visualization of how nanomaterials have larger surface area than bulk materials with the same volume.

provide a good connection for the electrons to transfer from the dye to the semiconductor. A well known anchoring group is the carboxylic acid group. The carboxylic acid's interaction with anatase TiO_2 is probably the most widely researched anchoring, as the combination has resulted in highly-efficient DSSCs [33]. However, the knowledge about this interaction might not be transferable to other surface-anchor pairs. O'Rourke and Bowler [33] found that the anchors do not work equally well with all surface structures.

ZnO is a material which in some ways are fairly similar to anatase TiO_2 [8]. The band gap is approximately the same width and the edge of the conduction band is located at about the same energy level [18]. This means, that from an energy-level point of view, ZnO and TiO_2 should behave similarly. Advantages of ZnO over TiO_2 include faster electron transport, more light scattering and simple manufacture [20]. ZnO grows anisotropically, allowing many different morphologies to assemble, including flowers, stars, rods and sheets, even at low temperatures [9, 35].

A huge limitation of ZnO is its chemical instability [8]. Due to the high isoelectric point of approximately 9, ZnO dissolves very easily [20]. Both acidic and basic media will dissolve ZnO [8]. This makes acidic anchoring groups a bad match with ZnO. The acid will dissolve ZnO, and the resulting Zn^{2+} -ions will form complexes with N719 and become insoluble precipitates that clog the pores and lower the efficiency of the cell [10]. TiO_2 has an isoelectric point of about 6, which makes it more stable [20].

The positioning of the energy levels of the different components in the cell is essential. Since ZnO is an n-type semiconductor, the following description will be for such. The energy bands of the dye must be positioned around the conduction band of the semiconductor. This is illustrated in Figure 2.7. The LUMO-level of the dye should be over the conduction band in the semiconductor and the HOMO-level should lay under [8]. That way, when an electron is excited from the HOMO-level to the LUMO-level of the dye,

it can be transferred to the energetically favorable semiconductor conduction band. The electrons will then move through the semiconductor and into the outer circuit.

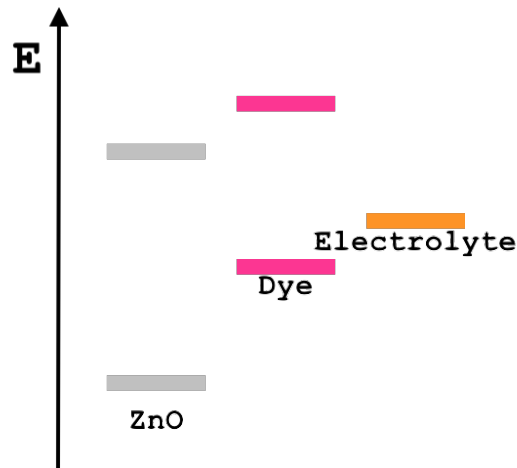


Figure 2.7: Illustration of the energy levels in dye sensitized solar cells.

2.4.2 Efficiency loss

There are four main loss mechanisms: transmission loss, thermalization loss, recombination loss and loss due to resistance in cell [36, 8]. Transmission loss is loss due to photons not having enough energy to excite electrons. Thermalization loss, on the other hand, is due to photons having too much energy, exciting the electrons higher than the energy gap. The dye can only fully utilize the energy of photons with energy equal to its HOMO-LUMO energy gap. This is also true for the band gap of the semiconductor. The only way to minimize these two types of losses, it is to choose a panchromatic dye, able to absorb light of many wavelengths. Recombination loss is loss due to electrons recombining with holes in the cell before reaching the outer circuits. These lost electrons do not contribute to the photocurrent and the conversion efficiency of the cell decreases. Recombination can happen in several places in the cell. The electrons can recombine before leaving the dye, which can be prevented by good connection between the dye and the semiconductor. Furthermore, the electron can fall down to the valence band, intermediate surface states or be lost by reducing the electrolyte. ZnO is supposed to be suitable to limit this type of mechanism, as it has an electron transport which is 10 times faster than TiO_2 . The resistance in the cell arise from diffusion of the ionic-species in the electrolyte, losses at the

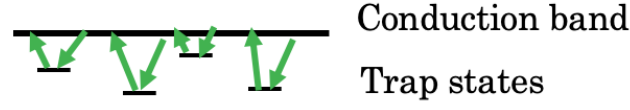


Figure 2.8: Illustration of the movement of electrons by hopping in ZnO [38]. The lines illustrates energy levels in the semiconductor as a function of space.

counter electrode, transport resistance in the ZnO and a series resistance in the circuitry. According to Sharma *et al.* [5], the process of dye-regeneration generates a lot of loss. The resistances will be discussed further in Chapter 2.5.3.

Transport resistance is the resistance the electrons experience as it travels through the metal oxide-electrode [37]. The electron transport in the cell is according to Hagfeldt under debate [8], although an accepted theory is hopping between trap states and the conduction band in the semiconductor, as illustrated in Figure 2.8, or by diffusion in a single state [38]. Trap states are therefore good for conduction by hopping, but bad for conduction by diffusion, where trap states will limit the transport.

2.4.3 Efficiency calculations

The losses in the cell will affect its performance. How well a solar cell performs is usually reported in term of its conversion efficiency (η), which is the ratio between the power density of the solar irradiance (P_{in}) and the power density produced in the cell (P_{out}),

$$\eta = \frac{P_{out}}{P_{in}}. \quad (2.3)$$

The power density produced in the cell can be found through the product of the potential (V) and current density (J) produced in the cell [14],

$$P = VJ. \quad (2.4)$$

The highest potential is obtained when the cell is in open circuit condition. This voltage is called the open circuit voltage (V_{oc}). At the V_{oc} , no current is flowing through the cell. This potential is related to the difference in energy between the semiconductor's Fermi level and the redoxpotential of the electrolyte [5]. The maximum current density is called the short circuit current density (J_{sc}) and is the current when the potential is zero. The maximum power density is somewhere in between these two extremes, and is called the maximum power point (P_{max}), with corresponding potential, V_{max} , and current density,

J_{sc} . It is desirable for V_{max} and J_{max} to be as close to V_{oc} and J_{sc} as possible. How close they are has been termed fill factor (FF), given by

$$FF = \frac{J_{max}V_{max}}{J_{sc}V_{oc}}. \quad (2.5)$$

Combining equations 2.4 and 2.5 with Equation 2.3 gives the maximum conversion efficiency (η_{max}),

$$\eta_{max} = \frac{P_{max}}{P_{in}} = \frac{V_{oc}J_{sc}FF}{P_{in}}. \quad (2.6)$$

Note that the current density is the current per unit area, and is convenient to use when comparing cells of different sizes. In this work, it is the total current produced that will be discussed, due to circumstances that will be described in Chapter 2.5.1. The same relationships hold for the current as for the current density, except that it will be the total power and not the power density that will be calculated.

2.5 Characterization

2.5.1 Characterization cell

The Zahner photoelectrochemical cell (PECC-2), which is imaged in Figure 2.9, is a cell to easily characterize DSSC-photoanodes. The photoanode is mounted onto the designated area and the cell is then filled with electrolyte. The benefit of using this cell is that the only aspect that changes from experiment to experiment is the sample itself. This eliminates variability in the assembly of the cell.

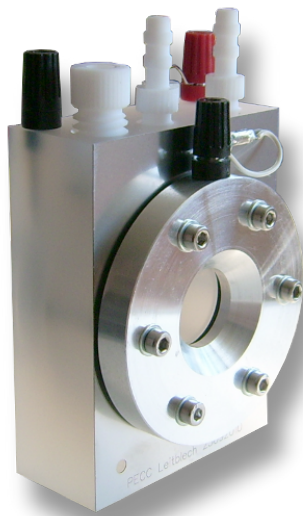


Figure 2.9: A PECC-2 cell used to characterize photoelectrodes [39].

The cells allow square samples up to a size of 3 cm x 3 cm, however not all of the sample is exposed to the electrolyte and the light source. A circular area of 3.1 cm², enclosed by an rubber o-ring, is exposed to the electrolyte. The circular opening exposing the working electrode to the light has an area of 2.5 cm².

The light source illuminates an area of 1 cm², but it is not unlikely that a greater area was effectively illuminated during the testing, as the light spreads. In retrospective, the samples should have been covered with tape or such, to expose only an area of 1 cm² or smaller to the light, to be able to get a correct value for the current density generated in the cell. This was, however, not realized until after several samples were already tested. The photoelectrochemical characterization in the PECC-2 is destructive and old samples cannot be re-characterized. The value of comparability between samples was therefore weighted to be more valuable than comparability to literature. The values presented within this thesis are comparable, as the distance from the light source to the cell was equal each time. For future characterization, the cell area should be smaller than the light beam to avoid this problem.

2.5.2 Current-voltage curves and quantum efficiency

The current, voltage and fill factor of a solar cell is usually presented in an current-voltage curve (IV-curve). A typical IV-curve of ZnO-cells is presented in Figure 2.10a. In this plot it is can be seen why the fill factor is often referred to as the "*squareness*" of the IV curve, as a curve of fill factor 1 would be a rectangle. An IV-measurement is performed illuminating the cell, while sweeping the potential over the cell from the open circuit voltage to 0 V and measuring the corresponding current. An ideal cell would maintain the same current for all potential up until the open circuit voltage where the current would be 0 A, giving a fill factor close to 1. The best ZnO cells in literature typically have fill factors around 0.6 [20].

A cell with a high FF is said to have a diode behavior, in analogy to the current-voltage characteristic of a diode. A bad cell, with a low FF, will have an Ohmic behavior, like a normal resistor following Ohm's law. The relationship between the current and the voltage would then be linear.

The standard test conditions for solar cells are at a temperature of 25 °C and the AM1.5 solar spectrum [14]. These conditions are used to compare results between publications. It is also possible to measure the IV-curves at a single wavelength. For dye sensitized solar cells this can be beneficial as the semiconductor will contribute some to the photocurrent by absorption of photons in the UV-range. By choosing a wavelength only the dye can absorb, the performance of only the dye can be evaluated. To find wavelengths where the dye performs well, incident photon-to-electron conversion efficiency (IPCE) measurements

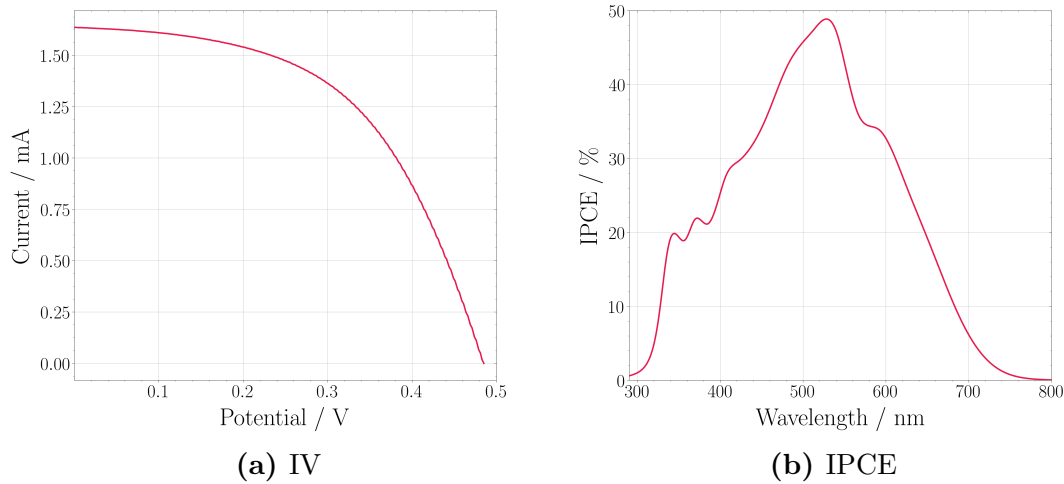


Figure 2.10: A typical (a) IV-curve and (b) IPCE-spectrum of ZnO-DSSC in this work. The fill factor of the IV-curve is 0.545.

are performed.

IPCE is a measurement to assess the quantum efficiency of the solar cell [14]. The measurement gives insight into how much of the solar energy is converted into electrical energy through photons exciting electrons. The quantum efficiency is measured as a function of the wavelength or energy of the incident light. The quantum efficiency of a cell is independent of the intensity of the incident light [14]. IPCE measurements are presented as wavelength versus IPCE in percent or AW^{-1} , and an IPCE spectrum of a cell made by the author is presented in Figure 2.10b. Several peaks can be observed in the plot. At short wavelengths, peaks corresponding to adsorption in the semiconductor and substrate material can be observed, these are the two peaks below 400 nm. Peaks at longer wavelengths are due to adsorption in the dye-molecules. These two areas will be referred to the ZnO-region (<400 nm) and the dye-region (>400 nm). Note that the dye N719 also absorbs light in the ZnO-region [24]. The total quantum efficiency of a cell can be found by integrating the IPCE-spectrum with regards to the wavelength, and can be useful when evaluating the change in performance of a cell.

The IPCE measurements are performed under open circuit conditions. The quantum efficiency of the cell can therefore be related to the short circuit current through

$$I_{\text{sc}} = \frac{Aq}{hc} \int \Theta(\lambda) IPCE(\lambda) d\lambda. \quad (2.7)$$

Here A is the area of the cell, q is the electron charge, $\Theta(\lambda)$ is the photon flux and $IPCE(\lambda)$ is the quantum efficiency as a function of wavelength (λ) [30]. If the experimental short circuit current is equal the calculated short circuit current, the collection efficiency in the

cell is good [30]. The collection efficiency is the solar cell's ability to collect generated photo-electrons. A high collection efficiency suggests that the current is independent of the recombination in the cell. This is an assumption made when modeling the resistances in the cell.

2.5.3 Electrochemical impedance spectroscopy

In a DSSC, the charge transport is affected by interfaces and mass transport within the cell. Each part of the cell gives rise to a type of resistance, and since the recombination is dependent on the voltage in the cell, it will affect the shape of the IV-curve. Both the fill factor and the open circuit voltage is dependent on the recombination of electrons [30]. To evaluate the resistance in the cell, electrochemical impedance spectroscopy (EIS) is used. This technique separates the contributions of different components or aspects in the cell.

In a resistive circuit, the voltage (V) is proportional to the current (I), with the resistance of the circuit (R) being the factor of proportionality [40]. This relationship is the well known Ohm's law:

$$V = IR. \quad (2.8)$$

The resistance is a magnitude, measured in Ohms. In circuits with reactive components, such as capacitors, the relationship is dependent on both the magnitude and the phase of the current. To describe this the impedance (Z) of the circuit must be evaluated. The impedance relates the current and the voltage in the same way as the resistance

$$V = IZ, \quad (2.9)$$

but the impedance is complex and changes with frequency. The frequency dependency is the base of EIS [41]. The impedance of a resistive component does not have an imaginary part.

EIS is a technique to evaluate the solar cell's performance at certain points along the IV-curve of the solar cell [41]. The solar cell is illuminated and a DC-potential is applied in addition to a small, oscillating AC-potential while the current response is recorded. These measurements are performed at different frequencies (f), giving information about the frequency dependence of the impedance. The results are usually plotted as either Bode-plots or complex impedance plots, with a magnitude ($|Z|$) and complex phase angle (ϕ). By doing EIS, the contributions for each element in the cell can be evaluated individually [41]. The data is fitted to an equivalent circuit to evaluate each component [37]. The processes inside a DSSC can be described by the equivalent circuit in Figure 2.11. There are five main features to the circuit: The series resistance (R_s) in the contacts,

the transport resistance in the ZnO, the interface between the ZnO and the electrolyte is modeled as a series of parallel circuits of a resistor (r_{rec}) and a capacitor (c_{μ}), there is an impedance element raising from the diffusion of ions in the electrolyte (Z_{D}) and finally the interface between the electrolyte and the counter electrode is also modelled as a resistor (R_{RC}) and a capacitor (C_{RC}) in parallel.

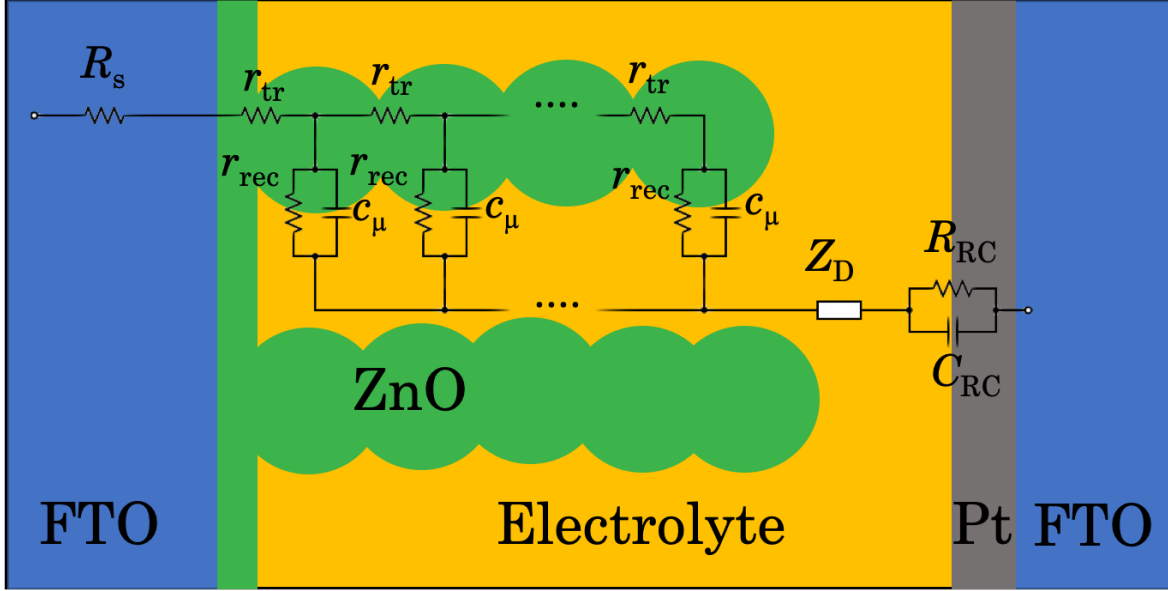


Figure 2.11: Equivalent circuit of a DSSC.

The total impedance (Z_{tot}) in the cell can be described as the sum of the series resistance (R_s), the impedance at the counter electrode (Z_{RC}), the impedance related to the diffusion of ions in the electrolyte (Z_{D}), and the transmission line impedance (Z_t),

$$Z_{\text{tot}} = R_s + Z_{\text{RC}} + Z_{\text{D}} + Z_t. \quad (2.10)$$

The series resistance does not have a complex component and a large R_s will give an Ohmic behavior at large potentials [14]. The impedance at the counter electrode is given by

$$Z_{\text{RC}} = \frac{1}{\frac{1}{R_{\text{RC}}} + \frac{j\omega}{R_{\text{RC}}\omega_{\text{RC}}}}, \quad (2.11)$$

where R_{RC} is the resistance across the interface at the counter electrode, and ω_{RC} is

$$\omega_{\text{RC}} = \frac{1}{R_{\text{RC}}C_{\text{RC}}}, \quad (2.12)$$

where C_{RC} is the capacitance at the same interface. The impedance from diffusion is

given by

$$Z_D = R_D \frac{\tanh[(j\omega/\omega_D^p)^{1/2}]}{(j\omega/\omega_D^p)^{1/2}}, \quad (2.13)$$

where R_D is the diffusion resistance, ω_D^p is the characteristic frequency of diffusion [37]. And finally, the transmission line impedance is given by

$$Z_t = \left(\frac{R_{tr}R_{rec}}{1 + j\omega/\omega_{rec}}\right)^{1/2} \coth\left[\left(\frac{R_{tr}}{R_{rec}}\right)^{1/2}\left(1 + \frac{j\omega}{\omega_{rec}}\right)^{1/2}\right], \quad (2.14)$$

where R_{tr} is the total transport resistance in the semiconductor, R_{rec} is the recombination resistance at the surface of the semiconductor, ω_{rec} is the radian frequency of the charge transfer process.

For a more detailed description of the model concerning the processes inside the cell, please refer to Fabregat-Santiago *et al.* [37] and the project work of Erring Hansen [42].

2.5.4 Time constants

Intensity-modulated photocurrent spectroscopy (IMPS) and intensity-modulated photovoltage spectroscopy (IMVS) are techniques to gain knowledge about the time constants of recombination and transport in the cell [43]. In both techniques, the cell is illuminated by a constant light intensity superpositioned with a small oscillation of light on top. The frequency of the oscillation is changed to gain the frequency dependence of the photocurrent and the photovoltage.

IMPS measures the response in the current, when the potential set to 0 V, and IMVS measures the response in the potential, when the current is set to 0 A. Therefore, IMPS gives information about the performance near the short circuit current, and IMVS gives information near the open circuit voltage.

Figure B.5 shows plots of IMPS- and IMVS-measurement. The minimum of the curve (f_{IMVS}) is related to the recombination time (τ_{rec}) in the cell through

$$\tau_{rec} = \frac{1}{2\pi f_{IMVS}}. \quad (2.15)$$

Similarly, the frequency of the minimum of the IMPS-curve (f_{IMPS}) is related to the transport time (τ_{tr})

$$\tau_{tr} = \frac{1}{2\pi f_{IMPS}}. \quad (2.16)$$

The recombination time should be long, meaning the recombination resistance is large, and the transport time should be short, meaning the transport resistance is low. The transport

time should at least be shorter than the recombination time, if not most electrons would not reach the outer circuit.

2.5.5 Recombination modeling in Python

If EIS is measured at different potentials close to the open circuit potential, the theory described in Chapter 2.5.3 can be utilized to find the resistances in the cell, and from that, recreate the IV-curve of the cell. When resistance found at each potential is plotted on a log scale, they should form a linear line. The slope and intercept of the line is used to fit the IV-curve. If the IV-curve can be recreated from the EIS-data, the results of both techniques are strengthened. It is also possible to evaluate the performance of only the ZnO and the dye-molecules by subtracting the resistance contributions of the other parts of the cell. This will reveal if it is processes in the ZnO and dye or the rest of the cell that causes poor performances.

This modeling is based on the theories of Fabregat-Santiago [37] and the coding is based on the project work of Erring Hansen [42]. The codes used can be found in Appendix C.

The model employs a method of complex least squares described by Orazem and Tribollet to find the optimal parameters (\mathbf{P}) that fit the data [44]. The objective function used is

$$S(\mathbf{P}) = \sum_{k=1}^N \frac{(Z_{\text{re}}(\omega_k) - \hat{Z}_{\text{re}}(\omega_k|\mathbf{P}))^2}{\sigma_{\text{re},k}^2} + \sum_{k=1}^N \frac{(Z_{\text{im}}(\omega_k) - \hat{Z}_{\text{im}}(\omega_k|\mathbf{P}))^2}{\sigma_{\text{im},k}^2}, \quad (2.17)$$

where $S(\mathbf{P})$ is the sum of least squares, N is the number of data points recorded, ω_k is the angular frequency of the measurements, $Z_{\text{re}}(\omega_k)$ is the real part of the experimental impedance, $Z_{\text{im}}(\omega_k)$ is the imaginary part of the experimental impedance, $\hat{Z}_{\text{re}}(\omega_k|\mathbf{P})$ is the real impedance calculated from the model, $\hat{Z}_{\text{im}}(\omega_k|\mathbf{P})$ is the imaginary part of the impedance calculated from the model, $\sigma_{\text{re},k}^2$ and $\sigma_{\text{im},k}^2$ are the variance in the measurements. In this modeling they are both set to 1. The parameters (\mathbf{P}) that the model tries to optimize are related to the theory described in Chapter 2.5.3:

- R_s
- $\sqrt{R_{\text{rec}}R_{\text{tr}}}$
- ω_{rec}
- ω_{tr}
- β (A constant related to the recombination in the cell)
- R_{RC}

- ω_{RC}
- R_D

In this modelling, the "scipy.optimize.least_squares()" function is utilized with the Levenberg–Marquardt algorithm. An initial guess on the parameters in \mathbf{P} must be supplied. The Levenberg–Marquardt algorithm is also described by Orazem and Tribollet [44].

2.5.6 Profilometer

A profilometer measures the thickness of a sample by running a stylus over the sample and measuring the vertical deflection as a function of one horizontal position. It is a quick and simple method that gives a two-dimensional picture of the thickness. A limitation, however, is that the profilometer does not measure the whole sample. There could be variations in some areas of the sample which will not be detected by the stylus. Yet, the profilometer does give an indication as to what the thickness of the sample is, and can therefore be used as an initial test to see which samples are worth investigating further.

2.5.7 Scanning electron microscopy

A scanning electron microscope (SEM) uses electrons instead of light to image samples. Since electrons have a shorter wavelength than light, it is possible to image objects that are smaller than the diffraction limit of light [45]. A beam of electrons, accelerated towards the sample by an applied voltage is scanned over the surface. When the electrons hit the surface they interact with the atoms in the material and secondary electrons and backscattered electrons are shot back from the sample. These can be detected to form an image of the sample. Secondary electrons give a view of the sample's morphology, while backscattered electrons may also give an elemental dimension to the image. In addition to the secondary and backscattered electrons, characteristic X-rays are also emitted from the sample. If these X-rays are measured and plotted as a function of energy, the elements present in the sample can be determined. Each element will emit X-rays of specific energies [46]. This technique is called Energy-dispersive X-ray spectroscopy (EDX).

2.5.8 X-ray diffraction

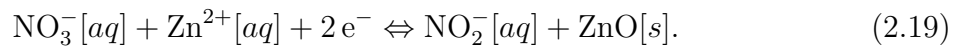
X-ray diffraction (XRD) is a method to study the crystal structure of a material [45]. It is based on reflection of X-rays from crystal planes in the material, based on Bragg's Law:

$$2d \sin \theta = n\lambda, \quad (2.18)$$

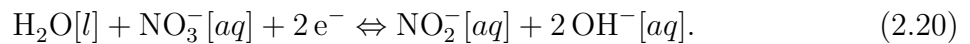
where d is the lattice plane spacing, θ is the incident angle, n is a positive integer and λ is the wavelength of the X-ray. The measurement scans over different angles and measures the intensity of the reflected X-rays. At angles that hit lattice planes in a way so that equation 2.18 holds, the intensity of the reflected X-rays will be much higher. The results are presented as plots of 2θ versus intensity. Characteristic peaks of the material will be present in the plot, and these peaks can be analyzed to evaluate the crystalline phases of the sample.

2.6 Electrodeposition

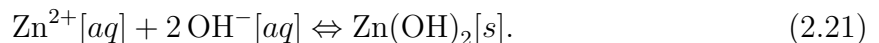
Electrodeposition is a simple manufacturing technique to deposit a material onto a conductive substrate. According to Yoshida *et al.* [47], the ZnO deposited is both porous and crystalline. For ZnO, a common way to perform electrodeposition is by cathodic reduction of nitrate ions from an aqueous solution of zinc nitrate ($\text{Zn}(\text{NO}_3)_2$) onto FTO-glass [48, 49, 50]. The total reaction of the electrodeposition is



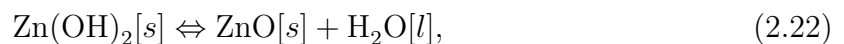
This total reaction is composed of three steps. At the working electrode the nitrate ions in the solution are reduced,



This reaction elevates the pH in the solution making Zn^{2+} react with the produced hydroxyl-groups forming $\text{Zn}(\text{OH})_2$ through



The $\text{Zn}(\text{OH})_2$ is spontaneously transformed into ZnO,



which precipitates onto the electrode surface. At room temperature the transformation of $\text{Zn}(\text{OH})_2$ to ZnO and water has a change in enthalpy (ΔH) of 3 kJ mol^{-1} and a change in entropy (ΔS) equal $33\text{ J K}^{-1}\text{ mol}$ [51, 52]. A positive enthalpy and entropy means that the reaction is spontaneous at elevated temperatures. The change in Gibbs free energy (ΔG) of a system is related to the entropy and the enthalpy

$$\Delta G = \Delta H - T\Delta S. \quad (2.23)$$

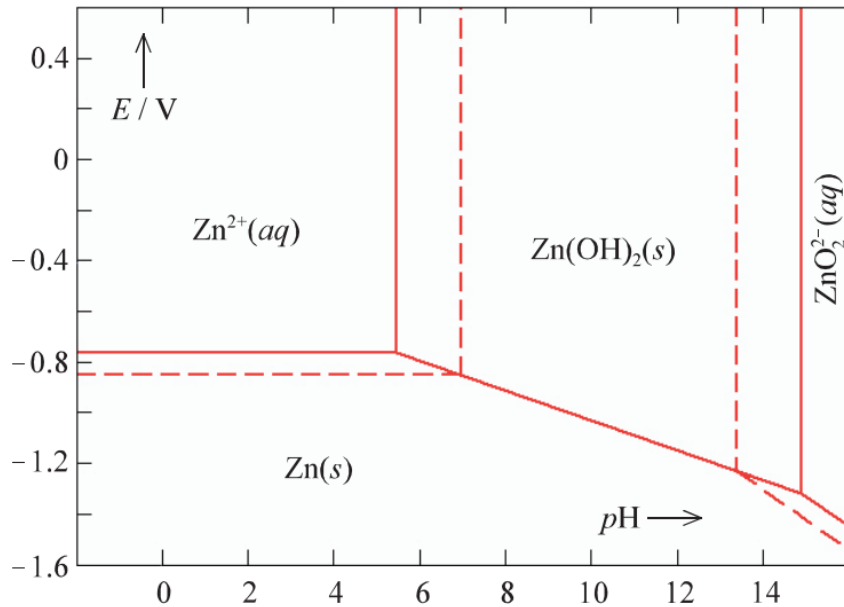
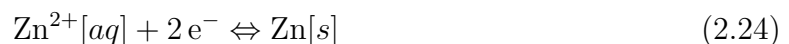


Figure 2.12: Pourbaix-diagram of zinc [19]. The dashed line is for an ionic activity of 10^{-3} , while the solid line is for an activity of 1.

At 40°C the change in Gibb's free energy of the reaction is equal to -4.33kJ mol^{-1} . A negative ΔG means it is a thermodynamically spontaneous reaction at 40°C .

The pH-dependency of the process is evident from the Pourbaix-diagram, displayed in Figure 2.12. A Pourbaix diagram, also known as a potential-pH diagram, is a diagram visualizing which state of an element is thermodynamically stable when the pH and potential changes [19]. The figure shows that above a potential of approximately -0.8 V, Zn^{2+} is the stable state below a pH of 5.5. Above, $Zn(OH)_2$ is stable. This supports that reaction 2.21 happens when the pH increases above 5.5 due to production of OH^- . According to Otani *et al.* [49], the pH at the working electrode is between 6 and 7 during the deposition, while the bulk pH is between 5 and 5.5. Otani *et al.* also showed how the pH at the electrode is dependent on the temperature of the zinc nitrate bath, with higher electrode pH at higher temperatures [49].

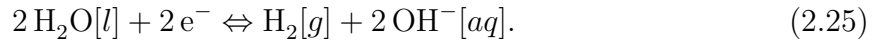
If the potential is too low (more negative), the reaction



might take place, depositing metallic zinc onto the electrode. From the Pourbaix diagram, this happens at all pH-levels.

Another reaction might also occur at the working electrode, namely the reduction of

water to hydrogen gas and hydroxyl-groups, according to



This reaction is beneficial for the production of porous ZnO films, as the film will grow around the H₂ bubbles at the electrode. However, too much gas bubbles will make it hard for the ZnO to deposit on the surface.

The electrodeposition of ZnO from a zinc nitrate bath will be referred to as the standard electrodeposition (SE).

Another way to promote porous growth is to introduce the dye eosin Y to the nitrate bath. This results in a hybrid dye/ZnO electrodeposition, where the ZnO is loaded with dye molecules during the deposition, manufacturing DSSC-anodes in one single step. Yoshida and coworkers have reported this synthesis and its mechanisms over several papers [53, 54, 13, 55]. Their proposed theory is that the dye adsorbs to the surface of the ZnO and inhibits growth in that area. This forces the ZnO to grow around the dye, creating a pore. The resulting ZnO films are colored pink. Yoshida and Minoura [13] reported that the method is sensitive to the magnitude of the applied potential. Applying a too low potential creates a film with dye molecules built into the ZnO, without being accessible from the outside. The electrodeposition with eosin Y in the nitrate bath will be referred to as hybrid electrodeposition (HE).

The HE-electrodes could be directly used in a solar cell, but this dye loading is not optimal. During HE, the dye molecules adsorb in multi-layers. Only the dye molecules directly in contact with both the ZnO and the electrolyte will be able to fully contribute to the photocurrent. For dyes not in contact with the ZnO, the electron transfer will be limited, and dye molecules not in contact with the electrolyte will not get regenerated. This leads to huge losses in the cell.

The solution to this problem is to remove the dye molecules deposited during the HE and then reload the electrode in a new dye solution [13]. During the reloading, the dye molecules will adsorb to the ZnO in a monolayer and the electrolyte will have access to all dye molecules. The dye removal can be done by soaking the electrodes in a bath of potassium hydroxide (KOH) at a pH of about 10.5. The process is illustrated in Figure 2.13. If the pores in the ZnO are interconnected, all the dye molecules can be removed. A pH of 10.5 will not dissolve the ZnO, as can be seen in the Pourbaix diagram in Figure 2.12. The KOH bath is therefore also a test to see if the electrodes are of good quality. The dye used in the reloading does not have to be eosin Y, it can be whatever dye that is desirable. However, it is beneficial to use eosin Y in the HE as it is cheap and non-hazardous [28].



Figure 2.13: Left: Eosin Y (stars) adsorbs in multilayers onto the ZnO during the hybrid electrodeposition. Middle: The eosin Y can be removed by KOH at a pH of 10.5, leaving bare ZnO. Right: Dye molecules re-adsorb in a monolayer.

In general, the electrodeposition of ZnO is thought to be limited by the charge transfer at the interface [54]. As the ZnO grows thicker, the current flowing to the solid/liquid interface will decrease, and the growth of ZnO will slow down.

It is possible to use other solutions than $\text{Zn}(\text{NO}_3)_2$ to electrodeposit ZnO. Yoshida *et al.* [55] exchanged $\text{Zn}(\text{NO}_3)_2$ with ZnCl_2 . The mechanisms of ZnCl_2 will, however, not be discussed, as $\text{Zn}(\text{NO}_3)_2$ is the solution used in this work. Yoshida *et al.* found that films produced from electrodeposition in a $\text{Zn}(\text{NO}_3)_2$ bath were "[...]not homogeneous and poorly reproducible." [55] They applied the potential during the electrodeposition potentiostatically, meaning at constant potential.

Other electrochemical techniques for electrodeposition are galvanostatic and potentiodynamic. In the galvanostatic technique, a constant current is applied. In potentiodynamic application, the potential is cycled between two set vertex potentials a certain amount of times at a set sweeping rate. It was the potentiodynamic technique that was used in the preceding project work [12].

2.7 Doctor blading

Doctor blading is a simple technique to apply a thin film of nanoparticles [56]. The nanoparticles are made into a paste with a solvent and a binding agent. This paste is deposited onto a substrate by sliding a tool over the surface. A glass rod or a squeegee blade can be used for this purpose. The substrate must be covered by tape to expose only the areas where the thin film is desired. The thickness of the tape affects the thickness of the thin film. The doctor blading method is visualized in Figure 2.14. After the film is deposited, it should first be dried to evaporate the solvent and then annealed to interconnect the particles.

The experience with doctor blading from the project work was that adhesion to the substrate can be a problem [12]. To solve this the method of depositing doctor blading layers on top of a standard electrodeposition film was developed. This improves adhesion,



Figure 2.14: Illustration of the doctor blading process.

and indications that the electrodeposited layer underneath acted as a light scattering layer in the cell were also observed.

This doctor blading method does not fulfill the desire of creating electrodes at low temperatures. It is, however, an easy method to create well performing DSSC-photoanodes with ZnO that can be used as a reference for other ZnO-electrodes.

2.8 Atomic Layer Deposition

Atomic layer deposition (ALD) is a method of depositing layers of material with atomic precision [57]. It is a vapor phase method which can deposit monolayers of the desired material, made possible by the self-limiting growth of the precursor. The deposition of metal-oxides happens in two steps: The surface is first chemically activated with water, hydroxylating the surface, secondly, the metal precursor reacts with the hydroxyl-groups and forms the desired metal-oxide, in this case titanium dioxide. The reaction chamber is purged alternating between water and metal precursor. Since the metal-precursor only reacts with the hydroxyl-groups that are attached to the surface, only one layer of TiO₂ can form per purging of precursor and water. The byproducts of the reaction are removed from the reaction chamber by N₂-gas.

Chapter 3

Experimental

The materials and chemicals used are listed in Appendix A.

3.1 Electrode manufacture

The process of making DSSCs photoanodes was performed as follows:

1. Prepare the FTO for deposition of ZnO
2. Deposit ZnO into the surface of FTO. In this work this was done by electrodeposition or doctor blading.
3. If the samples were made by hybrid electrodeposition the deposited "place holder" dye has to be removed.
4. The ZnO-film is loaded with dye molecules
5. The finished electrode is assembled in a PECC-2 cell and the cell is filled with electrolyte.

An electrode holder was designed and 3D-printed to support the electrodes during the electrodeposition. The distance between to working electrode and the counter electrode placements was 3.5 cm. The reference electrode was placed in the middle between the two. The electrode stand was printed in PLA-plastic with an Ultimaker 2+ 3D-printer. The model and the printed holder are shown in Figure 3.1.

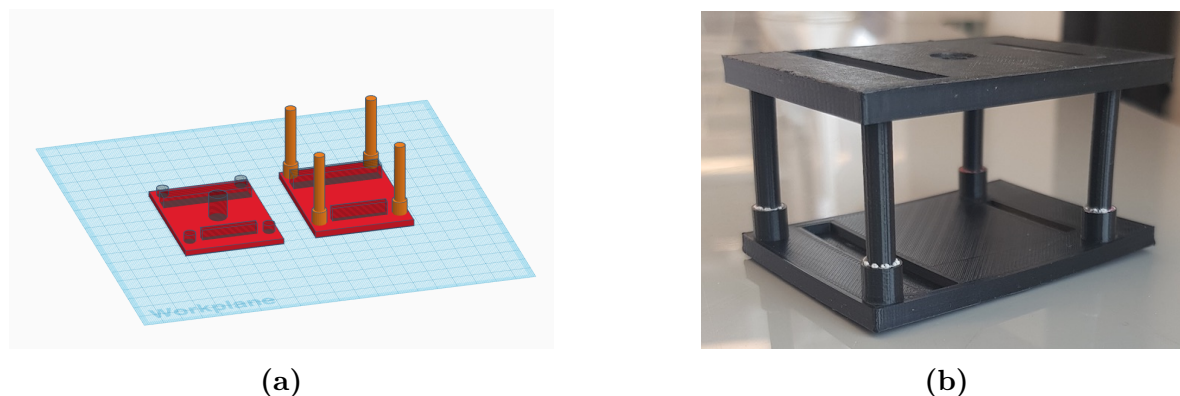


Figure 3.1: 3D-model (a) and image (b) of the electrode holder. It was designed to keep the distance between the electrodes equal for all experiments.

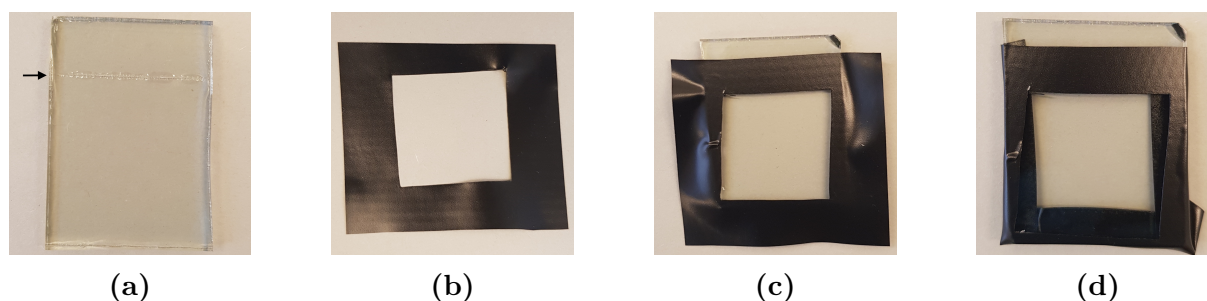
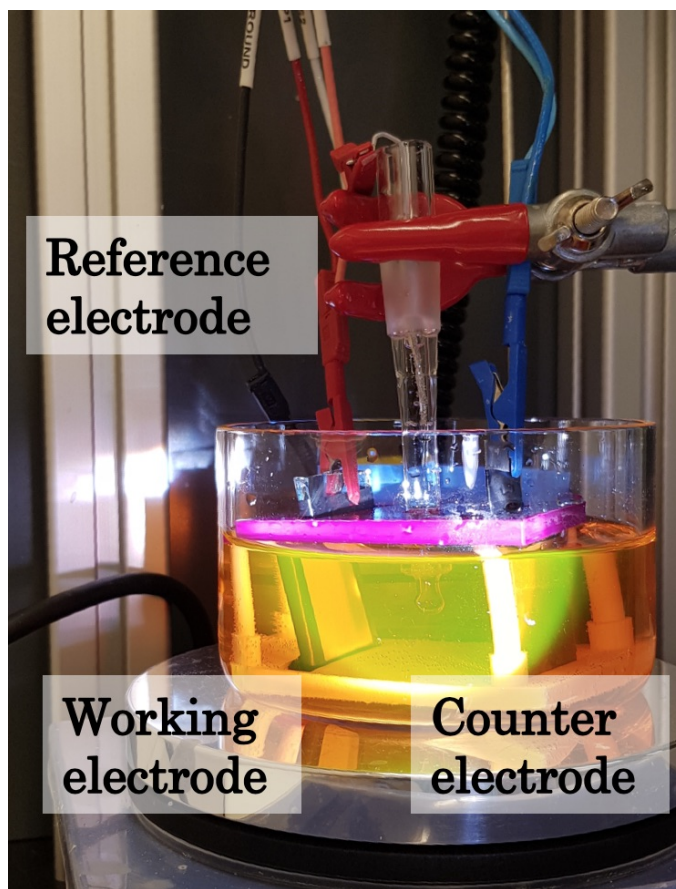


Figure 3.2: Preparation of FTO sample. (a) FTO, (b) tape (c) tape covering sample, (d) fully prepared sample. Notice the cut in the FTO in Figure (a).

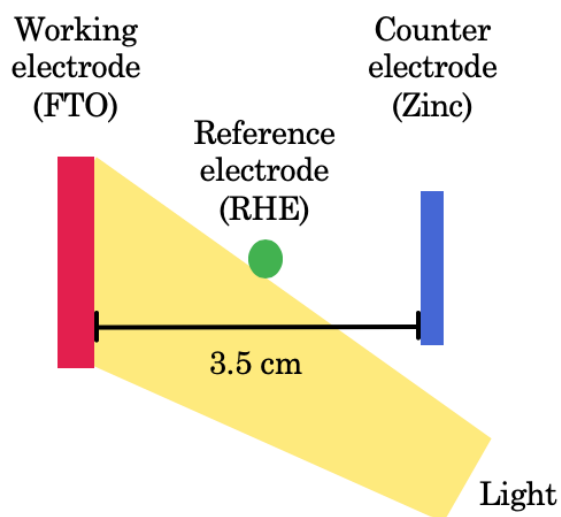
The electrodeposition of zinc oxide was based on the work done by Nayak [50], and Yoshida with coworkers [13, 55]. Three different electrodeposition methods were used. Standard electrodeposition (SE) is with only a $\text{Zn}(\text{NO}_3)_2$ -solution, hybrid electrodeposition (HE) is with eosin Y in the $\text{Zn}(\text{NO}_3)_2$ -solution, and photoassisted hybrid electrodeposition (PHE) is HE illuminated by a Science Tech 201 solar simulator.

Electrodeposition was performed in an aqueous solution of 0.1 mol dm^{-3} , 0.5 mol dm^{-3} or 1 mol dm^{-3} $\text{Zn}(\text{NO}_3)_2$ with or without $50 \mu\text{mol dm}^{-3}$ eosin Y. The eosin Y was dissolved in ethanol at a ratio of 1 mg eosin Y per mL ethanol prior to mixing with the zinc nitrate solution. A three-electrode setup was used with a Bio-Logic potentiostat. FTO served as the working electrode, a zinc sheet served as the counter electrode and a reversible hydrogen electrode (RHE, 0.5 mol dm^{-3} H_2SO_4) was used as a reference electrode. The zinc nitrate solution was either at room temperature or heated to 40°C by a hot plate. The solution was not stirred during electrodeposition.

Prior to the synthesis, the FTO substrate was cut into pieces of $3 \text{ cm} \times 4 \text{ cm}$. A cut was made on the non-conductive side of the sample, dividing the pieces into two sections of $3 \text{ cm} \times 3 \text{ cm}$ and $3 \text{ cm} \times 1 \text{ cm}$, as shown in Figure 3.2a. The reason for this was to be



(a)



(b)

Figure 3.3: The setup used during the electrodeposition. (a) Image of the actual setup and (b) a drawing of the set up as seen from above.

able to cleave the glass piece to fit in the PECC-2 sample holder, while still being able to place the electrode clip on the glass during the electrodeposition. The glass pieces were cleaned with DI-water and ethanol, dried with an airflow of nitrogen gas and covered with insulation tape to expose only an area of 2.5 cm x 2.5 cm of the conductive side of the glass to the zinc nitrate solution. The insulation tape process is shown in Figures 3.2b-3.2d.

Three different electrochemical techniques were used: potentiostatic, galvanostatic and potentiodynamic. Potentiostatic deposition was performed at a constant potential of -1 V, -0.9 V or -0.8 V vs RHE for 30 minutes. Galvanostatic deposition was performed with a current density of 0.16 mA cm^{-2} , 0.32 mA cm^{-2} , 1 mA cm^{-2} or 2 mA cm^{-2} for 30 minutes. Potentiodynamic deposition was performed cycling between -1 V and -0.2 V 21 times at a sweep rate of 5 mV s^{-1} .

After deposition, the samples were cleaned by soaking them in a beaker of DI-water. The samples were then dried in air for minimum 30 minutes. For HE and PHE the samples were soaked in a KOH-solution at a pH of 10.5 for 60 minutes, to remove the deposited eosin Y. After this treatment, the samples were cleaved to remove the excess glass and cleaned with DI-water.

The process of investigating the different aspects of electrodeposition of ZnO is presented in Figure 3.4. Some techniques or aspects were disregarded when they were found unsatisfactory.

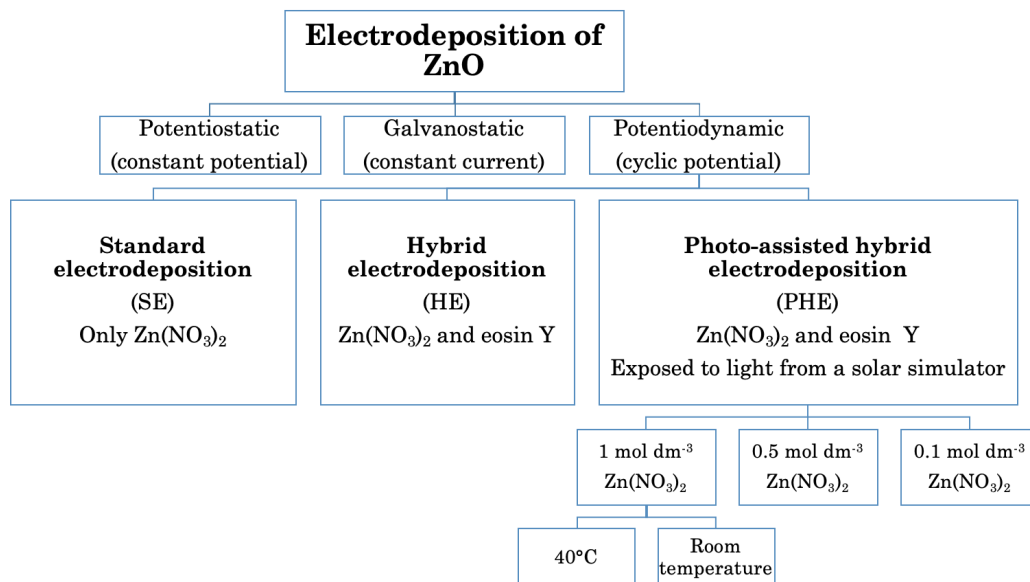


Figure 3.4: The process of optimizing the electrodeposition of zinc oxide.

The doctor blading method followed the one published by Guo *et al.* [56]. A ZnO-paste was made from 25 wt% ZnO nanoparticles (dispersed in H₂O), 8 wt% ethyl cellulose and 67 wt% terpeneol. Samples with SE-ZnO were covered with insulation tape, exposing only the ZnO. The ZnO-paste was spread over the substrate by sliding a glass rod over the sample. After carefully removing the tape, the samples were dried at 100 °C in a drying oven for 30 minutes. A second layer of ZnO-paste was deposited the same way, but with a double layer of insulation tape. After a second round of drying, the samples were annealed at 350 °C for 4 hours in a Carbolite horizontal tube furnace. The atmosphere was synthetic air.

The ALD was performed with a Veeco ALD. The edges of exposed FTO around the ZnO were cleaned with ethanol and covered with kapton tape. The ALD of TiO₂ was performed at a temperature of 160 °C and a pressure of 34.53 Pa, in an N₂ atmosphere at a flow rate of 20 sccm. The titanium precursor was TDMA. 100 nm of TiO₂ was deposited through 1980 deposition cycles. After deposition, the tape was removed and the edges were cleaned with 2-propanol. To oxidize the samples to TiO₂, the samples were heated in a Carbolite horizontal tube furnace at 500 °C for 3 hours.

Finally, the samples were dried at 125 °C for 30 minutes before dye loading. The dye solution was either N719 or eosin Y at a concentration of 0.5 mmol dm⁻³ in ethanol. The samples should be dry and warm when immersed in the dye solution [24]. The samples were left in the staining bath for 2 hours. During staining the samples were in the dark. After staining the samples were rinsed with ethanol and dried in a flow of nitrogen gas.

3.2 Photoelectrochemical characterization

The finished electrodes were assembled in a Zahner photo electrochemical cell (PECC-2) immediately after staining. An I⁻/I³⁻ electrolyte was used for the photoelectrochemical characterization. The electrolyte was composed of 0.6 mol dm⁻³ tetrabutylammonium iodide, 0.5 mol dm⁻³ lithium iodide, 50 mmol dm⁻³ iodine and 0.5 mol dm⁻³ 4-tert-butylpyridine in acetonitrile [56].

The photoelectrochemical measurements were performed by a Zahner controlled intensity modulated photospectroscopy (CIMPS) measurement system. Incident photon-to-electron conversion efficiency (IPCE) measurements were performed with the potential set to 0 V over the cell at wavelengths from 290 nm to 800 nm. The frequency of the light was set to 1 Hz and the background light was on. The IV measurements were done at a wavelength of 512 nm. 512 nm was the closest wavelength to the dye-peak that the CIMPS allowed. The intensity of the light was around 82.6 W m⁻¹. The size of the light beam was 1 cm². Electrochemical impedance spectroscopy (EIS) was performed at

10 potentials from the open circuit voltage at an interval of 10mV (towards 0 V). The frequency range was from 10 mHz to 100 kHz and the amplitude of the oscillation was 10 mV. Intensity modulated photocurrent spectroscopy (IMPS) and intensity modulated photovoltage spectroscopy (IMVS) was performed in the frequency range of 10 mHz to 1 kHz, the oscillation of light was set to an amplitude of 10 mA. The light source was set to 512 nm for EIS, IMPS and IMVS.

3.3 Material characterization

To compare the outcome of the different synthesis routes, the samples were inspected with regards to color and coverage, their deposition currents were compared, and their thickness were measured with a Dektak 150 stylus profilometer.

X-ray diffraction was performed, on ZnO that was scraped off the electrode, using a Bruker D8 Focus between 5° and 90°. The measurement took 30 minutes. The XRD-analysis was done with the Bruker "DIFFRAC.EVA" software. The surface of the finished electrodes were investigated with either a Zeiss Ultra 55 SEM or a FEI APREO SEM. Energy dispersive X-ray spectroscopy was performed on a Zeiss Ultra 55.

Chapter 4

Results

4.1 Electrodeposition of zinc oxide

All samples in this section (4.1) are made by electrodeposited ZnO and sensitized with N719 for the photoelectrochemical characterization. The concentration of $\text{Zn}(\text{NO}_3)_2$ was 1 mol dm^{-3} , except in Chapter 4.1.4, where different concentrations were investigated. The temperature of the nitrate bath was 40°C , except in Chapter 4.1.4, where different temperatures were investigated.

4.1.1 Electrochemical technique

Images of samples from the different electrochemical techniques are presented in Figure 4.1. The potentiodynamic deposition resulted in white films that covered the whole substrate uniformly. Potentiostatic and galvanostatic depositions, on the other hand, either deposited black films, had trouble with adhesion to the FTO-surface, or covered the sample non-uniformly. Due to the white color and the uniform coverage, the potentiodynamic method was chosen for further optimization.

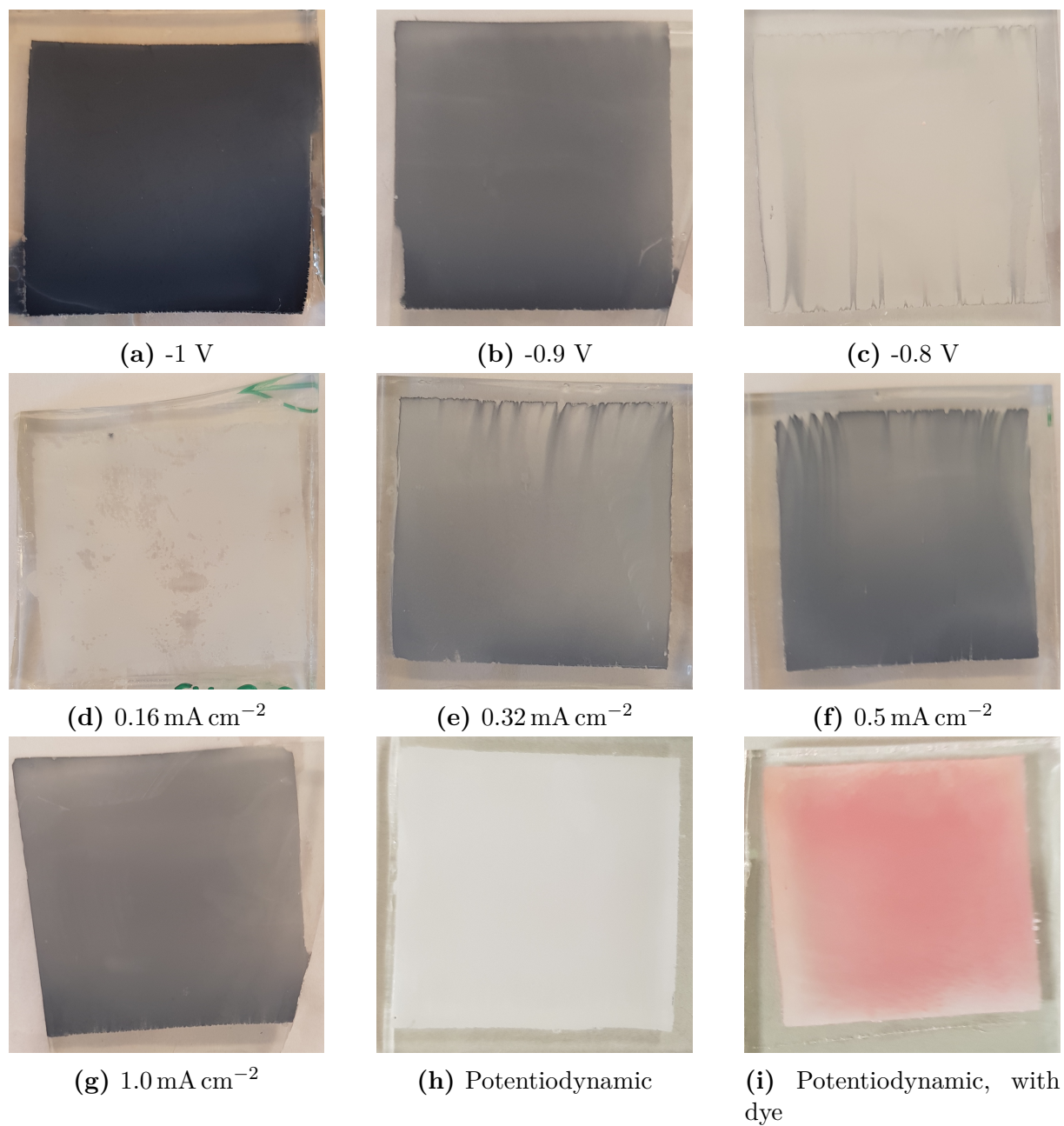


Figure 4.1: Images of samples made applying different potentials or currents. a-h were standard electrodepositions, while (i) was a hybrid electrodeposition. (a) to (c) underwent potentiostatic electrodeposition ranging from -1 V to -0.8 V, (d) to (g) underwent galvanostatic electrodeposition ranging from 0.16 mA cm^{-2} to 1 mA cm^{-2} , while (h) and (i) underwent potentiodynamic deposition, the latter with eosin Y.

4.1.2 SE, HE and PHE

The deposition current generated during photoassisted hybrid electrodeposition (PHE) was higher than during hybrid electrodeposition (HE), as is evident from Figure 4.2. In fact, the deposition current generated during PHE was the highest for all electrodeposition techniques, indicating that the exposure to light has an effect when dye molecules are present in the $\text{Zn}(\text{NO}_3)_2$ -solution. The standard electrodeposition (SE) and HE generated currents can be described as equal, based on the variability observed from sample to sample of the same technique.

The profilometer scans presented in Figure 4.3, show that the sample which generated the most current (PHE), also had the thickest film. HE resulted in thicker films than SE, even though they generated approximately the same amount of current during the deposition. The PHE and HE films were pink like the sample in Figure 4.1i, indicating that eosin Y had deposited onto the ZnO during deposition. Note the different scales on the horizontal axis (mm) and the vertical axis (μm) in Figure 4.3.

Still, samples were quite rough, as can be seen in the SEM-images in Figure 4.4. The scanning electron micrographs revealed that the SE had grown nanosheets with hierarchical flowers growing on top, HE had a higher density of flowers, and PHE did not display any distinct flowers, but had a lot more structure in the form of sheets.

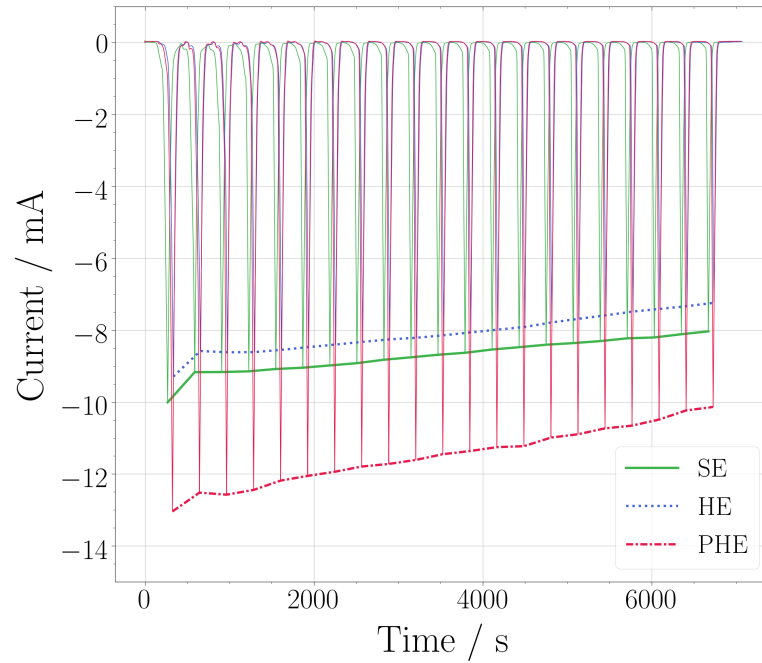


Figure 4.2: Deposition current during standard electrodeposition (SE), hybrid electrodeposition (HE) and photoassisted hybrid electrodeposition (PHE).

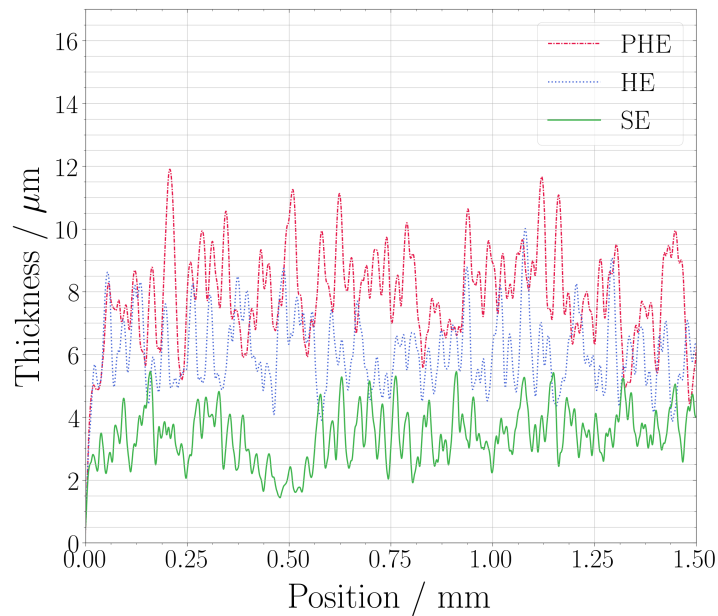
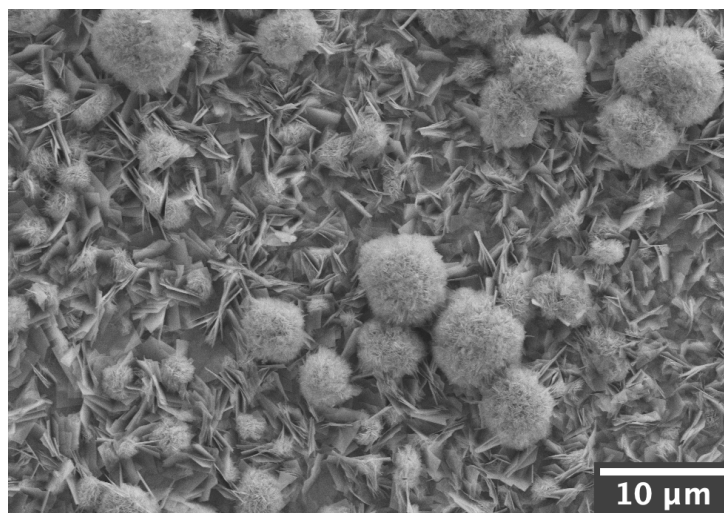
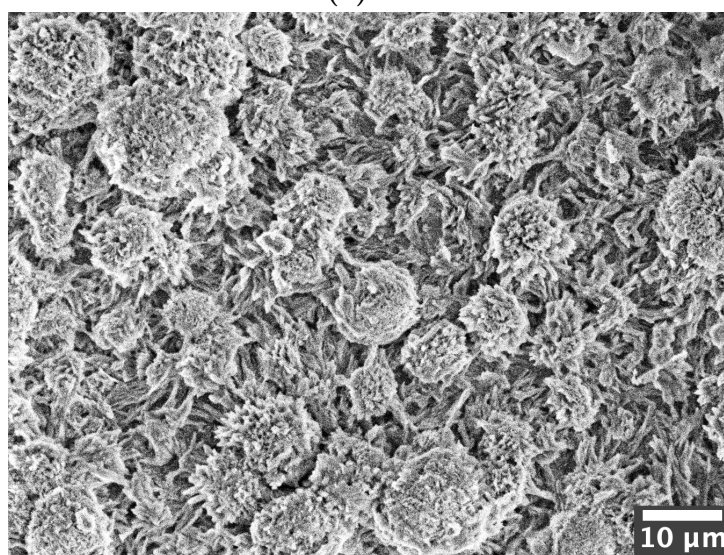


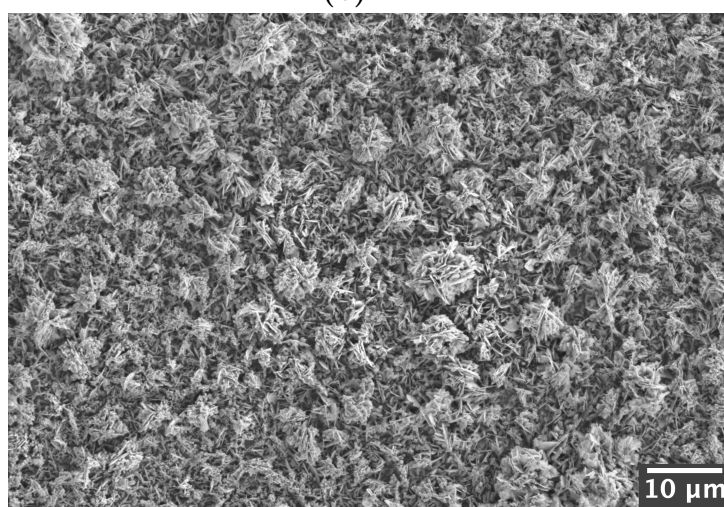
Figure 4.3: Thickness along 1.5 mm starting from the top edge of films made by standard electrodeposition (SE), hybrid electrodeposition (HE) and photoassisted hybrid electrodeposition (PHE).



(a) SE



(b) HE



(c) PHE

Figure 4.4: SEM micrographs of (a) standard electrodeposition and (b) hybrid electrodeposition and (c) photoassisted hybrid electrodeposition.

Figure 4.5 compares the IPCE-curves of SE, HE, and PHE samples sensitized with N719. The SE sample produced no significant photocurrent, while HE and PHE exhibit one peak at around 535 nm, and two peaks in the range 300 nm - 400 nm. In addition, a small peak at 395 nm can be observed. The first peak, at 344 nm, corresponds to absorption by the band gap of SnO_2 at 3.6 eV [58]. The FTO-substrate is made of SnO_2 . The second peak, at 367 nm, corresponds to absorption by the band gap of ZnO around 3.3 eV. The rest of the spectra is due to absorption by N719. These characteristics were observed for all ZnO/N719 cells in this work.

The IV-curves of a HE-sample and a PHE-sample are shown in Figure 4.6. Their open circuit voltages and short circuit currents are similar, but their fill factors were different, reading 0.35 and 0.52 for HE and PHE, respectively. However, as is presented later, the IV-curves vary greatly between samples produced by the same method. The IV-curve of HE displays an almost ohmic characteristic, while diode behavior was observed for the PHE. Again, the SE samples were unable to produce a photocurrent.

PHE was chosen for further optimization, based on the rougher surface, the better performance in the IPCE- and IV-measurements and the fact that it was the thickest sample.

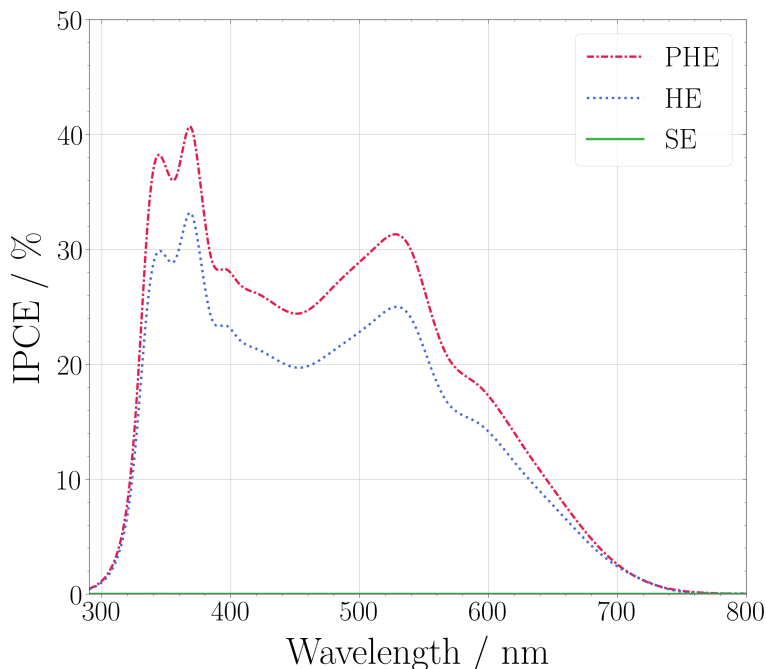


Figure 4.5: The IPCE spectra of standard electrodeposition (SE), hybrid electrodeposition (HE) and photoassisted hybrid electrodeposition (PHE). The quantum efficiency of the SE-sample was so low, no peaks can be seen when compared to HE and PHE. The SE-curve is hugging the wavelength axis. The cells were sensitized with N719.

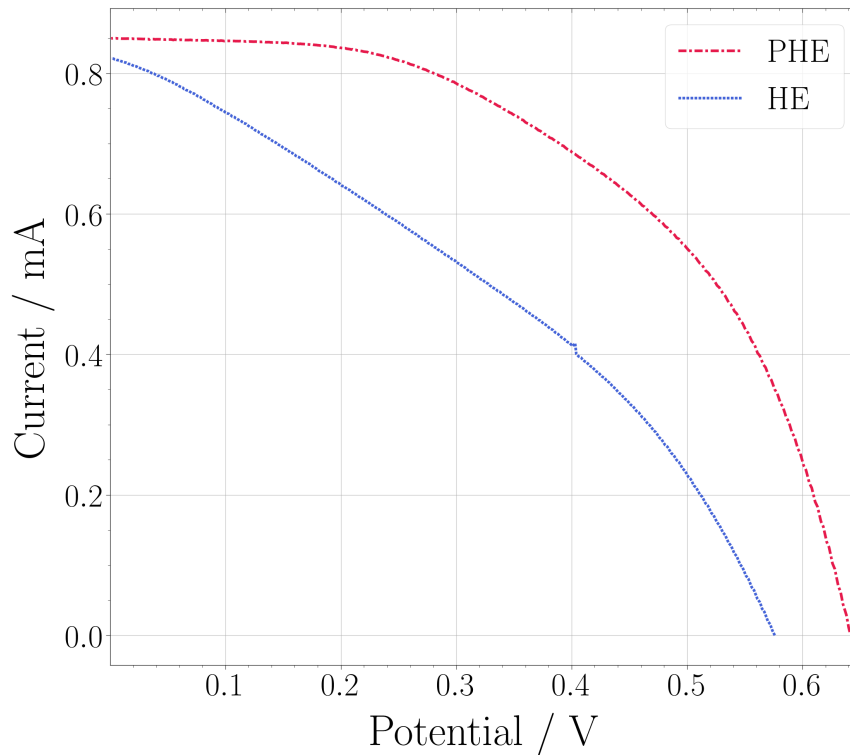


Figure 4.6: IV-curves at 512 nm, generated from a hybrid electrodeposition sample (HE) and a photoassisted hybrid electrodeposition sample (PHE). The fill factors of the curves were 0.353 and 0.520, respectively. The cells were sensitized with N719.

Sample-to-sample variations

Sample-to-sample variations were observed. Figure 4.7 displays the IPCE-curves of 3 different PHE samples. Samples 1 and 2 are from the same $\text{Zn}(\text{NO}_3)_2$ -batch while Sample 3 is from a different batch. All samples display the same shape of the IPCE-curve, but Sample 3 had a lower dye-peak, and sample 1 had higher SnO_2 and ZnO peaks.

The IV-curves in Figure 4.8 show that Sample 3, which generated the lowest photocurrent, had the highest fill factor. Their open circuit voltages were similar for all 3 samples.

The deposition currents of the samples were similar, as presented in Figure 4.9. Even though the deposition current of Sample 2 was somewhat lower, the difference is not observed in the thickness of the samples. The profilometer scans of all three samples are shown in Figure 4.10. Though there are some slight differences in the thickness, they cannot be related to the deposition current.

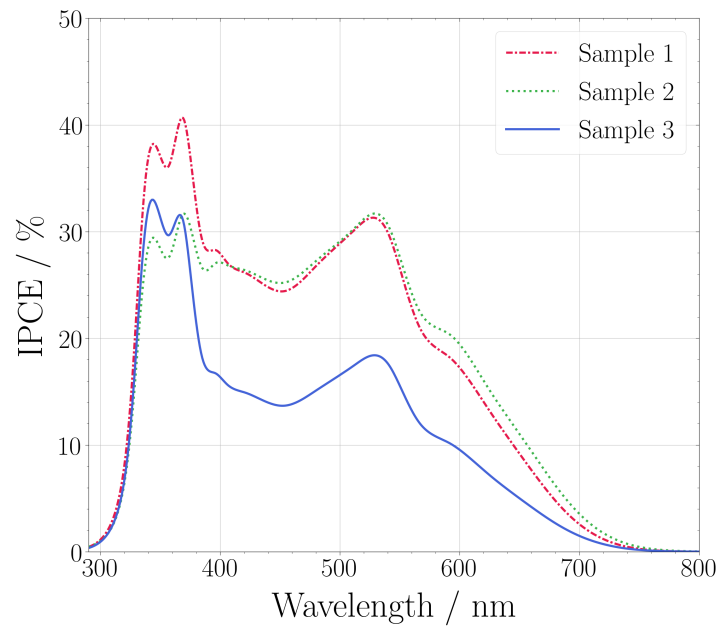


Figure 4.7: IPCE-curves of 3 samples made by photoassisted hybrid electrodeposition, sensitized with N719.

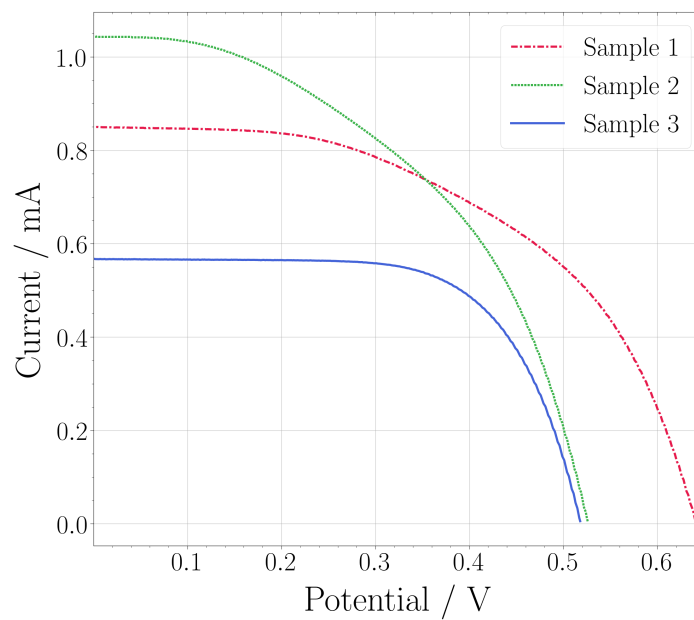


Figure 4.8: IV-curves at 512 nm of 3 samples made by photoassisted hybrid electrodeposition, sensitized with N719.

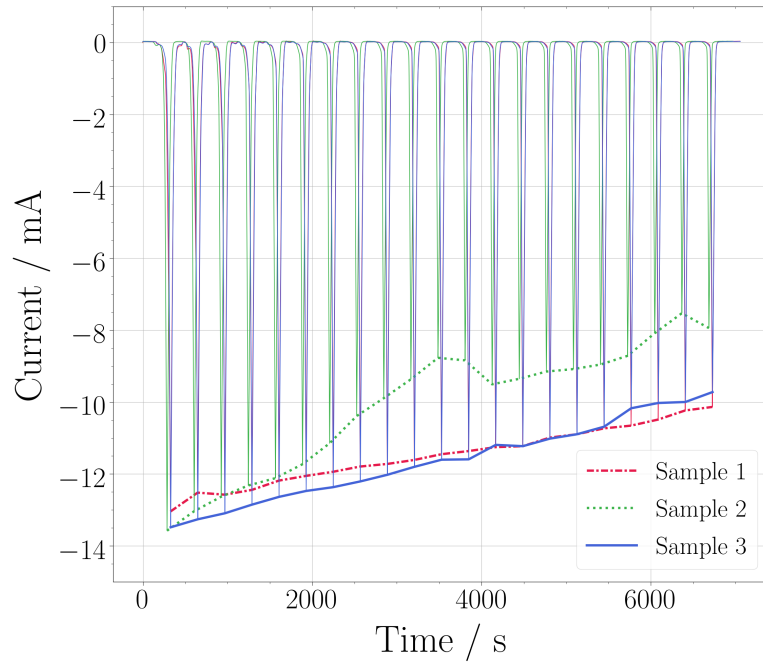


Figure 4.9: Current generated during the photoassisted hybrid electrodeposition of 3 different samples.

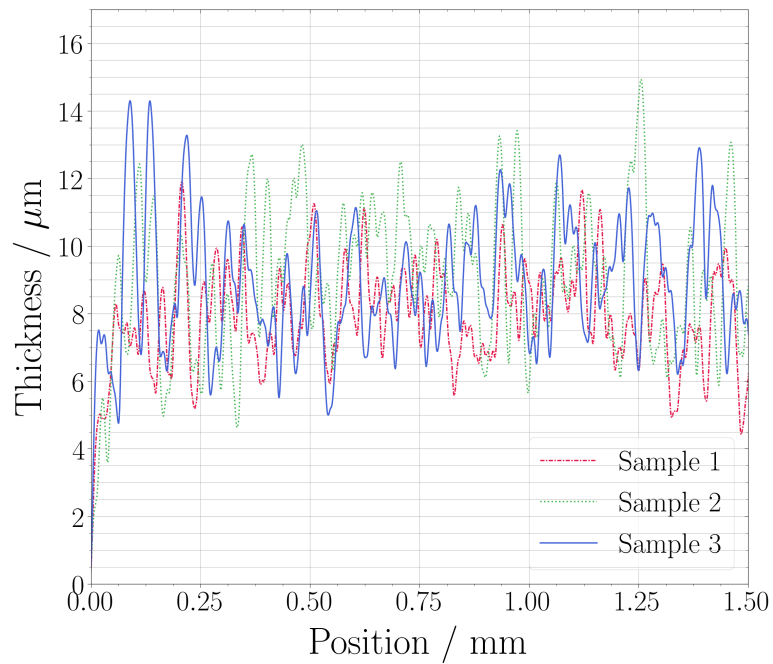


Figure 4.10: Profilometer scans of 3 samples made by photoassisted hybrid electrodeposition.

Table 4.1 summarizes the photovoltaic performances of three PHE-electrodes and one HE-electrode. The best performing PHE-cell had a conversion efficiency at 512 nm of 3.42%. The short circuit current at 512 nm, calculated from the IPCE-spectra by Equation 2.7, were equal to the measured short circuit current for all samples, except Sample 1.

Table 4.1: Fill factor (FF), conversion efficiency at 512 nm ($\eta_{512\text{nm}}$), measured short circuit current (I_{sc}) and calculated I_{sc} for 3 cells with photoassisted hybrid electrodeposition (PHE) -electrodes and one cell with hybrid electrodeposition (HE) electrode.

Sample	FF	$\eta_{512\text{nm}}$	I_{sc} from IV	I_{sc} from IPCE
PHE - Sample 1	0.520	3.42%	0.85 mA	1.03 mA
PHE - Sample 2	0.477	3.22%	1.04 mA	1.04 mA
PHE - Sample 3	0.677	2.36%	0.57 mA	0.60 mA
HE	0.353	2.02%	0.82 mA	0.81 mA

4.1.3 Crystal structure of electrodeposited films

Figure 4.11 shows the X-ray diffraction patterns of material made by PHE, before and after drying at 125 °C. The *before* material had only dried in room temperature, and the dominant material appeared to be $\text{Zn}_5(\text{NO}_3)_2(\text{OH})_8$. ZnO was the most prominent phase *after* drying at 125 °C. Some of the $\text{Zn}_5(\text{NO}_3)_2(\text{OH})_8$ peaks were still present after drying (9°, 26°, 42°, 44°, 58° and 59°).

EDX confirmed that the surface of an SE sample was composed of zinc and oxygen. The EDX results can be found in Appendix B.

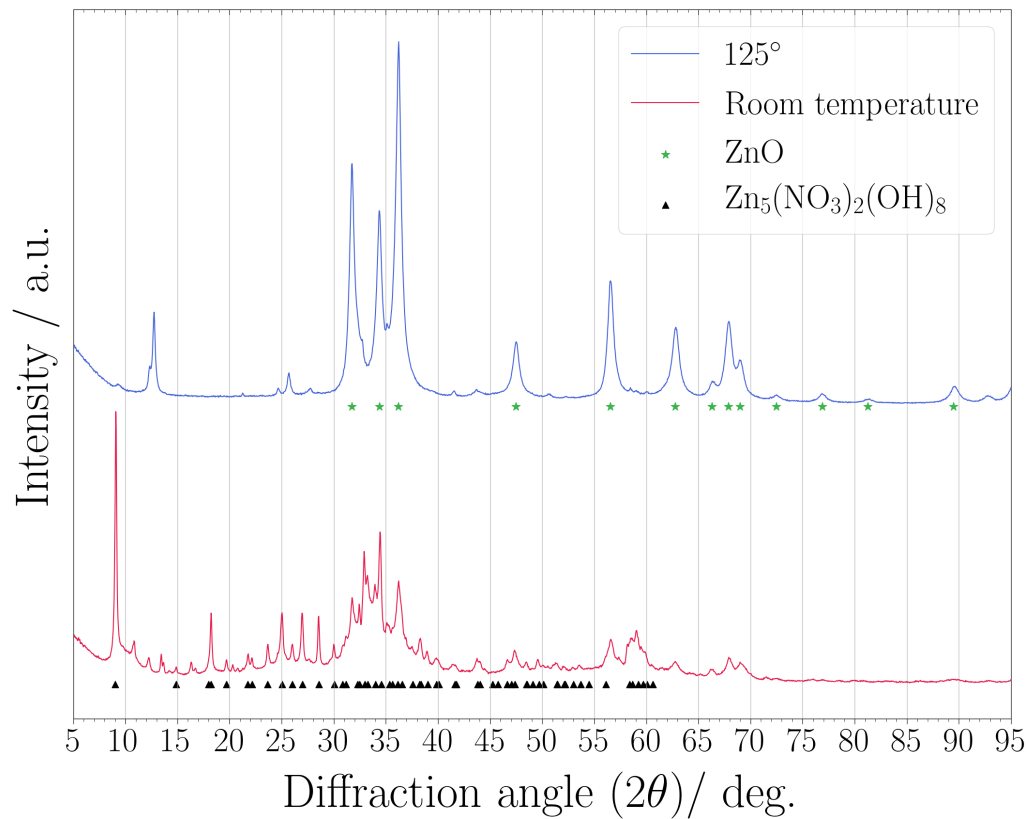


Figure 4.11: X-ray diffraction patterns of material deposited by photoassisted hybrid electrodeposition. The measurements were performed before (bottom) and after (top) drying at at 125 °C. The peak locations of ZnO (★) and Zn₅(NO₃)₂(OH)₈ (▲) are also shown.

4.1.4 Changes in deposition environments

Temperature

Figure 4.12 compares the current generated for a PHE at room temperature (RT) and at 40 °C. At room temperature, the deposition current diminished much faster. After cycle 10, the current generated is too small for any significant amount of ZnO to be deposited. The film made at 40 °C was almost twice as thick as the one made at room temperature. The profilometer scans of the two samples can be found in Appendix B.

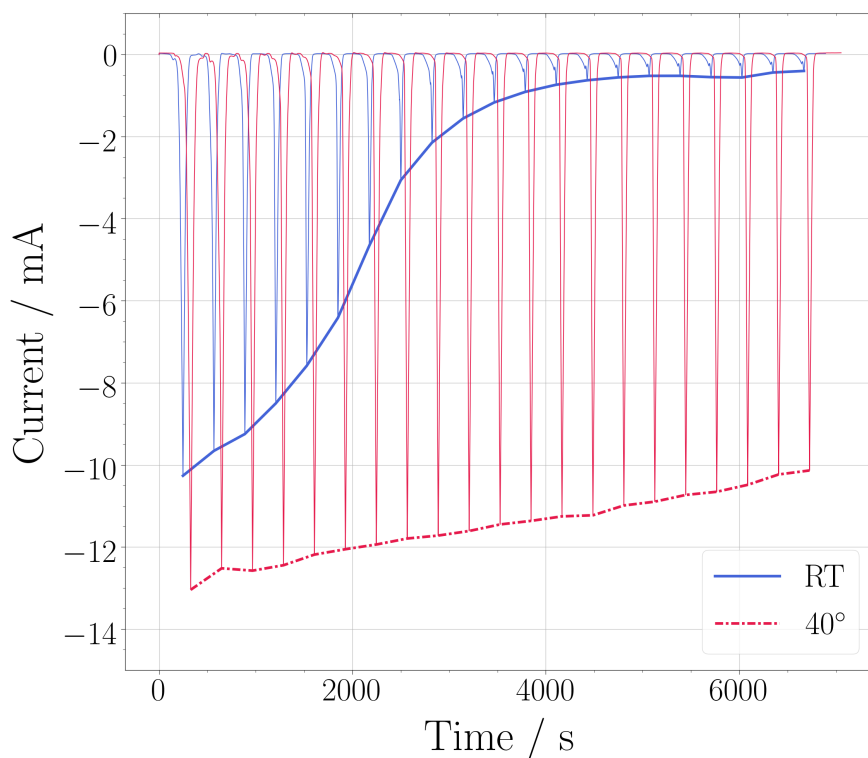


Figure 4.12: Recorded current during photoassisted hybrid electrodeposition at room temperature (RT) and at 40 °C.

Concentration

Figure 4.13 compares the current during PHE of three samples made from different concentrations of zinc nitrate. The increase in deposition current, especially during the first five cycles, for $0.1 \text{ mol dm}^{-3} \text{ Zn(NO}_3)_2$ was uncharacteristic of the system, but was observed for all trials at this concentration. The deposited film was flaking off the substrate, making it unusable for further characterizations. The flaking film is shown in Figure 4.14. The deposition current in $0.5 \text{ mol dm}^{-3} \text{ Zn(NO}_3)_2$ diminishes over time. This was observed for several trials at this concentration. The deposition current in $1 \text{ mol dm}^{-3} \text{ Zn(NO}_3)_2$ was stable, and did not diminish significantly from cycle to cycle. This was observed for several trials, as was presented in Figure 4.9.

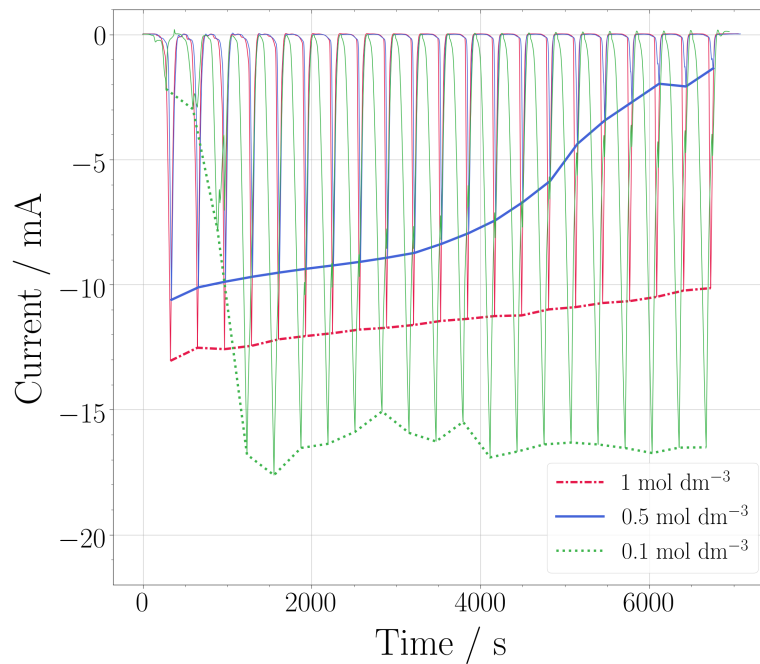


Figure 4.13: Current generated during photoassisted hybrid electrodeposition of three different concentration of $\text{Zn}(\text{NO}_3)_2$: 1 mol dm^{-3} , 0.5 mol dm^{-3} and 0.1 mol dm^{-3} .

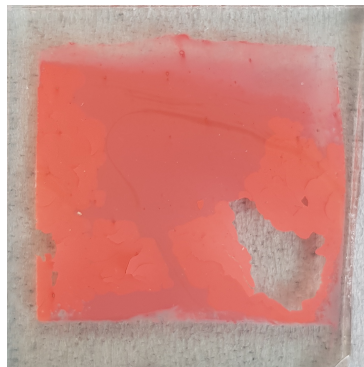


Figure 4.14: An electrode made from a 0.1 mol dm^{-3} $\text{Zn}(\text{NO}_3)_2$ -electrolyte. The film was flaking off the substrate.

In Figure 4.15, the IV-curves of samples made from 1 mol dm^{-3} (Sample 1 from Chapter 4.1.2) and 0.5 mol dm^{-3} are shown. Both samples were sensitized with N719. The short circuit current was over 4 times as high for the sample made from the highest concentration. The open circuit voltage was approximately the same, and similar to other $\text{ZnO}/\text{N719}$ cells in this work. Their IPCE-curves can be found in Appendix B.

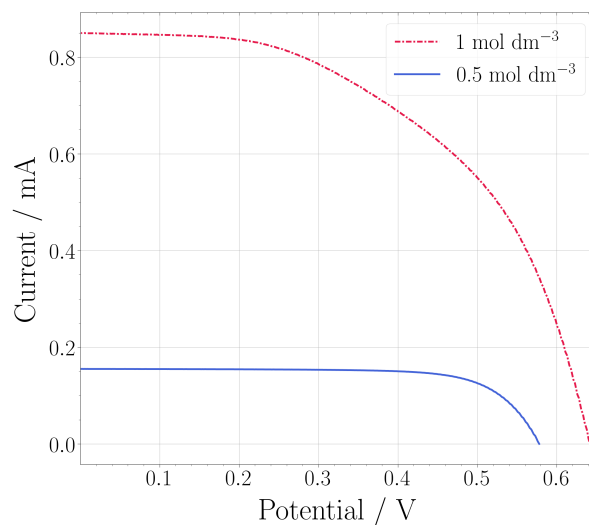


Figure 4.15: The IV-curve of two samples made from different concentrations of $\text{Zn}(\text{NO}_3)_2$. The solid line is made from 1 mol dm^{-3} $\text{Zn}(\text{NO}_3)_2$ and the dotted line is made from 0.5 mol dm^{-3} $\text{Zn}(\text{NO}_3)_2$.

Photoassisted standard electrodeposition

There was no significant difference in the current generated during standard electrodeposition performed in the dark, as compared to the photoassisted standard electrodeposition, as can be seen in Figure 4.16. The concentration of $\text{Zn}(\text{NO}_3)_2$ was 0.5 mol dm^{-3} for both samples.

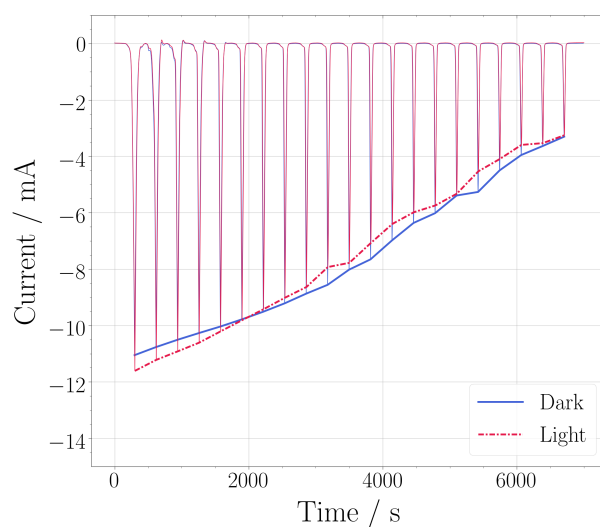


Figure 4.16: Comparison of the current generated during standard electrodeposition in the dark and photoassisted standard electrodeposition.

4.2 Degradation

The samples used to investigate the degradation were made of two layers of doctor blading on top of a standard electrodeposition layer. Figure 4.17 shows photographs of a sample before dye staining (a), the two samples after dye staining (b and c) and after 15 days of photoelectrochemical measurements (d and e). An image of another sample is also included (f), which shows a PHE sample sensitized with eosin Y, which was only tested for 2 hours. No eosin Y was left on the eosin Y-samples where they had been in contact with the I^-/I_3^- electrolyte. There was still N719 left on the N719-sample.

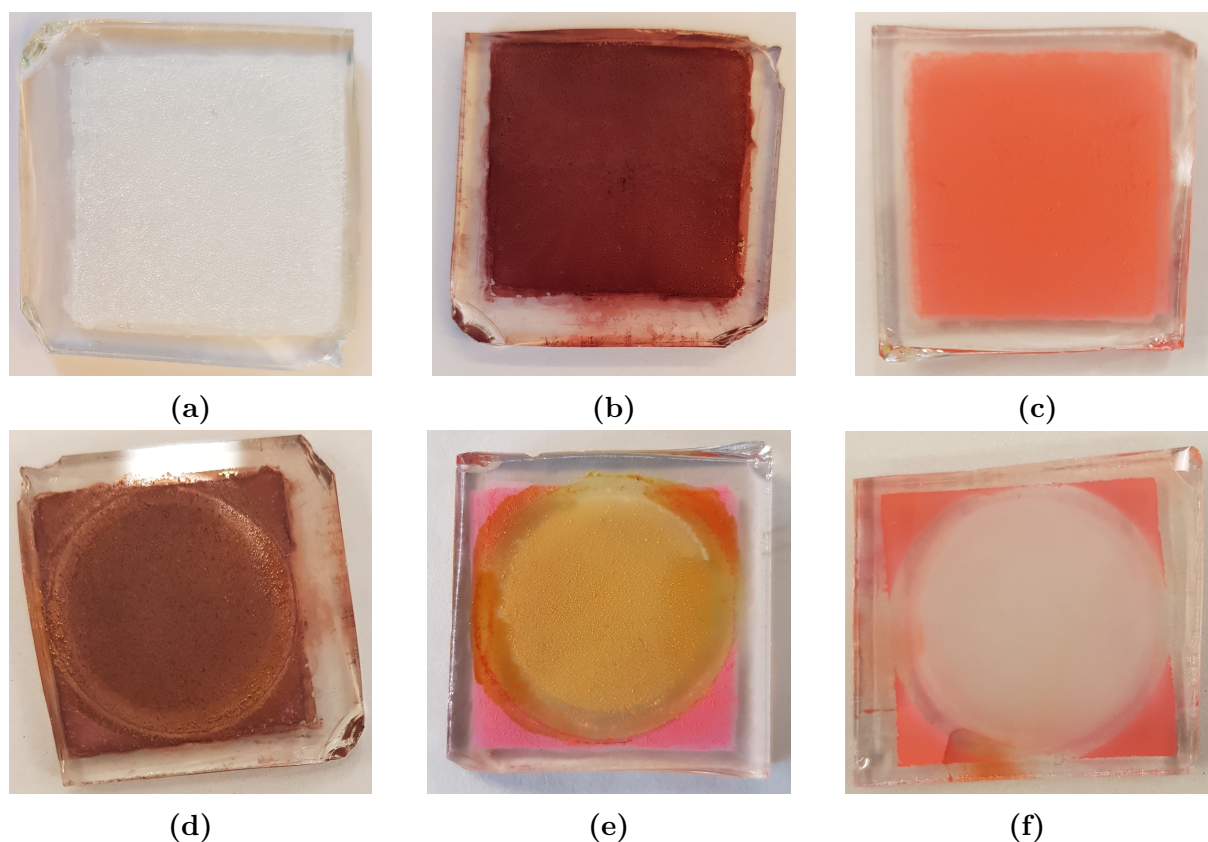
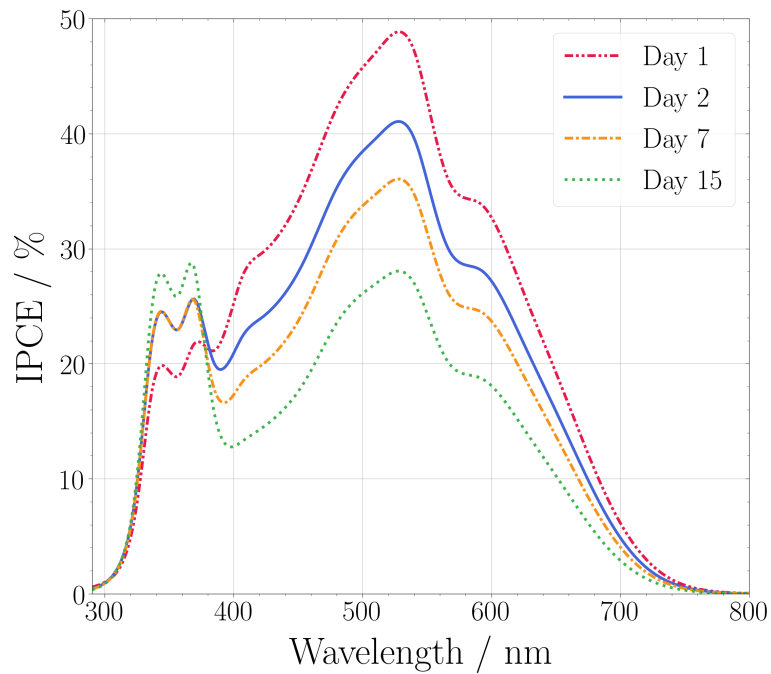


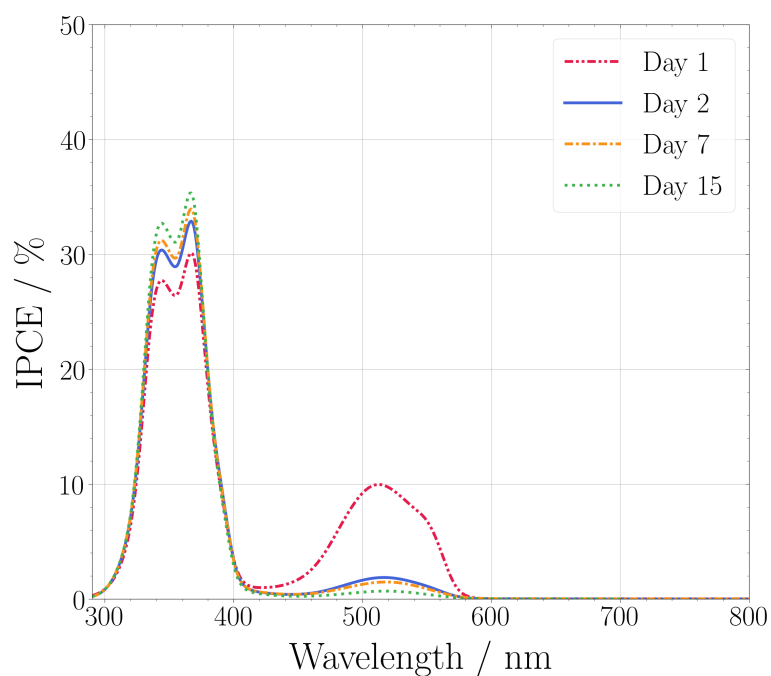
Figure 4.17: Images of samples used to investigate the degradation of the ZnO. (a) A doctor bladed electrode before staining, (b) an electrode stained with N719, (c) an electrode stained with eosin Y, (d) the N719-electrode after 15 days, (e) the eosin Y-electrode after 15 days and (f) a photoassisted hybrid electrode stained with eosin Y after 2 hours of measurements.

The change in the IPCE-spectra over time for the samples sensitized with eosin Y and N719 can be seen in Figure 4.18. The N719 sample performs better than the eosin Y sample during the whole period. The dye-peak of eosin Y has almost completely disappeared from day 2 and onward, The ZnO-peak increases when the dye-peak decreases for both samples. The total quantum efficiency of the N719-sample had decreased with

13.3% by day 2, 25.3% by day 8 and 37.7% by day 15.



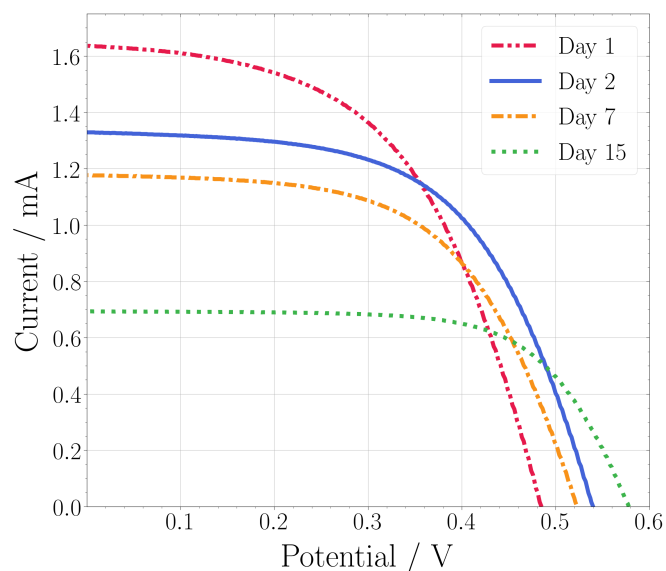
(a) N719



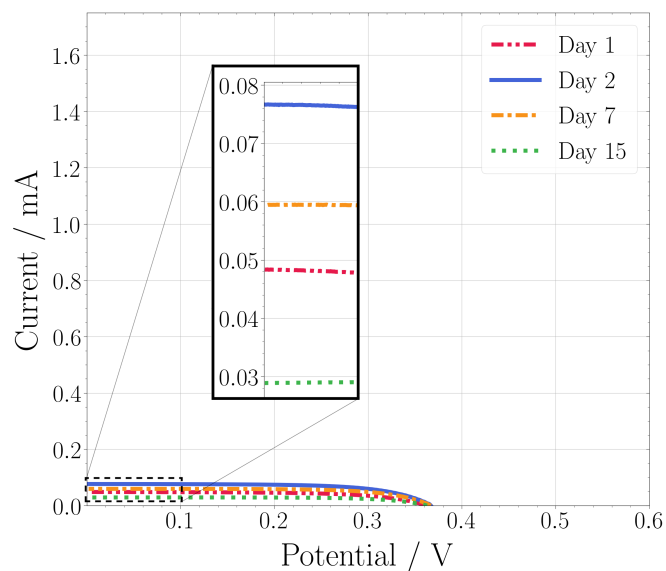
(b) Eosin Y

Figure 4.18: Stability of the IPCE-spectra for a sample stained with (a) N719 and (b) eosin Y.

The IV-curves for the same two samples are presented in Figure 4.19. The N719 sample degrades from day to day, following the degradation trend observed in the IPCE-spectra. The eosin Y sample produces little current all days. It does not degrade following the IPCE-spectra, but all short-circuit currents are within a range of $50 \mu\text{A}$.



(a) N719



(b) Eosin Y

Figure 4.19: Stability of the IV-curve for a sample stained with (a) N719 and (b) eosin Y. The inset in (b) is a zoom of the short circuit region of the eosin Y-cell.

Table 4.2 summarizes the performance of the N719 sample and the eosin Y sample on day 1 and day 15. The fill factor increased for both samples. The conversion efficiency at 512 nm on day 1 was 5.03% for the N719 sample. For the N719 sample, the recorded short circuit current (I_{sc}) matched the I_{sc} calculated from Equation 2.7 on day 1, but was 0.24 mA to high on day 15. For the eosin Y sample, the calculated I_{sc} was off by one order of magnitude on day 1. Since the photocurrent generated in the eosin Y cell was smaller than 0.1 mA on all days, the cell was not investigated any further.

Table 4.2: Fill factor (FF), conversion efficiency at 512 nm (η_{512nm}), short circuit current (I_{sc}) from IV and I_{sc} from IPCE of N719 and eosin Y on day 1 and 15

Sample	FF	η_{512nm}	I_{sc} from IV	I_{sc} from IPCE
N719 1	0.526	5.03%	1.63 mA	1.61 mA
N719 15	0.670	3.22%	0.69 mA	0.93 mA
Eosin Y 1	0.629	0.13%	0.048 mA	0.34 mA
Eosin Y 15	0.677	0.086%	0.029 mA	0.023 mA

In Table 4.3, the time constants of the N719-cell can be found. The recombination time is longer than the transport time on both days. Both time constants decrease during the degradation process. The values are calculated based on the theory in Chapter 2.5.4, and the data plots can be found in Appendix B.

Table 4.3: Transport time (τ_{tr}) and recombination time (τ_{rec}) in the N719 cell on day 1 and day 15.

Day	τ_{tr}	τ_{rec}
1	11.71 ms	113.42 ms
15	6.21 ms	76.6 ms

Figure 4.20 shows complex impedance plots at open circuit voltage on day 1 and day 15 for the N719-cell. The model fits the data better on day 1 than on day 15.

Figure 4.21 uses the model to recreate the IV-curve on day 1 and 15. The measured IV-curve is plotted along with the fitted curve based on the model. The resistances used to make the fitted curve are presented in Figure 4.22. The open circuit voltage had changed during the trial period, which is the reason why the resistances are calculated for different values.

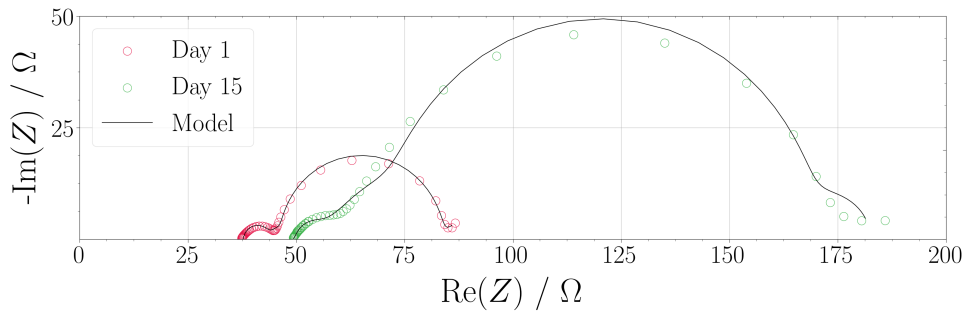


Figure 4.20: Electrochemical impedance spectroscopy (EIS) at open circuit voltage on day 1 and day 15. The open circuit voltage was 0.5 V when EIS was performed on day 1 and 0.6 V on day 15. The circles represent the measured data, while the black line is the impedance calculated from the model.

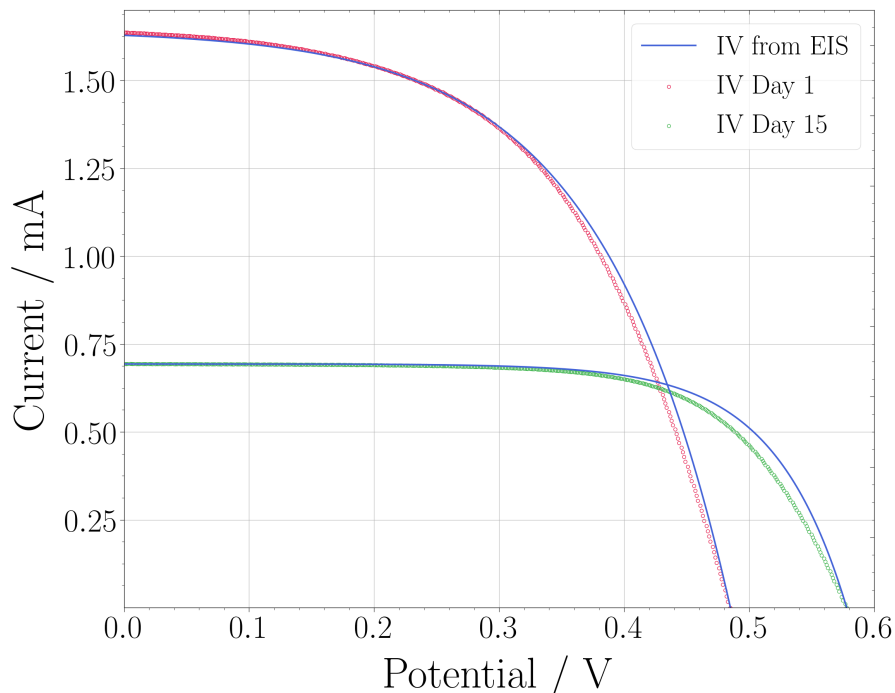


Figure 4.21: The IV-curve measured on day 1 and 15 for the N719 sample, in addition the the IV-curve generated from the electrochemical impedance modelling and the model-curve corrected with the series resistance, diffusion resistance and cathode resistance removed.

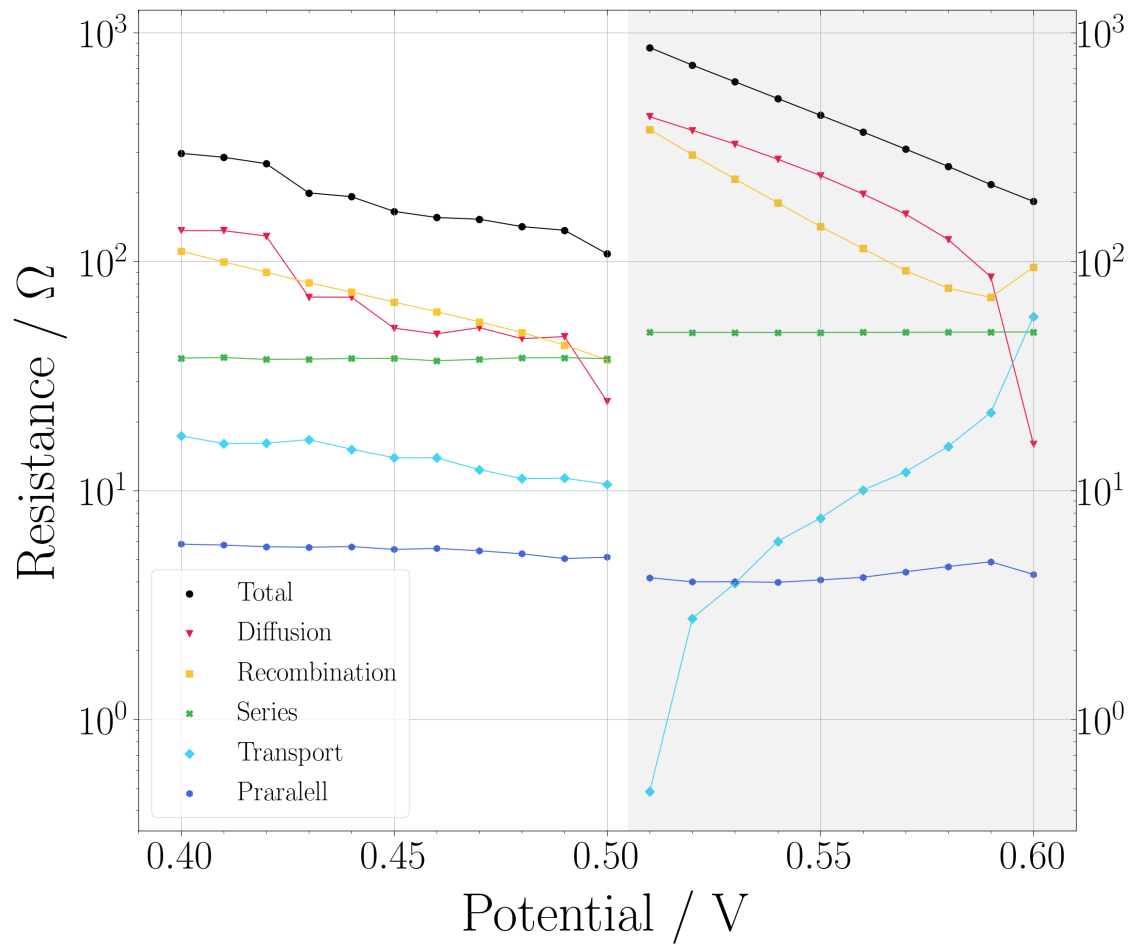


Figure 4.22: The resistances in the N719 cell on day 1 (white section) and day 15 (shaded gray section). The open circuit voltage in the cell had increased, and the EIS measurements were therefore not performed at equal potentials.

4.3 Atomic layer deposition of titanium dioxide

The sample used to investigate the effect of a thin layer of TiO_2 was made of two layers of doctor blading on top of a standard electrodeposition layer. Figure 4.23 shows the sample after each ALD-manufacturing step. After the ALD-deposition, the sample turned black (b). After the heat treatment it became light-colored again (c), though not completely white. The sample did not change color after dye-sensitization (d). The dye loading was increased to 24 hours to see if the staining process was slow, but this did not help.

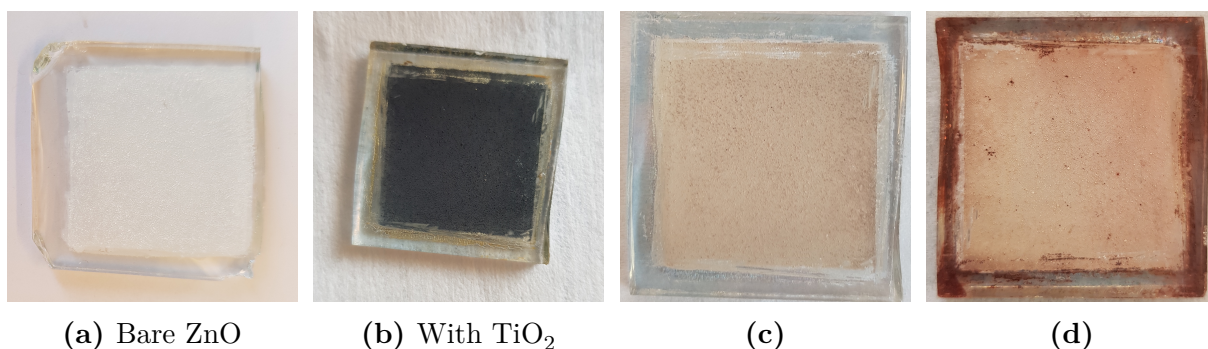
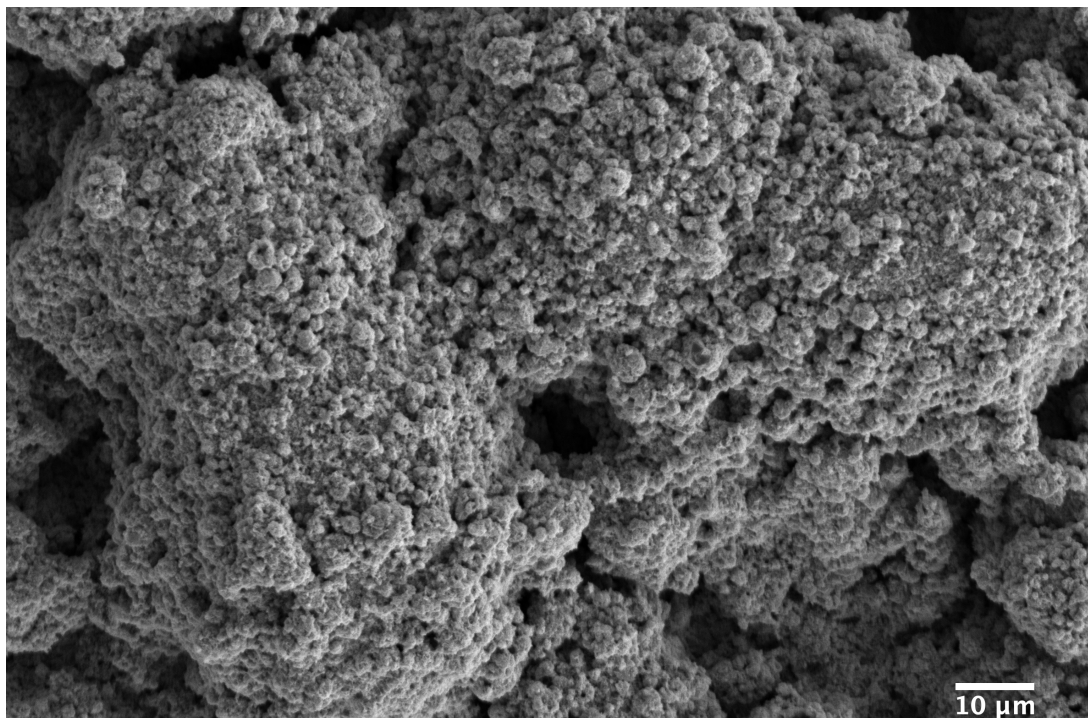
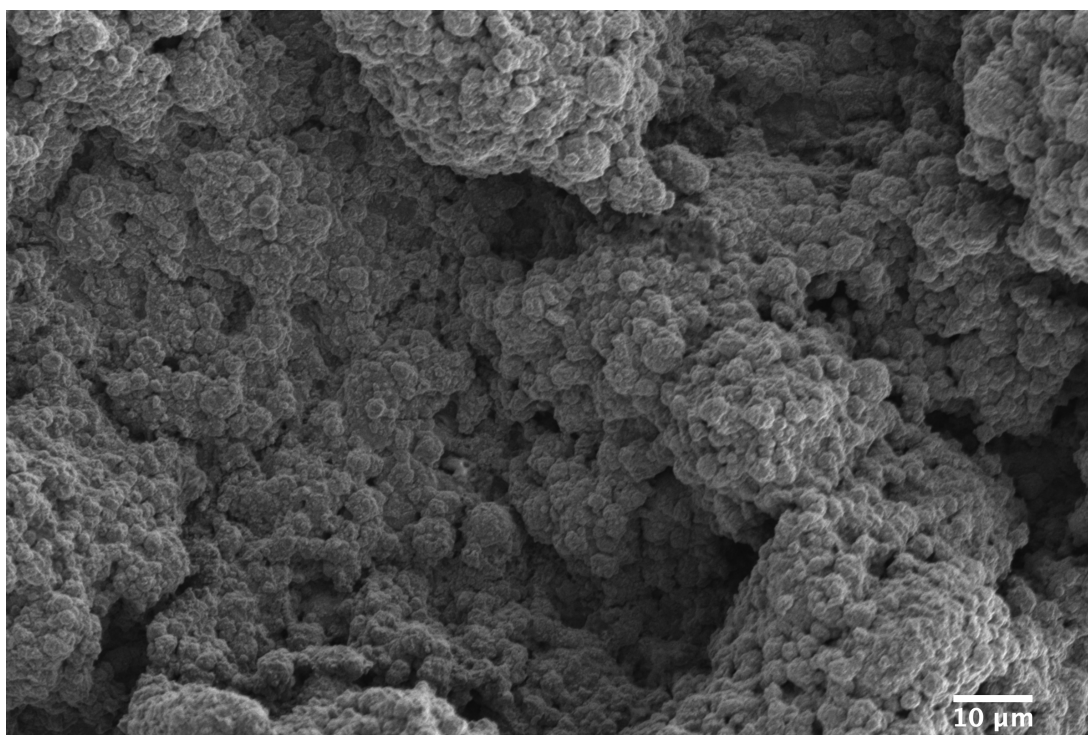


Figure 4.23: The ALD-sample, (a) before ALD, (b) after ALD, (c) after heat treatment at 500°C , and (d) after dye loading.

Figure 4.24 shows SEM micrographs comparing the surface of a sample with and without TiO_2 deposited on top. The sample without TiO_2 appears to be more porous.



(a)



(b)

Figure 4.24: SEM images of a doctor blading sample (a) before and (b) after ALD-deposition of TiO₂.

Chapter 5

Discussion

5.1 Electrodeposition of zinc oxide

5.1.1 Comparison of electrochemical technique

There are five reactions that might take place during the electrodeposition of ZnO, making the ZnO growth hard to control. At too negative potentials, Equation 2.24 might take place and deposit metallic zinc. If Equation 2.25 is dominant, too much hydrogen will be produced at the working electrode and the ZnO will be unable to deposit onto the surface. The electrodeposition is dependent on the local pH-increase caused by the increasing amount of OH^- as Equation 2.20 or Equation 2.25 takes place. The OH^- is, however, not stationary, and might move into the bulk solution by diffusion. The actual pH at the electrode is therefore hard to control. Careful application of the potential is needed for optimal results.

Large current densities and high potentials during the the galvanostatic and potentiostatic applications produced what appears to be metallic zinc. This is the black color that can be observed in figures 4.1a, 4.1b, 4.1e 4.1f and 4.1g. It is undesirable in terms of light absorption, as the black color will absorb all the light and make it impossible for the dye-molecules to generate current through photoexcitation. Also, since it is a metal, the charge separating abilities of a semiconductor would be lost. The electrodes that turned black are therefore regarded as useless, and the deposited material was not investigated further.

Too low potentials and currents results in inhomogeneous films. At low currents, the galvanostatic technique did not result in a uniform coverage, as seen in Figure 4.1d. This was also a problem experienced by Yoshida and his group when working with zinc nitrate baths [55]. When small currents flow through the cell, little reduction of NO_3^- or water is taking place. This results in a slow increase in pH. The slow production gives the OH^-

groups time to diffuse into the bulk of the solution, lowering the pH near the electrode. The result is less precipitation of ZnO onto the surface. The pH-increase might also not have been homogeneous over the whole sample, as some areas were left without ZnO deposited. Enough current must be ensured during the deposition.

As the potential or current was measured at the crocodile clip at the top of the FTO-piece, and not directly at the interface between the nitrate solution and the working electrode, the actual potential or current at the interface is not known. Therefore, the potentiostatic and galvanostatic deposition can give variable results when different substrates are used. The deposition is performed at potentials in the region right between deposition of metallic zinc and ZnO, as observed in Figure 4.1 between (b) and (c), and (d) and (e). A small change in substrate size could change the result of the deposition. A shorter distance for the electrons to travel through the FTO means a smaller voltage drop before the interface. Yoshida *et al.* used a potentiostatic deposition technique and reported that their results were very variable both with regards to coverage and reproducibility [55].

Potentiodynamic application of potential seemed to balance the different reactions, resulting in white ZnO, as shown in Figure 4.1. Since the potential was swept, it did not stay at too negative potentials long enough for metallic zinc to deposit. The sweeping allowed some diffusion to happen, which seemed to make the pH at the electrode homogeneous, yet high enough for ZnO to deposit. Due to depositing films with the best coverage and color, the potentiodynamic technique was chosen for further optimization.

5.1.2 Comparison of SE, HE, and PHE

Dye molecules in the nitrate bath results in thicker films. In Figure 4.2, the deposition currents of SE and HE are approximately the same, but the profilometer scans in Figure 4.3 revealed that the HE-sample is thicker than the SE-samples. The only difference between the two depositions was the addition of eosin Y in the nitrate solution. It is therefore reasonable to believe that the eosin Y is the cause of the thicker films. This follows the theory presented by Minoura and Yoshida [13], saying that ZnO is forced to grow around the eosin Y molecules.

The dye molecules also have an effect on the surface structures of the ZnO film. As seen in figures 4.4a and 4.4b, the surface structures of HE and SE were different. It is especially the hierarchical flower-structures that are different. In the HE sample, the flowers are grown more numerous and the flower itself appear denser. The underlying nanosheet-structures of both samples are similar to the structures reported by Nayak [50] and Yoshida *et al.* [53], but they did not report of the flower-structures.

The dye-molecules can contribute to even thicker films if exposed to light. PHE had a

higher deposition current and resulted in thicker films than HE, as seen in figures 4.2 and 4.3. More current flowing in the cells, reduces more nitrate ions following Equation 2.20. The only difference between HE and PHE is the exposure to light. The extra current generated in PHE is attributed the photoelectrons generated in the eosin Y molecules.

The effect of light is the most interesting finding in this thesis. However, it might not be necessary to expose the electrodeposition to a solar simulator light source to get this effect. Figure 4.16 shows how the exposure to light had no effect on the current during deposition without eosin Y in the zinc nitrate solution. The extra photocurrent during PHE could therefore not have been produced in the ZnO. Hence, it must be the eosin Y that absorbs photons and assists the electrodeposition. Eosin Y has an absorption peak around 517 nm [25] and a light source of this wavelength might therefore be sufficient. Due to practical reasons and to the lack of equipment, this was not investigated further. Not using a solar simulator emitting light in the UV-range as a light source would be beneficial from an HSE-point of view. Optimizing the light exposure could give even better films.

The surface structure of PHE was the roughest, with nanosheets covering the whole sample. Nanosheets are, according to Vittal *et al.* [9], the optimal structures for fast electron transport and high dye adsorption. PHE did not produce the characteristic hierarchical flowers, as HE and SE did. The surface structure can also be related to the photogenerated electrons. In HE and SE, the reduction of nitrate is dependent on an electron to travel through the deposited ZnO, while in PHE electrons are also generated directly at the surface of the electrode. The reduction can therefore happen in more places and the growth can be distributed across the surface.

The differences observed in the IPCE-spectra of Figure 4.5, can be attributed to the aforementioned difference in sample-thickness and structure. The general shapes of the plots are the same, but the PHE has higher quantum efficiency for all wavelengths where the cell is active. The generated photocurrent is related to the amount of dye-molecules adsorbed at the surface of the electrode. Since the sample is thicker it can be assumed that the surface area is larger. Therefore, more dye can adsorb and more photons can be converted to electrons.

The flowers in the HE-sample might create a large resistance in the cell. The IV-curve of the HE-sample showed an Ohmic characteristic in Figure 4.6. The linear shape is due to resistances in the cell. Since the PECC2-cell was used, all parts in the cell, except the ZnO, were equal for all electrodes characterized. A possible explanation for the poor performance of HE is that the connection between the flower structures and the substrate is bad, creating recombination at the contact between the flowers and the substrate. In addition, the flowers also appear dense, indicating that dye-molecules might not have been

able to get inside the flowers. If this was the case, the electrons would have a long way to travel through the ZnO to reach the outer circuit. The cell was not characterized with regards to the resistances in the cell, but the IV-curve reveal big problems.

The PHE film is transformed into ZnO after drying. The XRD-analysis revealed that $\text{Zn}_5(\text{NO}_3)_2(\text{OH})_8$ was the deposited material when PHE was performed, as observed in Figure 4.11. This was also observed in other works by Nayak [50] and Hou [59]. The formation of $\text{Zn}_5(\text{NO}_3)_2(\text{OH})_8$ happens when ZnO or $\text{Zn}(\text{OH})_2$ is in an aqueous solution with $\text{Zn}(\text{NO}_3)_2$ [60]. Both ZnO and $\text{Zn}(\text{OH})_2$ are produced during the electrodeposition. According to Hou, the amount of $\text{Zn}_5(\text{NO}_3)_2(\text{OH})_8$ present after the electrodeposition depends on the concentration of $\text{Zn}(\text{NO}_3)_2$ [59], with lower concentrations resulting in less $\text{Zn}_5(\text{NO}_3)_2(\text{OH})_8$. However, the material is transformed back into ZnO by drying at 125 °C. The electrodes were heated to 125 °C to remove water from the surface to obtain optimal dye coverage [24]. The electrodes are therefore zincite ZnO when used in DSSCs.

Based on the superior IV and IPCE performance in addition to thicker films and nanosheet structure, PHE was chosen for further investigation.

5.1.3 Changes in deposition environments

Concentration

Most of the research on ZnO DSSCs from electrodeposition used a $\text{Zn}(\text{NO}_3)_2$ -concentration of 0.1 mol dm^{-3} [49, 13, 53, 54, 55]. Since the concentration used in the project work was ten times larger, it felt necessary to investigate what concentration could be sufficient [12].

At low concentrations of NO_3^- , production of hydrogen is the dominant reaction. The PHE deposition with 0.1 mol dm^{-3} $\text{Zn}(\text{NO}_3)_2$ did not stick to the surface, while the deposition current was quite high, as seen in Figure 4.13. It is therefore possible that equation 2.25 took place, producing hydrogen at the electrode, making ZnO unable to stick to the surface. At a lower concentration of NO_3^- , a higher ratio of water is present at the electrode/electrolyte-interface. As H_2 -bubbles start to form, a mechanic force from the bubbles will create movement in the liquid at the electrode. This will make it harder for the pH to increase near the electrode, and thus less ZnO will deposit. Bubbles can also stick to the surface of the electrode, forcing ZnO to grow around. Since the samples were manufactured either in complete darkness or while exposed to a solar simulator, the electrode was not observed during the deposition due to practical and safety reasons. It can therefore not be confirmed if the hydrogen is the reason. Nevertheless, the samples were not suited for further use, and the 0.1 mol dm^{-3} solution was discarded for further experiments. Again, Yoshida *et al.* [55] used 0.1 mol dm^{-3} and reported of trouble with

the coverage as well.

The highest concentration of $\text{Zn}(\text{NO}_3)_2$ also produced the best performing electrodes. As shown in Figure 4.15, the photocurrent generated at 512 nm was much lower for the electrode made from a concentration of 0.5 mol dm^{-3} than from 1 mol dm^{-3} . Also the deposition current was lower for the lower concentration, as seen in Figure 4.13. The deposition current even diminished towards the end of the deposition. The obvious difference between the two is the amount of ions in the nitrate solution. The accessibility of ions in the solution is higher when the concentration is higher, which makes it easier for reactions to happen. Another factor that might affect the deposition is the ratio of eosin Y to $\text{Zn}(\text{NO}_3)_2$. As NO_3^- is reduced to NO_2^- and ZnO precipitate, NO_3^- and Zn^{+2} need to diffuse to the surface. The eosin Y molecules are larger than the NO_3^- and Zn^{+2} -ions, which might make it harder at lower concentrations to reach the electrode by diffusion. Though the mechanisms behind are uncertain, it has been empirically shown that higher concentrations of $\text{Zn}(\text{NO}_3)_2$ produce better films. The $\text{Zn}(\text{NO}_3)_2$ -concentration during PHE was therefore chosen to be 1 mol dm^{-3} .

Temperature

Temperature is an important factor which can be difficult to control by this easy set up. Diffusion, pH and the thermodynamic driving forces of the reaction are dependent on the temperature, which again affects the deposition [52]. There was a drastic difference between the deposition at room temperature and at 40°C as seen in Figure 4.12.

The temperature during the deposition could explain the variability observed from sample to sample. Since there is no stirring and the temperature is measured at a single point, it is possible that there is a temperature gradient in the cell. Also, the light exposure by the solar simulator might have affected the temperature in the bath. Though the heating might have been accounted for by a feedback loop from the thermometer to the hot plate, the exact temperature of the nitrate bath is not known.

For better control of the temperature, a closed cell in a water bath can be used. Other works on electrodeposition go to even higher temperature, such as 70°C . This was not possible with this set-up due to two reasons, evaporation of water and the glass transition temperature of the PLA-plastic in the electrode holder. 40°C is sufficient to create working electrodes in an easy, low temperature way. Otani *et al.* found that the material deposited at temperatures of 40°C lost the hexagonal facets of zincite [49]. No clear hexagonal structures were observed in this work either. However, the three distinct XRD-peaks of ZnO present between 30° and 40° in the top graph of Figure 4.11, confirm zincite after the heat treatment at 125°C .

5.1.4 Future outlook of electrodeposition

Based on the discussion above, PHE arises as the best way, so far, to make ZnO by electrodeposition. By introducing dye-molecules to the nitrate solution, and exposing the synthesis to light, the electrodeposited electrodes have improved from not generating a photocurrent at all (SE), to a conversion efficiency of 3.42% at 512 nm (PHE). This makes PHE a promising low-temperature ZnO deposition method.

However, PHE is a sensitive deposition method. The conversion efficiency at 512 nm of PHE cells varied from 2.36% to 3.42%. The reason for this is unclear, as all films were deposited in the same way. The many reactions taking place is the most likely explanation. Other factors are temperature variations, concentration gradients, intensity of incident light, and electrode connection to the potentiostat, which are all aspects of the electrodeposition that are difficult to control in the simple set-up used in this work. A more advanced and closed set-up might limit sample variations.

High temperature electrode manufacture still produce better electrodes than low temperature electrode manufacture. When sensitized with N719, the conversion efficiency at 512 nm was 5.03% for the doctor bladed cell (high temperature), and 3.42% for the best PHE-cell (low temperature). The IPCE-dye peak of the doctor bladed cell on day 1 in Figure 4.18a is much higher than the best PHE-cell in Figure 4.7. From the project work, it is known that the doctor bladed electrodes are porous and much thicker (approximately 23 μm), and therefore have a larger area where the dye-molecules can adsorb [12].

In addition to the dye adsorption, the connection between the ZnO particles can be a reason for the difference in performance. The only difference between the two electrodes was the ZnO. The doctor bladed samples were annealed to ensure good connections between the particles. For PHE, the material deposited was $\text{Zn}_5(\text{NO}_3)_2(\text{OH})_8$, which was transformed into ZnO by drying at 125 °C. How well this transformation was is, however, uncertain. There were still some intensity peaks that were not characteristic of ZnO after the heat treatment, such as 9 °, 26 °, 42 ° and 44 °. There is a possibility that there are many grain-boundaries in the PHE-film acting as recombination centers. More characterization of the PHE-cells is needed to determine the cause of the lesser performance and improve to the deposition method even further.

5.2 Degradation

The performance of the N719-electrode was high on day 1. The short circuit current, the open circuit voltage and the fill factor were all high, as seen in Figure 4.19a. At 512 nm, the conversion efficiency of the cell was 5.03%, which is the highest recorded value for all cells made by the author. The performance is strengthened by the fact that the IPCE-spectra gave the same short circuit current at 512 nm as the IV-measurement, as seen in Table 4.2. It is difficult to compare to literature as this characterization is performed under monochromatic light, and not standard test conditions. Nevertheless, the electrodes with two doctor bladed nanoparticle layers on top of a SE-layer are promising high-temperature electrodes. As is evident from the following discussion, dye-molecules compatible with ZnO need to be discovered.

5.2.1 Anchoring groups

The anchor groups serve an important role in keeping the dye molecules adsorbed to the surface of ZnO. The bleaching of the eosin Y-electrode is evident in the loss of color between Figure 4.17c and 4.17e. All of the pink color had been removed in the area where the electrode had been in contact with the electrolyte, and only the yellow color of the electrolyte was left. This severe bleaching was not observed for the N719-electrode from Figure 4.17b to 4.17d. N719 has two carboxylic anchoring groups, while eosin Y does not have any anchoring groups. The lack of binding to the surface of ZnO is likely the cause of the bleaching.

The removal of eosin Y from the electrode surface happens fast. In Figure 4.17f, a completely bleached electrode is imaged after just 2 hours of characterization. Anta *et al.* [20], suggest that *tert*-butylpyridine (TBP) in the electrolyte helps speed up the bleaching process of ZnO/eosin Y-electrodes. TBP is an additive that is added to increase the open circuit voltage in the cell through raising the position of the conduction band of the semiconductor. It operates by adsorbing to the surface of ZnO. If the connection between ZnO and TBP is stronger than between ZnO and eosin Y, the eosin Y will be removed.

When the dye molecules are removed from the surface, no photocurrent is generated. In Figure 4.18b, the IPCE-dye peak from 440 nm to 580 nm, corresponding to absorption in eosin Y, had almost completely disappeared on day 2. This indicates that little electron transfer is taking place between the dye and ZnO. The IV-curves in Figure 4.19b also confirms low photocurrent generation of less than 0.1 mA on all days. Since the dye molecules are removed from the electrode, the electron transfer from dye to semiconductor is very unlikely. The eosin Y electrodes are therefore useless for DSSC-application.

5.2.2 Degradation of the ZnO/N719-electrode

Even though the acidic anchoring groups are better than no anchoring groups, they degrade ZnO too fast. It is a known fact that the carboxylic acid groups of N719 degrade ZnO [10]. The total quantum efficiency of the N719-electrode dropped by 37.7% from day 1 to day 15. This fast degradation could be observed in both the IPCE- and IV-characteristics in Figure 4.18a and Figure 4.19a. The fast degradation was also observed in the project work when the total quantum efficiency diminished by 24.5% in 8 days, which is similar to the decrease between day 1 and 8 in this work (25.3%). A 37.7% decrease in 2 weeks is not acceptable, and the lifetime of the electrodes need to be improved if ZnO-cells are to be commercialized. Silicon solar cells have an expected lifetime of more than 20 years, and are considered to be expired when they drop below 80% of their original conversion efficiency [61]. That limit was reached within 1 week for the cells in this work. The degradation remains the main bottleneck for ZnO-DSSCs.

The degradation happens though the removal of dye and ZnO from the electrode. This has been reported by Keis *et al.* [10] and Ke *et al.* [11], and now also by this work. The removal of dye is evident from visual inspection, comparing Figure 4.17b and Figure 4.17d. Even though the bleaching of the N719-electrode was not as severe as for the eosin Y-electrode, it is evident that dye removal has taken place. The removal of ZnO from the electrode has not been directly confirmed by measurements, however the following discussion of the resistances in the cell, give indications that also ZnO has been dissolved. Dissolution of ZnO to Zn^{2+} and O^{2-} at low pH-values follows the Pourbaix-diagram in Figure 2.12.

The degradation of the electrode affects the performance in several ways. The following discussion will be based on the equivalent circuit in Figure 2.11, and the modeling of the resistances in the cell, presented in Figure 4.22. The total resistance in the cell had increased from day 1 to day 15. It is clear from Figure 4.22 that the parallel resistance and the series resistance had remained close to unchanged. This is reasonable, since the PECC2-cell was used, keeping the counter electrode and the circuitry in the cell stable. The diffusion resistance and the recombination resistance had increased, while the transport resistance had decreased. These three resistances are all related to the electrode, and a change in them agrees with the degradation of the electrode.

The decreased transport resistance is most likely due to shorter paths for the electrons to travel. When ZnO in the electrode is dissolved, the ZnO-layer left will be thinner than the original. A shorter path means that the electrons have to visit fewer trap-states along the way to the FTO, and the resistance experienced in the ZnO is therefore lower. The dye molecules left after bleaching are also the closest to the FTO. The remaining dye-molecules will inject electrons into the ZnO closer to the FTO than the ones that were

removed. The electron-path was therefore shorter and the transport time faster. The shorter transport time in the Table 4.3 supports the decrease in transport resistance.

The removal of dye-molecules, Zn^{2+} and O^{2-} from the electrode and their addition into the electrolyte is most likely the reason for the increase in diffusion resistance. With more ions in the electrolyte, the collision rate of the redox-species will increase, and its diffusion in the electrolyte is hindered. Also, the formation of $\text{Zn}^{2+}/\text{N719}$ -complexes agglomerating in the pores of the electrode can increase the diffusion resistance. The complexes will make it harder for the redox-species to reach and regenerate dye-molecules still at the ZnO-surface.

The origin of the change in recombination resistance is unknown. The modelling of the resistances in Figure 4.22 indicates that the recombination resistance had increased, while the recombination time from the IMVS in Table 4.3 had decreased. This means that fewer electron hole pairs recombine, but the recombination that occurs, is happening faster. Less recombination could simply be due to less electrons being injected, since dye-molecules have been removed. The possible changed recombination centers in the cell are the zinc oxide, the dye-molecules, or changed energy levels in the cell.

The dissolution of ZnO may have created more intermediate surface states where recombination can happen. As ZnO is removed from the electrode, the surface-to-volume ratio of the ZnO will increase. This makes a larger part of the electrode possible recombination sites for electrons. A thinner electrode will give the electrons a shorter path to the recombination sites, making the recombination time shorter.

The probability of recombination with the electrolyte or the dye-molecule could have changed. The open circuit voltage in the cell had increased, meaning that the position of the energy levels in the cell had shifted. This may have changed the overlapping between the conduction band in ZnO and density of states in the electrolyte and the dye, changing the probability of recombination.

Dye-molecules might be recombination centers. The amount of light absorption in the region where only the dye was active had decreased during the trial, as seen in the IPCE-spectra in Figure 4.18a, while the peak in the ZnO region had increased. N719 is also active in the same short-wavelength region as ZnO [24]. If the dye-molecules were the recombination centers, it makes sense that the IPCE in this region would increase, and that the recombination resistance increase as the dye-molecules are removed.

To summarize, it is unknown what the recombination centers in the cell are. The creation of intermediate surface states due to dissolution of the ZnO fit with the shorter recombination time, while the larger recombination resistance could be a consequence of less electrons being injected into the ZnO. The dye molecules are also probable recombination centers.

The modeling of the recombination in the cell was not perfect. Figure 4.20 shows that the model does not fit the data on Day 15, and the calculated IV-curve on day 15 in Figure 4.21 does not overlap with the data-set as well as it did on Day 1. Another odd observation is the increase in recombination resistance from 0.59 V to 0.60 V on day 15, the line should have been linear. Since only one cell was measured, the statistical evidence for the recombination is non-existent. More characterization is needed to determine the effects of degradation with certainty. However, the degradation of ZnO/N719 cells is extreme and was observed both in this work and in the project work. Efforts should be put towards finding alternative, ZnO-friendly, dye-molecules or solutions to protect the ZnO, instead of investigating the commonly agreed upon poor combination of ZnO and N719.

5.3 Atomic layer deposition of titanium dioxide

100 nm of TiO_2 clogs the pores in the ZnO. The electrode covered with TiO_2 , imaged in Figure 4.23, did not stain properly. This was uncharacteristic both of the doctor bladed electrode and TiO_2 in general. N719 is a dye which normally works well with TiO_2 electrodes [24]. A possible explanation is that the layer of TiO_2 clogged the pores, making most of the electrode inaccessible to the dye molecules. Li *et al.* found that too thick layers of TiO_2 clog the electrodes [62]. The SEM-images in Figure 4.24 also give an indication of this. The sample without the TiO_2 appears to be more porous than the one with TiO_2 .

The TiO_2 thickness of 100 nm was chosen as an initial test to ensure complete coverage of the ZnO. If the dye molecules were given access to the ZnO, they could degrade the ZnO, creating a hollow shell of TiO_2 . The idea was to start with a thick layer and then decrease the layer thickness if needed. The experiment confirmed that 100 nm was too thick, as the electrode did not stain properly. Trials with thinner layers were unfortunately not possible, as a pump in the ALD-machine broke down.

It is not clear what the crystal structure or oxidation state of the deposited TiO_2 was. This might have affected the staining, as the anchoring between the dye and the semiconductor is surface dependent [33]. According to Kim *et al.* [63], the TiO_2 deposited by ALD is amorphous or nanocrystalline when deposited at temperatures lower than 225 °C. Sun *et al.* found material deposited at 25 °C to be amorphous [64]. An amorphous material is not optimal with regards to electron transport, as it introduces many trap states [64]. Further investigations of the state of the TiO_2 by X-ray photoelectron spectroscopy (XPS) and XRD would be needed gain knowledge about the deposited material. This was, however, not prioritized since more ALD-samples could not be made.

Sun and his coworkers [64], found that the performance of ALD- TiO_2 /ZnO cells increased when sensitized with N719, but decreased when sensitized with an organic dye called D149. N719 is a dye that works well with TiO_2 , while D149 is reported to work well with ZnO [8]. Sun *et al.* [64] concluded that the method did not improve the cells significantly. Be that as it may, the fact that the performance is slightly increased with N719, and not decreased, is interesting. As discussed in the previous section, N719 degrades ZnO fast, and this is the real problem with ZnO-electrodes. If the ALD layer cooperates well with N719, it could prolong the lifetime of ZnO/N719-cells. Further investigations, including the long-term stability of the cells with ALD- TiO_2 is needed.

Chapter 6

Conclusions

The work has demonstrated that it is possible to make dye-sensitized solar cells with zinc oxide as the semiconducting material. It is an advantage to be able to deposit zinc oxide at a low temperature using electrodeposition, and important improvements to this technique have been made. Changing from a standard electrodeposition to a photoassisted hybrid electrodeposition improved the photoelectric performance of the electrodes from not producing any photocurrent at all, to achieving a conversion efficiency at 512 nm of 3.22%. Still, the best performing ZnO-electrode in this work was made by one layer of standard electrodeposition followed by two layers of doctor blading, which is a high-temperature synthesis. When sensitized with N719 and illuminated by 512 nm, it achieved a conversion efficiency of 5.03%.

The best way to perform electrodeposition of ZnO from a nitrate bath found so far is a photoassisted hybrid electrodeposition. The deposition was performed with a potentiodynamic application of potential between -1 V and -0.2 V. The $\text{Zn}(\text{NO}_3)_2$ -concentration was 1 mol dm^{-3} , the temperature was 40°C , and eosin Y was present in the nitrate bath, while the whole solution was exposed to light from a solar simulator. The produced electrodes needed to be dried at 125°C to transform the deposited material from $\text{Zn}_5(\text{NO}_3)_2(\text{OH})_8$ to zincite-ZnO. Electrodeposition of ZnO is a sensitive technique, and further optimization of the synthesis is needed to ensure equal results every time.

Acidic anchoring groups of the dye molecule N719 degrade ZnO-electrodes fast. 37.7% of the cell's original total quantum efficiency was lost within 15 days. The cells degrade by dye-desorption and dissolution of ZnO. The degradation causes a larger diffusion resistance in the cell's electrolyte. It was confirmed that anchoring groups are important to keep the dye molecules at the surface. Even though the acidity of carboxylic acid groups degrades ZnO, using dye molecules without the group at all is no option, as ZnO-cells sensitized with eosin Y was useless after a few hours. An optimal dye for ZnO should yield high quantum efficiency and not degrade the ZnO. In order for ZnO to be considered a real

competitor to TiO₂ DSSCs, a dye that meets these requirements must be identified.

100 nm of TiO₂ deposited on top of ZnO by ALD does not help in protecting ZnO-electrodes from degradation. In fact, it ruins the electrodes by clogging the pores. Thinner layers should be investigated further.

Dye sensitized solar cells with ZnO are possible to make, and the performance of the cells is promising. Advances were made in the electrodeposition of ZnO, especially the finding that the exposure to light helps the increase the growth of ZnO during hybrid electrodeposition. For ZnO-DSSCs advance, dye-molecules which does not corrode ZnO is needed. This is the real bottle neck of ZnO-based DSSCs.

Chapter 7

Further work

The main bottle-neck for ZnO-DSSCs is the fast degradation. Dye-molecules that does not dissolve ZnO is needed for the ZnO-DSSCs to compete with other solar cell technologies. An extensive search for the best dye is needed.

Electrodeposition of ZnO

There are many aspects with the photoassisted hybrid electrodeposition that could be optimized further.

Light exposure

Eosin Y only absorbs light from 440 nm to 580 nm. Optimizing the light exposure during the photoassisted electrodeposition to obtain the maximum effect of the light should be done. Also improving the set up, to get a higher light intensity at the electrode could improve the deposition.

Concentration of eosin Y

The same concentration of eosin Y was used for all hybrid electrodepositions and photoassisted hybrid electrodepositions. The eosin Y have an effect on the structure of the deposited material. Finding an optimal amount if eosin Y could improve the electrodes. This could also be seen with regards to the concentration of $\text{Zn}(\text{NO}_3)_2$.

The potentiodynamic technique

The vertex potentials and the sweeping rate in the potentiodynamic application of potential could also be optimized further. It was not investigated if other intervals resulted in equal or better films. The deposition in this work lasted for two hours, and it would be beneficial from a production point of view if a faster deposition procedure is obtained.

Make complete cells

Make complete cells that are comparable to the other cells made by our group. Then fully characterize the resistances in the electrode with the EIS to understand where electrodeposited ZnO needs improving. It important is to characterize the cells with a light

beam that is larger than the cell area to be able to find the current density, and thus be able to compare to other cells.

More characterization

A thorough characterization of the deposited material should be conducted with more XRD and SEM in addition to X-ray photoelectron spectroscopy.

Make flexible solar cells

One of the selling arguments for electrodeposition is the low synthesis temperature. Making flexible DSSCs with electrodeposited ZnO would be an interesting next step.

Other applications

It is possible to explore other applications for the PHE thin films than DSSCs. The films produced are easy to make, created at a low temperature, and does not require many tools to create. It is quite simple to scale the production. Though there might be problems with the electron conduction in the FTO as the samples grow larger, but for samples of 6.25 cm^2 , no noticeable difference in thickness was observed between the area closest to and furthest away from the contact clip to the potentiostat.

Degradation

To gain statistical power in the degradation of the ZnO-electrode, several more trials to investigate the degradation should be conducted. The structure of the surface before and after could be characterized, along with the total dye-adsorption and the composition of the electrolyte. However, it obvious that the degradation of N719/ZnO-electrodes is so fast that the cells are not of any commercial value. Efforts should be put into finding dye-molecule better suited for ZnO, and improve the morphology and crystallinity of ZnO.

ALD

As for the ALD of TiO_2 on top of ZnO, there is a lot more that could be investigated. An easy test to do is to see if a thinner layer of TiO_2 will line the inside of the pores without filling them. This was initially the plan to do, but the ALD broke down. If a thinner layer does not work, it is possible to further characterize the deposited TiO_2 . It would be beneficial to see what state the material is in right after deposition to understand why it is black. This can be done by X-ray photoelectron spectroscopy. The crystal structure of the film could be characterized by grazing incident X-ray reflection. If a thinner layer works, then long-term stability of the cells should be investigated. There is also the possibility to try the ALD on top of the electrodeposited films, to improve their stabilities. Again, a much thinner TiO_2 -layer is needed.

Bibliography

- [1] IPCC, Summary for Policymakers. In: Global warming of 1.5 °C. An IPCC special report on the impacts of global warming of 1.5 °C above pre-industrial levels and related global greenhouse gas emission pathways, in the context of strengthening the global response to the threat of climate change, sustainable development, and efforts to eradicate poverty [V. Masson-Delmotte, P. Zhai, H. O. Pörtner, D. Roberts, J. Skea, P.R. Shukla, A. Pirani, W. Moufouma-Okia, C. Péan, R. Pidcock, S. Connors, J. B. R. Matthews, Y. Chen, X. Zhou, M. Gomis, E. Lonnoy, T. Maycock, M. Tignor, T. Waterfield, (eds.)], World Meteorological Organization, Geneva, Switzerland, 2018.
- [2] L. Mostue, Energi 21 - summary report strategy 2018 (2018).
- [3] B. O'Regan, M. Grätzel, A low-cost, high-efficiency solar cell based on dye-sensitized colloidal TiO₂ films, *Nature* 353 (1991) 737–740.
- [4] J. Gong, J. Liang, K. Sumathy, Review on dye-sensitized solar cells (dsscs): Fundamental concepts and novel materials, *Renewable and Sustainable Energy Reviews* 16 (8) (2012) 5848 – 5860.
- [5] K. Sharma, V. Sharma, S. S. Sharma, Dye-sensitized solar cells: Fundamentals and current status, *Nanoscale Research Letters* 13 (1) (2018) 381.
- [6] G. Instruments, Dssc: Dye sensitized solar cells basic principles and measurements, downloaded 26.03.2019.
- [7] Solaronix, Solaronix solar cells (2014).
URL <http://www.solaronix.com/solarcells/>
- [8] A. Hagfeldt, G. Boschloo, L. Sun, L. Kloo, H. Pettersson, Dye-sensitized solar cells, *Chemical Reviews* 110 (11) (2010) 6595–6663.
- [9] R. Vittal, K.-C. Ho, Zinc oxide based dye-sensitized solar cells: A review, *Renewable and Sustainable Energy Reviews* 70 (2017) 920–935.

- [10] K. Keis, J. Lindgren, S.-E. Lindquist, A. Hagfeldt, Studies of the adsorption process of ru complexes in nanoporous zno electrodes, *Langmuir* 16 (10) (2000) 4688–4694.
- [11] L. Ke, S. Dolmanan, L. Shen, P. Pallathadk, Z. Zhang, H. Liu, Degradation mechanism of zno-based dye-sensitized solar cells, *Solar Energy Materials and Solar Cells* 94 (2) (2010) 323–326.
- [12] M. Nyhaug, Fabrication of zinc oxide photoanodes for use in dye-sensitized solar cells by combining the methods electrochemical deposition and doctor blading, TMT4510 Nanotechnology, Specialization Project, Supervised by Svein Sunde (2018).
- [13] H. Minoura, T. Yoshida, Electrodeposition of ZnO/dye hybrid thin films for dye-sensitized solar cells, *Electrochemistry* 76 (2008) 109–117.
- [14] J. Nelson, *The physics of solar cells*, 1st Edition, Imperail Collage Press, Covent Garden, London, 2003.
- [15] F. H. Alharbi, S. Kais, Theoretical limits of photovoltaics efficiency and possible improvements by intuitive approaches learned from photosynthesis and quantum coherence, *Renewable and Sustainable Energy Reviews* 43 (2015) 1073 – 1089.
- [16] The National Renewable Energy Laboratory, Solar spectrum data set, downloaded on 15.11.2018.
URL <https://www.nrel.gov/grid/solar-resource/spectra.html>
- [17] C. Kittel, *Introduction to solid State Physics*, 8th Edition, John Wiley & Sons, 2005.
- [18] R. Memming, *Semiconductor electrochemistry* (2001).
- [19] K. B. Oldham, *Electrochemical science and technology : fundamentals and applications* (2013).
- [20] J. A. Anta, E. Guillén, R. Tena-Zaera, Zno-based dye-sensitized solar cells, *The Journal of Physical Chemistry C* 116 (21) (2012) 11413–11425.
- [21] R. Syafinar, N. Gomesh, M. Irwanto, M. Fareq, Y. Irwan, Chlorophyll pigments as nature based dye for dye-sensitized solar cell (dssc), *Energy Procedia* 79 (2015) 896 – 902, 2015 International Conference on Alternative Energy in Developing Countries and Emerging Economies.
- [22] R. Syafinar, N. Gomesh, M. Irwanto, M. Fareq, Y. Irwan, Potential of purple cabbage, coffee, blueberry and turmeric as nature based dyes for dye sensitized solar cell (dssc), *Energy Procedia* 79 (2015) 799 – 807, 2015 International Conference on Alternative Energy in Developing Countries and Emerging Economies.

- [23] D. Sinha, D. De, A. Ayaz, Performance and stability analysis of curcumin dye as a photo sensitizer used in nanostructured zno based dssc, *Spectrochimica Acta Part A: Molecular and Biomolecular Spectroscopy* 193 (2018) 467 – 474.
- [24] Solarinix, Switzerland, Ruthenizer 535-bisTBA (2013).
URL <http://shop.solaronix.com/sensitizing-dyes/ruthenium-dyes/ruthenizer-535-bistba.html>
- [25] R. W. Sabnis, *Handbook of Biological Dyes and Stains : Synthesis and Industrial Applications*, John Wiley & Sons, Incorporated, 2010.
- [26] E. Guillén, F. Casanueva, J. Anta, A. Vega-Poot, G. Oskam, R. Alcántara, C. Fernández-Lorenzo, J. Martín-Calleja, Photovoltaic performance of nanostructured zinc oxide sensitised with xanthene dyes, *Journal of Photochemistry and Photobiology A: Chemistry* 200 (2-3) (2008) 364–370.
- [27] G. Sharma, P. Balraju, M. Kumar, M. Roy, Quasi solid state dye sensitized solar cells employing a polymer electrolyte and xanthene dyes, *Materials Science and Engineering: B* 162 (1) (2009) 32 – 39.
URL <http://www.sciencedirect.com/science/article/pii/S0921510709000701>
- [28] SIGMA-ALDRICH Norway AS, Eosin Y sikkerhetsdatablad, CAS-number = 15086-94-9 (2018).
- [29] R. T. Ako, P. Ekanayake, D. J. Young, J. Hoblely, V. Chellappan, A. L. Tan, S. Gorelik, G. S. Subramanian, C. M. Lim, Evaluation of surface energy state distribution and bulk defect concentration in dssc photoanodes based on sn, fe, and cu doped tio₂, *Applied Surface Science* 351 (2015) 950 – 961.
- [30] J. Bisquert, R. A. Marcus, *Device Modeling of Dye-Sensitized Solar Cells*, Springer Berlin Heidelberg, Berlin, Heidelberg, 2014, Ch. 8, pp. 325–395.
- [31] J. A. Ben Rogers, S. Pennathur, *Nanotechnology - Understanding small systems*, third edition Edition, CRS Press, Boca Raton, Florida, USA, 2015.
- [32] J. Oh, W. Ghann, H. Kang, F. Nesbitt, S. Providence, J. Uddin, Comparison of the performance of dye sensitized solar cells fabricated with ruthenium based dye sensitizers: Di-tetrabutylammonium cis-bis(isothiocyanato)bis(2,2'-bipyridyl-4,4'-dicarboxylato)ruthenium(ii) (n719) and tris(bipyridine)ruthenium(ii) chloride (ru-bpy), *Inorganica Chimica Acta* 482 (2018) 943–950.

- [33] C. O'Rourke, D. Bowler, Dssc anchoring groups: A surface dependent decision, *Journal of Physics Condensed Matter* 26 (19).
- [34] L. Zhang, J. M. Cole, Anchoring groups for dye-sensitized solar cells, *ACS Applied Materials & Interfaces* 7 (6) (2015) 3427–3455.
- [35] C.-Y. Lin, Y.-H. Lai, H.-W. Chen, J.-G. Chen, C.-W. Kung, R. Vittal, K.-C. Ho, Highly efficient dye-sensitized solar cell with a zno nanosheet-based photoanode, *Energy Environ. Sci.* 4 (2011) 3448–3455.
- [36] S. Miyajima, ENR.L410 Introduction to photovoltaics, lectures (2018).
- [37] F. Fabregat-Santiago, G. Garcia-Belmonte, I. Mora-seró, J. Bisquert, Characterization of nanostructured hybrid and organic solar cells by impedance spectroscopy, *Physical Chemistry Chemical Physics* 13 (20) (2011) 9083–9118.
- [38] Q. Zhang, C. S. Dandeneau, X. Zhou, G. Cao, Zno Nanostructures for Dye-Sensitized Solar Cells, *Advanced Materials* 21 (2009) 4087–4108.
- [39] Zahner-Elektrik, Pec-cells, downloaded on 23.04.2019 (2019).
URL <http://zahner.de/products/photoelectrochemistry/pec-cells.html>
- [40] N. Storey, *Electronics : a systems approach* (2013).
- [41] G. Instruments, Dye solar cells – part 2: Impedance measurements, downloaded 26.03.2019.
- [42] H. E. Hansen, Reconstructing the IV-curve of dye-sensitized solar cells from impedance data, TMT 4510 Nanotechnology, Specialization Project, unpublished (2018).
- [43] G. Instruments, Dye solar cells – part 3 imps and imvs measurements, downloaded 26.03.2019.
- [44] M. E. Orazem, B. Tribollet, *Electrochemical impedance spectroscopy*, Electrochemical Society series, Wiley, Hoboken, N.J., 2008, Ch. 19, pp. 363–383.
- [45] B. Murty, *Textbook of nanoscience and nanotechnology* (2013).
- [46] A. J. Garret-Reed, D. C. Bell, *Energy-Dispersive X-Ray Analysis in the electron microscope*, BIOS Scientific Publisher Ltd, Oxford, UK, 2003.

- [47] T. Yoshida, M. Iwaya, H. Ando, T. Oekermann, K. Nonomura, D. Schlettwein, D. Wöhrle, H. Minoura, Improved photoelectrochemical performance of electrodeposited znO/eosiny hybrid thin films by dye re-adsorption, *Chemical Communications* 4 (4) (2004) 400–401.
- [48] T. Yoshida, M. Tochimoto, D. Schlettwein, D. Wöhrle, T. Sugiura, H. Minoura, Self-assembly of zinc oxide thin films modified with tetrasulfonated metallophthalocyanines by one-step electrodeposition, *Chemistry of Materials* 11 (10) (1999) 2657–2667.
- [49] S. Otani, J. Katayama, H. Umemoto, M. Matsuoka, Effect of bath temperature in the electrodeposition mechanism of zinc oxide film from nirtate solution, *Journal of The Electrochemical Society* 153 (8) (2006) C551–C556.
- [50] S. Nayak, Investigation of electrochemical oxygen reduction on semiconductor surfaces by attenuated total internal reflection infrared spectroscopy, chapter 9: Electrochemical atr-ir study of orr on zinc oxide thin films, Ph.D. thesis, Max-Planck-Institut für Eisenforschung GmbH (2013).
- [51] A. G. Blackman, L. R. Gahan, Aylward and Findlay's SI chemical data, 7th Edition, John Wiley and Sons, Australia, 2014.
- [52] S. S. Zumdahl, *Chemical principles*, sixth edition Edition, Hughton Mifflin Company, University of Illinois, 2009.
- [53] T. Yoshida, K. Terada, D. Schlettwein, T. Oekermann, T. Sugiura, H. Minoura, Electrochemical self-assembly of nanoporous znO/eosin y thin films and their sensitized photoelectrochemical performance, *Advanced Materials* 12 (16) (2000) 1214–1217.
- [54] T. Yoshida, T. Pauporté, D. Lincot, T. Oekermann, H. Minoura, Cathodic electrodeposition of znO/eosin y hybrid thin films from oxygen-saturated aqueous solution of zncl₂ and eosin y, *Journal of the Electrochemical Society* 150 (9) (2003) C608–C615.
- [55] T. Yoshida, J. Zhang, D. Komatsu, S. Sawatani, H. Minoura, T. Pauporté, D. Lincot, T. Oekermann, D. Schlettwein, H. Tada, D. Wöhrle, K. Funabiki, M. Matsui, H. Miura, H. Yanagi, Electrodeposition of inorganic/organic hybrid thin films, *Advanced Functional Materials* 19 (1) (2009) 17–43.
- [56] H. Guo, X. He, C. Hu, Y. Tian, Y. Xi, J. Chen, L. Tian, Effect of particle size in aggregates of ZnO-aggregate-based dye-sensitized solar cells, *Electrochimica Acta* 120 (2014) 23–29.

- [57] H. Knoops, S. Potts, A. Bol, W. Kessels, 27 - atomic layer deposition, in: T. F. Kuech (Ed.), *Handbook of Crystal Growth (Second Edition)*, second edition Edition, *Handbook of Crystal Growth*, North-Holland, Boston, 2015, pp. 1101 – 1134.
- [58] S. Zhang, Study of fluorine-doped tin oxide (fto) thin films for photovoltaics applications, Ph.D. thesis, Université Grenoble Alpes; Technische Universität, Darmstadt, Allemagne (3 2017).
- [59] Q. Hou, L. Zhu, H. Chen, H. Liu, W. Li, Growth of flower-like porous zno nanosheets by electrodeposition with $\text{Zn}_5(\text{OH})_8(\text{NO}_3)_2 \cdot 2\text{H}_2\text{O}$ as precursor, *Electrochimica Acta* 78 (2012) 55 – 64.
- [60] W. Stählin, H. R. Oswald, The crystal structure of zinc hydroxide nitrate, $\text{Zn}_5(\text{OH})_8(\text{NO}_3)_2 \cdot 2\text{H}_2\text{O}$, *Acta Crystallographica B*26 (1970) 860–863.
- [61] M. E. Flowers, M. K. Smith, A. W. Parsekian, D. S. Boyuk, J. K. McGrath, L. Yates, Climate impacts on the cost of solar energy, *Energy Policy* 94 (2016) 264 – 273.
- [62] Y. Li, L. Ma, Y. Yoo, G. Wang, X. Zhang, M. Ko, Atomic layer deposition: A versatile method to enhance tio 2 nanoparticles interconnection of dye-sensitized solar cell at low temperature, *Journal of Industrial and Engineering Chemistry* 73 (2019) 351–356.
- [63] W. D. Kim, G. W. Hwang, O. S. Kwon, S. K. Kim, M. Cho, D. S. Jeong, S. W. Lee, M. H. Seo, C. S. Hwang, Y.-S. Min, Y. J. Cho, Growth characteristics of atomic layer deposited tio2 thin films on ru and si electrodes for memory capacitor applications, *Journal of The Electrochemical Society* 152 (8) (2005) C552–C559.
- [64] H. Sun, H. Kurotaki, K. Kanomata, F. Hirose, M. White, T. Yoshida, Zno/tio 2 core-shell photoelectrodes for dye-sensitized solar cells by screen printing and room temperature ald, *Microsystem Technologies* 24 (1) (2018) 647–654.
- [65] Elteip 50 mm - artikkelnummer: 22-300.
URL <https://www.clasohlson.com/no/Elteip-50-mm/Pr220300000>

Appendix A

Chemicals and materials

A.1 List of chemicals and materials

Dyes

- Eosin Y from Sigma-Aldrich: dye content 99%
- Ruthenizer 535-bisTBA (N719) from Solaronix

Electrodeposition

- Zinc nitrate tetrahydrate from Merck: $\text{Zn}(\text{NO}_3)_2 \times 4 \text{H}_2\text{O} \geq 98.5\%$
- Zinc nitrate hexahydrate from Sigma-Aldrich: $\text{Zn}(\text{NO}_3)_2 \times 6 \text{H}_2\text{O}$, crystallized $\geq 99.0\%$
- Zinc foil from Alfa Aesar: 0.5mm thick, 99.994%

Doctor blading

- Zinc Oxide nano particles from Sigma-Aldrich: 20 wt% in H_2O , size $< 100 \text{ nm}$ (TEM)
- Ethyl Cellulose from Sigma-Aldrich: viscosity 10 cP, 5 % in toluene/ethanol 80:20(lit.), extent of labeling: 48% ethoxyl
- Terpeneol from Sigma-Aldrich: mixture of isomers, analytical standard

Electrolyte

- 4-tertbutylpyridine from Sigma-Aldrich: 98%
- Tetrabutylammonium iodide from Sigma-Aldrich: electrochemical analysis, $\geq 99.0\%$
- Iodine from Sigma-Aldrich: anhydrous, beads, -10 mesh, 99.999% trace metals basis

- Lithium iodide from Sigma-Aldrich: crystalline powder, 99.9% trace metals basis
- Acetonitrile from Sigma-Aldrich: anhydrous, 99.8%

Other

- Glass coated with fluorine doped tin oxide from Sigma-Aldrich: resistance $10 \Omega \text{ sq}^{-1}$, thickness 3mm, size: 300x300 mm
- Sulphuric Acid from VWR: 95%
- Potassium hydroxide from Merck: $\geq 85\%$, solid
- TDMA from Sigma-Aldrich: 99.999%
- Milli-Q DI-water
- Insulation tape from Clas Ohlson [65]

Appendix B

Supplementary results

B.1 Electrodeposition of ZnO

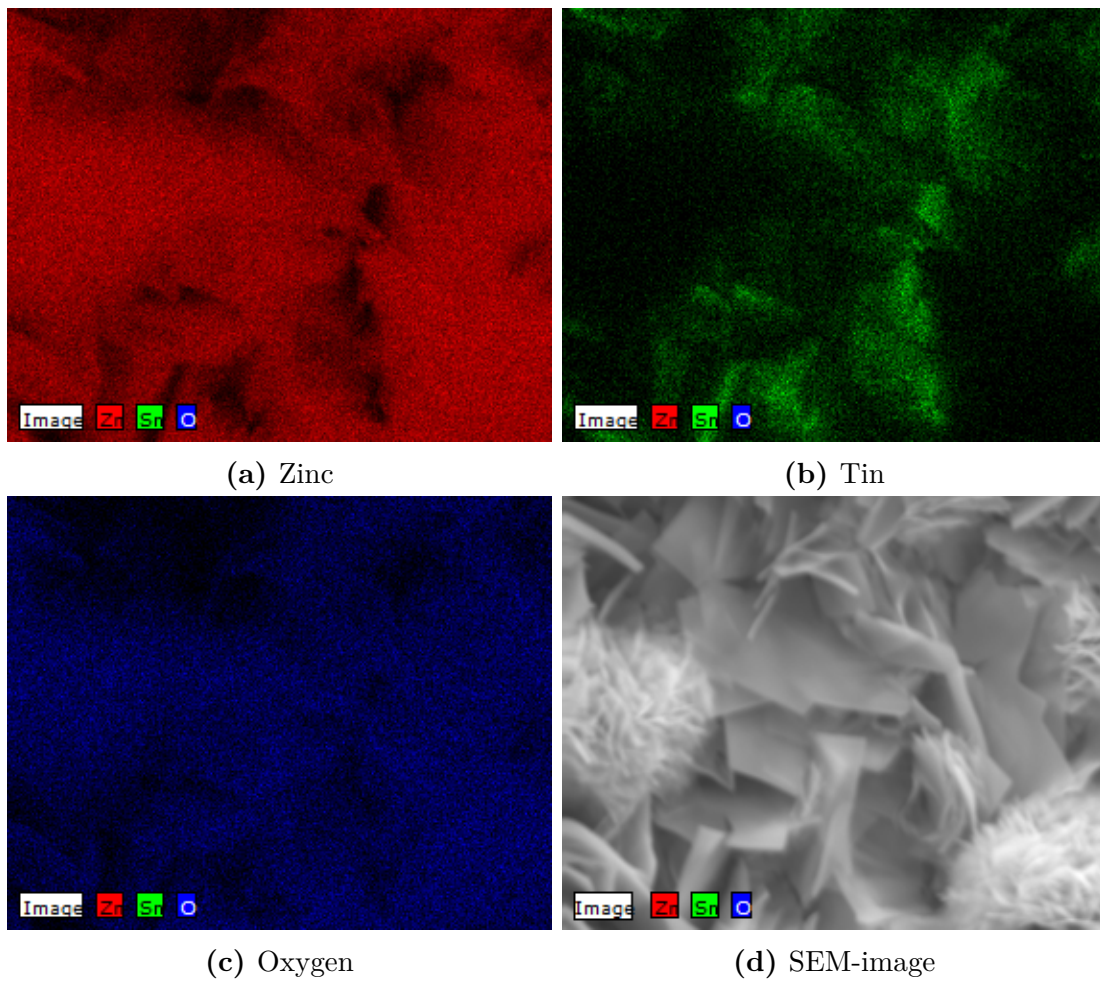


Figure B.1: Elemental EDX-maps of a ZnO film made by standard electrodeposition. The substrate is FTO (fluorine-doped tin oxide). (a) maps zinc, (b) maps tin, (c) maps oxygen, and (d) is a SEM-image of the area mapped.

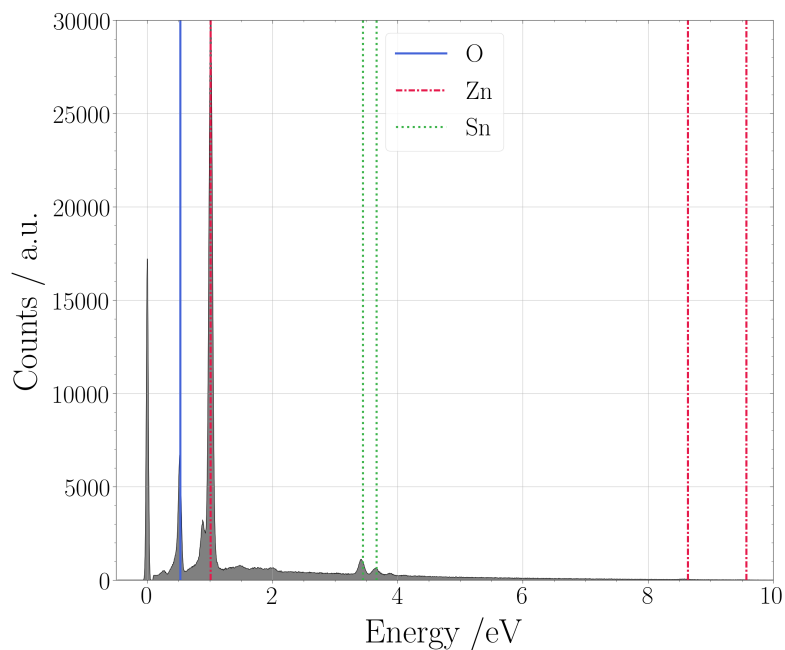


Figure B.2: EDX-spectrum of an SE-sample.

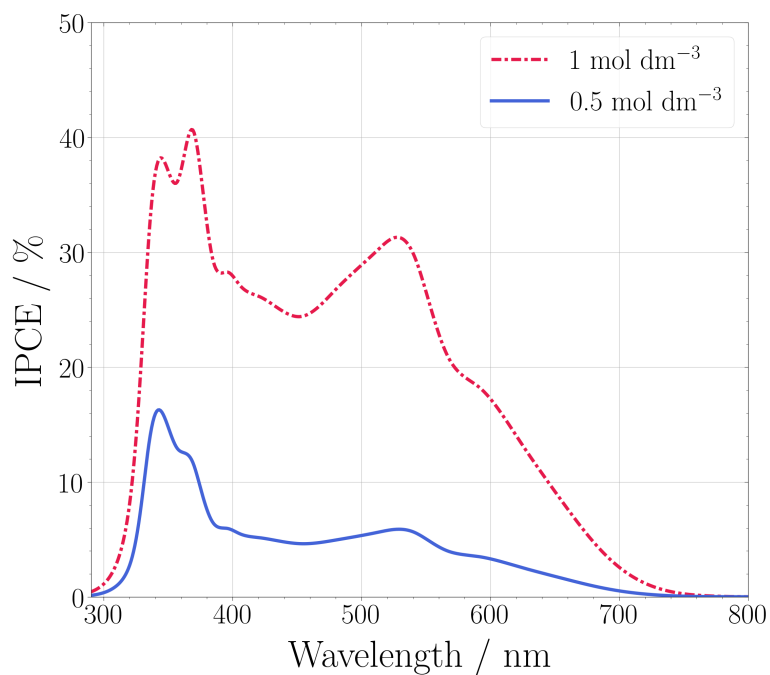


Figure B.3: IPCE-spectra of PHE electrodes made from $\text{Zn}(\text{NO}_3)_2$ -concentrations of 1 mol dm^{-3} and 0.5 mol dm^{-3} .

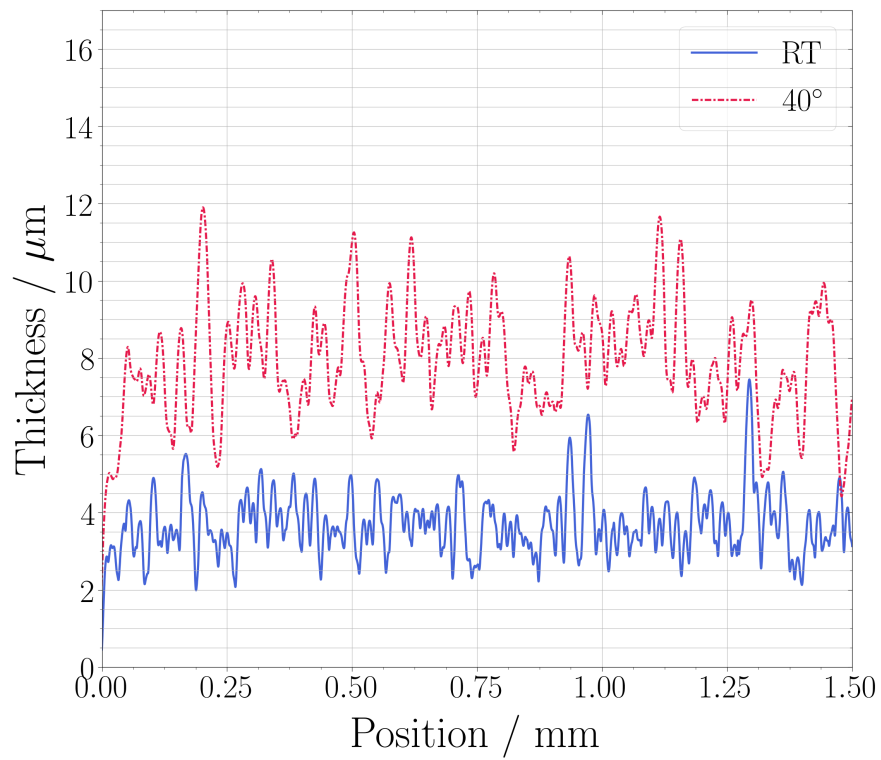
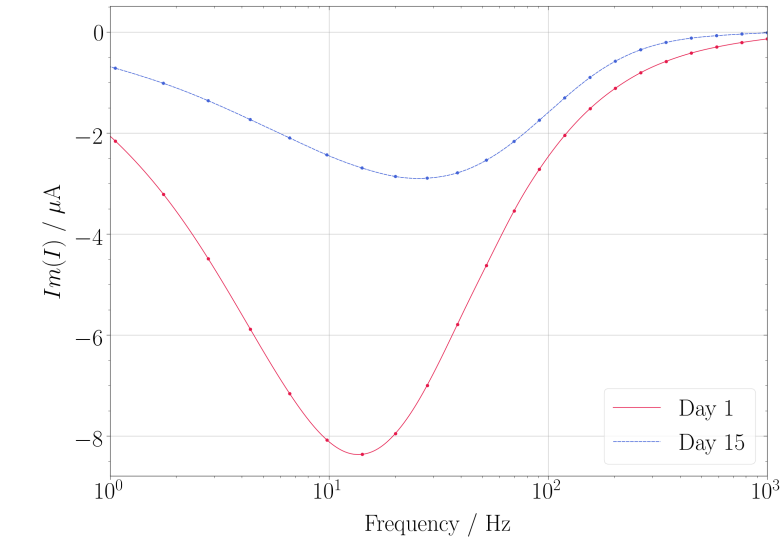
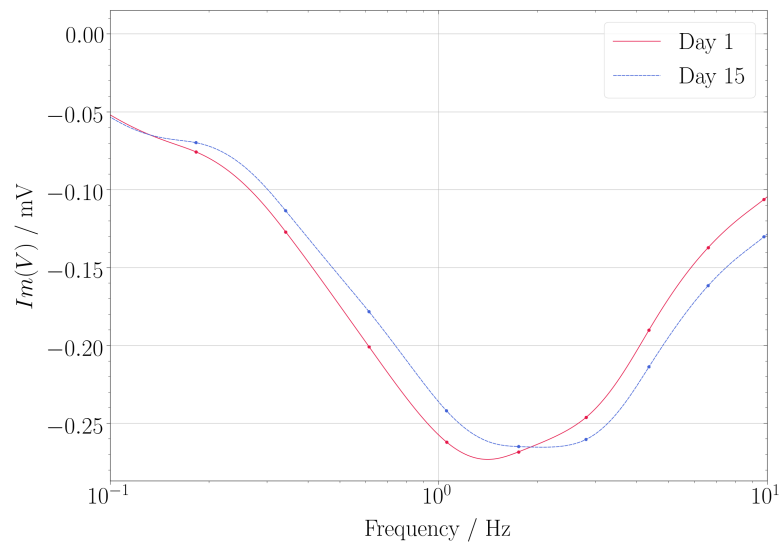


Figure B.4: Profilometer measurements of samples made from a nitrate solution at room temperature (RT) and at 40 °C.

B.2 Degradation



(a) IMPS



(b) IMSV

Figure B.5: (a) IMPS and (b) IMSV of the doctor bladed N719-electrode.

Appendix C

Python script

Note: On some lines, the code is too long to fit the page. In such cases, line shifts and tabulation is used in what are hopefully intuitive ways.

```
#-----#
#           Modelling           #
#           of the resistance in  #
#           dye-sensitized solar  #
#           cells                #
#   from electrochemical imepedance spectroscopy #
#           -----             #
#           Based on Matlab code #
#           by                   #
#           Henrik Erring Hansen #
#           and                  #
#           Svein Sunde          #
#                               #
#           To PYTHON by        #
#           Mari Nyhaug         #
#-----#
#####Preamble#####
import numpy as np
import cmath
import mpmath as mp
import math
import scipy.optimize as so
#####
```

```

#####
#-----FUNCTIONS-----#
#####

#--EIS data from DIRECTORY--#
#Function to get data from several measurements
#stored in the same folder.
#calls on the fuction getEIS(filename)
#Returns the 3D array rawData with the
#Zmodulus, PhaseAngle, frequency
#for all measurements stacked.
#Returns measurementPotentials which is an array of the
potentials the EIS-measurements are recorded at.

def getRawDataFromDirectory(DIRECTORY):
    files = os.listdir(DIRECTORY)
    #sorts the data files from largest measurement potential
    #to the smallest
    #(Requires the measurement potential to be
    #the only difference in the filenames)

    files.sort(reverse=True)
    rawData = []
    measurementPotentials = []

    for sample in files:
        if sample[:1] == '.':
            continue
        Zmodulus, PhaseAngle, frequency, potential =
            getEIS(DIRECTORY+sample)
        measurementPotentials.append(potential)
        rawData.append([Zmodulus, PhaseAngle, frequency])

    return rawData, measurementPotentials

#-----getEIS-----#
#fuction to get the EIS mesurement data (Zahner)

```

```

#Returns the modulus(Zmodulus) and
#phase angle (PhaseAngle) of the impedance
#according to  $Z = Zmodulus * \exp [jPhaseAngle]$ :

def getEIS(filename):
    data = open(filename, 'r')

    read = False
    started = False

    for line in data:
        words = line.split()
        if len(words) == 0:
            continue
        if words[0] == 'potential...':
            potential = abs(float(words[1]))
        if words[0] == 'Number':
            read = True
            continue
        if read == True:
            if started == False:
                frequency = float(words[1])
                Zmodulus = float(words[2])
                PhaseAngle = float(words[3])
                started = True
            else:
                frequency = np.hstack
                    ((frequency, float(words[1])))
                Zmodulus = np.hstack
                    ((Zmodulus, float(words[2])))
                PhaseAngle = np.hstack
                    ((PhaseAngle, float(words[3])))
    return Zmodulus, PhaseAngle, frequency, potential

#-----getIV-----#
# function to get the IV-measurements (Zahner)
def getIV(filename):

```



```

data = open(filename, 'r')

read = False
started = False

for line in data:
    words = line.split()
    if words != [] and words[0] == 'Number':
        read = True
        continue
    if read == True:
        if started == False:
            current = float(words[2])
            potential = float(words[1])
            started = True
        else:
            current = np.hstack
                ((current, float(words[2])))
            potential = np.hstack
                ((potential, float(words[1])))

potential = np.abs(potential)

return current, potential

#-----getX1-----#
# calls on the functions
#convertImpedanceToComplex(Zmodulus, PhaseAngle, frequency),
#leastSquareLM(x0, Zreal, Zimag, omega)
#and getResistance(x1).
#Returns the x1 from the model.

def getX1(rawData, x0):
    Zreal, Zimag, omega = convertImpedanceToComplex
        (rawData[0], rawData[1], rawData[2])
    x1 = leastSquareLM(x0, Zreal, Zimag, omega)
    x1 = getResistance(x1)

```

```

    return x1

#-----ConvertToComplexImpedance-----#

def convertImpedanceToComplex(Zmodulus, PhaseAngle, frequency):
    Zreal = np.zeros(len(Zmodulus))
    Zimag = np.zeros(len(Zmodulus))
    omega = np.zeros(len(Zmodulus))

    for i in range(len(Zmodulus)):
        z = Zmodulus[i]*cmath.exp(1j* np.deg2rad(PhaseAngle[i]))
        #Assumed to be the modulus of the impedance (Zahner)
        Zreal[i] = z.real
        #Assumed to be the phase angle (Zahner)
        Zimag[i] = z.imag
        omega[i] = frequency[i] * 2 * np.pi
    return Zreal, Zimag, omega

#----getResistance----#
#Calculates the transport resistance and the
#recombination resistance based on
#the parameters from the model
#Adds the two resistances to the x1-array.

def getResistance(x1):
    R_tr = np.sqrt((x1[1]**2) * (x1[2]/x1[3]))
    R_rec = R_tr * (x1[3]/x1[2])
    x1 = np.hstack((x1, R_rec))
    x1 = np.hstack((x1, R_tr))

    return x1

#-----Levenberg-Marquardt-Model-----#
#calls in the function nonLinearCurveToFit
#returns x1, an array of parameters
#based on the least-square optimization.

```

```

def leastSquareLM(x0, Zreal, Zimag, omega):
    x1 = (so.least_squares(nonLinearCurveToFit, x0,
                          args=(Zreal, Zimag, omega), method='lm')['x'])
    return x1

#-----Function (F) to fit to model-----#
#Fits the data to the theory by Fabregat-Santiago
#and optimized to complex-least-square theory by Orazem
#Sigma is assumed to be 1 and therefore omitted from code.

def nonLinearCurveToFit(x0, Zreal, Zimag, omega):

    #pre-allocate space
    # need space for both real and imaginary
    F = np.zeros(2 * len(omega))
    Zmodelreal = np.zeros(len(omega))
    Zmodelimag = np.zeros(len(omega))
    Zm = np.zeros(len(omega), complex)

    #calculate constants to make formulas easier to read
    v = x0[2] / x0[3]
    u = np.sqrt(v**x0[4])

    for k in range(len(omega)):

        Z_RC = 1 / (((1 / x0[5]) + ((1j * omega[k]) /
                                   (x0[5] * x0[6]))))
        Z_d = (x0[7] * np.tanh(np.sqrt(1j*omega[k]/x0[8])))/
              np.sqrt(1j * omega[k] / x0[8])

        #to make the function easier to read
        w = omega[k] / x0[2]

        Z_rec = (x0[1] / (np.sqrt(1 + (1j * (w**x0[4])))) *
                mp.coth(u * np.sqrt(1 + (1j * (w**x0[4])))))

```

```

#sum of all imedances
Zm[k] = (x0[0] + Z_d + Z_RC + Z_rec)
#real part of total impedance
Zmodelreal[k] = Zm[k].real
#imaginary part of total impedance
Zmodelimag[k] = Zm[k].imag

#F is the fuction to get optimized with regards
#to the parameters

# Real part
F[k] = Zreal[k] - Zmodelreal[k]

# Imaginary part
F[len(omega)+k] = Zimag[k] - Zmodelimag[k]
return F

#----make IV plot from EIS----#

#find the IV-curve from the EIS-data

def getIVfromEIS(
    x1, measurementPotentials, IVcurrent, IVpotential):

    #x1 is the fitted parameters from zmodel
    #make an array with all the potentials
    # and current-values we want to estimate (1000 points)
    v = np.linspace(max(measurementPotentials)+0.2, 0, 1000)
    iAL = np.linspace(0, max(IVcurrent), 1000)

    #pre-allocate space for resistances

    #resistance in the active semiconductor layer
    Ral = np.zeros(len(x1))

    #resistance in the cell

```

```

Rdc= np.zeros(len(x1))

#For all samples in x1:
# Ral: Adds together the Recombination Resistance (x1[9])
#and Transport Resistance (x1[10]) for all samples in x1.
# Rdc: Adds together Series Resistance (x1[0]),
#Parallel Resistance (x1[5]), Diffusion resistance (x1[7])
# Recombination Resistance (x1[9]) and
#Transport Resistance (x1[10])
# The Transport Resistance (x1[10]) is
#divided by 3 in both cases
for i in range(len(x1)):
    Ral[i] = x1[i][9]+x1[i][10]/3
    Rdc[i] = x1[i][0]+x1[i][5]+x1[i][7]+x1[i][9]+x1[i][10]/3

#Calculations for the WHOLE CELL (DC)
slope = np.polyfit(measurementPotentials, np.log(Rdc), 1)
beta = -slope[0] * k_b * T / q
c = np.exp(slope[1])
Rrec = c*np.exp(-beta*q*v/(k_b*T))
I0 = (k_b*T/(q*beta*c))

#Calculations for the ACTIVE SEMICONDUCTOR LAYER (AL)
# The series resistance, electrolyte diffusion and
#cathode resistance is removed
#Only the recombination resistance and transport resistance
#in the semiconductor is used to calculate the IV-curve
slopeAL = np.polyfit(measurementPotentials, np.log(Ral), 1)
betaAL = -slopeAL[0] * k_b * T / q
cAL = np.exp(slopeAL[1])
IOAL = (k_b * T / (q * betaAL * cAL))

#experimental short circuit current density
jsc = np.max(IVcurrent)

```

```

#eqn 91 and 42 from Fabregat-Santiago 2011

eq1 = lambda x: (k_b*T/(q*beta))/(jsc + I0 - x)
eq2 = lambda x: (k_b*T/(q*betaAL))/(jsc + IOAL - x)

V_01, rest = np.max(IVpotential) -
              scipy.integrate.quad(eq1, 0, jsc)
V_02, rest = np.max(IVpotential) -
              scipy.integrate.quad(eq2, 0, jsc)

V_IS = np.zeros(len(iAL))
V_f = np.zeros(len(iAL))

for i in range(len(iAL)):
    V_IS[i], rest = V_01 +
                    scipy.integrate.quad(eq1, iAL[i], jsc)
    V_f[i], rest = V_02 +
                   scipy.integrate.quad(eq2, iAL[i], jsc)

return V_IS, iAL, Rdc

# if other values from the model is desired
# add to the list after return

#####--USING THE FUNCTIONS--#####

##--INPUT--##
DIRECTORY = [] #path to folder with EIS-files.
IVpath = '' #Path to IV-data
#array with initial guess of the parameters
x0 = np.array([40, 20, 10, 90, 1, 10, 9*10**3, 10, 0.1])
#pre allocate space for model parameters
x1 = np.zeros([len(rawData), 11])

##--GET DATA--#

```

```

IVcurrent, IVpotential = etIV(IVpath)
rawData, measurementPotentials =
    r.getRawDataFromDirectory(DIRECTORY)

##--FIND PARAMETERS FROM MODEL--##

#find x1 for each EIS-measurement using
#getX1 from the file Z_model
for s in range(len(rawData)):
    if s == 0:
        x1[s] = Z.getX1(rawData[s], x0)
    else:
        x1[s] = Z.getX1(rawData[s], x1[s-1][0:9])

##--RECREATE THE IV-CURVE--##
V_IS, iAL, Rtot = getIVfromEIS(
    x1, measurementPotentials, IVcurrent, IVpotential)

#V_IS is the estimated voltage in the cell
#iAL is an array of 1000 currents from 0 to
#short circuit current
# Rtot is the an array of the total resistance in the cell
# at each measurement potential

#Plot desired data#

#####---#####-The END-#####---#####



#The input x0 guesses were:
#x0 on day 1:
x0 = np.array([40, 20, 10, 90, 1, 10, 9*10**3, 10, 0.1])
#x0 on day 15:
x0 = np.array([50, 100, 50, 90, 1, 10, 9*10**3, 10, 0.1])

```

Appendix D

Risk Assessment

The risk assessment is written in Norwegian. See next page.

NTNU		Utarbeidet av		Nummer		Dato	
		HMS-avd.		HMSRV2601		22.03.2011	
HMS		Godkjent av		Side		Ersätter	
		Rektor				01.12.2006	
<h1>Kartlegging av risikofylt aktivitet</h1>							
							

Enhet:

Institutt for materialteknologi

Dato:

20.02.2019

Linjeleder:

Svein Sunde

Deltakere ved kartleggingen (m/ funksjon):

Mari Nyhaug (student), Svein Sunde (veileder)

(Ansv. veileder, student, evt. medveiledere, evt. andre m. kompetanse)

Kort beskrivelse av hovedaktivitet/hovedprosess:

Masteroppgave om fargestofsceller med sinkoksid-elektroder.

Er oppgaven er rent teoretisk? (JA/NEI)

Nei

"JA" betyr at veileder innestår for at oppgaven ikke inneholder noen aktiviteter som krever risikovurdering. I dette tilfellet er det ikke nødvendig å fylle ut resten av skjemaet

Er det trygt å utføre arbeidet utenfor normal arbeidstid (8-17)? (JA/NEI)

JA

Signaturer:

Ansv. veileder:



Student:

Mari Nyhaug

ID nr.	Aktivitet/prosess	Ansv. veileder	Eksisterende dokumentasjon	Eksisterende sikringsiltak	Lov, forskrift o.l.	Kommentar
1	Generelt arbeid på lab 223	Mari		Briller, nitril-hansker, labfrakk, opplæring, avtrekkskap eller punktavsug, alle glass med kjemikalier skal merkes med innhold og konsentrasjon, kjemisk avfall kastes på anvist sted etter rutiner.		Arbeidet på lab 223 er av en "kjemisk art". Før arbeid med kjemikalier skal sikkerhetsdatabladene til disse være gjennomgått og risikoelementene ved arbeid med kjemikalier skal være kjent og vurdert.
2	Generelt arbeid på lab 003	Mari		Egnede UV-briller for arbeid med UV-stråling, opplæring, rutiner, ellers samme rutiner som på lab 223 (se pkt 1)		På lab 003 er det utarbeidet gode rutiner for hvordan man skal beskytte seg for UV-lys, og varsle andre om at lampen er i bruk.

3	Doctor blading	Mari	SDS: Etylcellulose, Terpineol, ZnO-nanopartikler dispergert i vann	Se generelt om lab 223.		Arbeider med nanopartikler. Det er ikke oppgitt at disse er farlige for mennesker, men kan være skadelig for livet i vann. Nanopartiklene er dispergert i vann.
4	Fargestofflegging	Mari	SDS: Etanol, N719 og Eosin Y	Se generelt om lab 223.		Små mengder, <20 mL hver gang.
5	Solcellekarakterisering (003)	Mari		Lyskilden står inne i en boks, se generelt om lab 003 i pkt 2		IV-karakteriseringen utføres med monokromatisk lys i synlig lys-regionen. IPCE-målingene går ned i UV-området. Potentiosaten er det største faremomentet.
6	Uttynning av konsentrert svovelsyre	Mari	SDS: Konsentrert svovelsyre	Hansker for syrearbeid, jobbe i avtrekkskap+ se generelt om lab 223		"Syre i vann går an" og arbeidet skjer i avtrekkskap, bruk ferdig uttynnet løsning hvis mulig.
7	Lage og håndtere elektrolytt	Mari	SDS: 4-tert-butylpyridine, acetonitrile, jod, litium iodinde, tetrabutylammonium iodide.	Arbeider i avtrekkskap + se generelt om lab på 223		Løsemiddelet (acetonitrile) er brannfarlig. Lagring av elektrolytten skal derfor skje etter retningslinjer på laben.
8	Arbeid med potentiosat både på 223 og 003	Mari		003: Elektrodene er inne i en boks under bruk.		Potentiosaten på 003 er mye mer beskyttet enn potentiosaten på 223. Forhåndsregler skal alltid utøves når man må være i kontakt med den.

9	Elektrokjemisk syntese av ZnO, lab 223	Mari	SDS: sinknitrat tetrahydrat eller sinknitrat heksahydrat, eosin Y, etanol	Se generelt om lab 223. Oppsettet står i en plastballe for å fange opp søl.		
10	Elektrokjemisk syntese av ZnO med solsimulator lab 003	Mari	Kjemikalier er samme som i pkt 9	Se generelt om lab 003. Oppsettet står i en plastballe for å fange opp søl.		Det er opparbeidet gode rutiner på laben for UV-lys. Det kjemiske delen av arbeidet i denne syntesen er lik som i pkt. 9. Faren ved bruk av solsimulatoren er at den ikke er dekket under bruk.

NTNU		Utarbeidet av		Nummer		Dato			
		HMS-avd.		HMSRV2603		04.02.2011			
HMS/KS		Godkjent av		Slide		Erstatter			
		Rektor				09.02.2010			
<h1>Risikovurdering</h1>									

Institutt for materialteknologi Dato:

20.02.2019

Enhet:
Linjeleder:

Deltakere ved risikovurderingen (m/ funksjon):

(Ansv. veileder, student, evt. medveiledere, evt. andre m. kompetanse)

Mari Nyhaug (student), Svein Sunde (Veileder)

Risikovurderingen gjelder hovedaktivitet:

Masteroppgave om fargestofsolceller med sinkoksid-elektroder.

Signaturer:

Ansvarlig veileder:

Student:

ID nr.	Aktivitet/prosess fra kartleggingsskjemaet	Mulig uønsket hendelse	Vurdering av sannsynlighet (1-5)	Vurdering av konsekvens				Risiko-verdi (menn-eske)	Kommentarer/ status Forslag til tiltak
				Menneske (A-E)	Ytre miljø (A-E)	Øk./materiell (A-E)	Om-dømme (A-E)		
1 og 2	Generalt arbeid på lab 223 og lab 003	Søl med kjemikalier slik at det kommer i kontakt med hud/løyne eller utgjøre en fare for andre på laben.	3	C				C3	Kjemikalier skal behandles med aktsomhet. Personlig verneutstyr skal alltid benyttes. Kjemikalier skal fraktes på en ansvarlig måte, oppbevares i korrekte beholdere og kastes etter retningslinjer på lab. Eksperimenter skal utføres kontrollert og gjennomtenkt

1 og 2	Generelt arbeid på lab 223 og lab 003	Brann	1	E					E1	Brann er farlig, særlig i rom som en kjemisk lab med mange brennbare/eksplosive kjemikalier og gassledninger. Riktig lagring, ryddige arbeidsområder og generelt god labkultur er viktige tiltak for at branner ikke oppstår. Man skal også gjøre seg kjent med nødutganger og slukkemidler på laben.
3	Doctor blading	Brenne seg på varm ovn/prøve.	2	B					B2	Braker hansker som er egnet for håndtering av varme objekter.
3	Doctor blading	Farer fra ethylcellulose - SDS: ingen farer	1	A					A1	Ingen farer i SDS
3	Doctor blading	Farer fra terpineo - SDS: H315 Irriterer huden. H319 Gir alvorlig øyeirritasjon.	3	B					B3	Braker vernebriller, labfrakk og nitril-hansker under bruk
3	Doctor blading	Farer fra ZnO-nanopartikler: ingen faresetninger om helse	1	A					A1	Siden dette er nanopartikler utøves forsiktighet likevel, pkt. 1 Avfall legges i egne poser

9	Elektrokjemisk syntese av ZnO, lab 223	<p>Farer ved Sinknitrat: H272 Kan forsterke brann; oksiderende. H302 Farlig ved svelging. H315 Irriterer huden. H319 Gir alvorlig øyirritasjon. H335 Kan forårsake irritasjon av luftveiene. H410 Meget giftig, med langtidsvirkning, for liv i vann.</p>	3	C			C3	<p>Med sikkerhetsiltak som alle rede er på plass på laben, er personskader ved svelging, hudkontakt og øyekontakt lite sannsynlig. At det er oksiderende og kan forsterke brann håndteres ved oppbevaring etter rutiner på lab. Personlig verneutstyr benyttes, se pkt 1 om generell håndtering av kjemikalier</p>
9	Elektrokjemisk syntese av ZnO, lab 223	Farer ved etanol og eosin Y, se pkt 4						se pkt 4 og pkt 1

9	Elektrokjemisk syntese av ZnO, lab 223	Kutte seg på glass	3	A				A3	<p>Det er en mulighet for å kutte seg på glasset mens man kutter det til egnede størrelser. Dette medfører i verste fall kutt på fingre eller heder. Nitridhansker brukes, disse beskytter noe, men ikke mot alt. Det regnes som lite sannsynlig at det påføres store skader som ikke kan ordnes med et plaster.</p>
---	---	--------------------	---	---	--	--	--	----	--

Risikoverdi = Sannsynlighet (1, 2 ...) x konsekvens (A, B ...). Risikoverdi A1 betyr svært liten risiko. Risikoverdi E5 betyr svært stor og svært alvorlig risiko.

		Konsekvens					
Verdi	Kriterier	Gradering	Menneske	Ytre miljø: Vann, jord og luft	ØK/materiell	Omdømme	
1	Svært liten: 1 gang pr 50 år eller sjeldnere	E	Svært alvorlig	Død	Svært langvarig og ikke reversibel skade	Drifts- eller aktivitetstans > 1 år.	Troverdighet og respekt betydelig og varig svekket
2	Liten: 1 gang pr 10 år eller sjeldnere	D	Alvorlig	Alvorlig personskade. Mulig uførhet	Langvarig skade. Lang restitusjonstid	Driftstans > 1/2 år, aktivitetstans opp til 1 år	Troverdighet og respekt betydelig svekket
3	Middels: 1 gang pr år eller sjeldnere	C	Moderat	Alvorlig personskade.	Mindre skade og lang restitusjonstid	Drifts- eller aktivitetstans < 1 md	Troverdighet og respekt svekket
4	Stor: 1 gang pr måned eller sjeldnere	B	Liten	Skade som krever medisinsk behandling	Mindre skade og kort restitusjonstid	Drifts- eller aktivitetstans < 1 uke	Negativ påvirkning på troverdighet og respekt
5	Svært stor :Skjer ukjentlig	A	Svært liten	Skade som krever førstehjelp	Ubetydelig skade og kort restitusjonstid	Drifts- eller aktivitetstans < 1 dag	Liten påvirkning på troverdighet og respekt

MATRISSE FOR RISIKOVURDERINGER ved NTNU

KONSEKVENNS	Svært alvorlig	E1	E2	E3	E4	E5
	Alvorlig	D1	D2	D3	D4	D5
	Moderat	C1	C2	C3	C4	C5
	Liten	B1	B2	B3	B4	B5
	Svært liten	A1	A2	A3	A4	A5
	Svært liten	Liten	Middels	Stor	Svært stor	
SANNSYNLIGHET						

Prinsipp over akseptkriterium. Forklaring av fargene som er brukt i risikomatrisen.

Farge	Beskrivelse
Rød	Uakseptabel risiko. Tiltak skal gjennomføres for å redusere risikoen.
Gul	Vurderingsområde. Tiltak skal vurderes.
Grønn	Akseptabel risiko. Tiltak kan vurderes ut fra andre hensyn.

